Astroparticle Physics 2022/23

1. Historical introduction - basic properties of cosmic rays
2. Hadronic interactions and accelerator data
3. Cascade equations
4. Electromagnetic cascades
5. Extensive air showers
6. Detectors for extensive air showers
7. High-energy cosmic rays and the knee in the energy spectrum of cosmic rays
8. Radio detection of extensive air showers
9. Acceleration, Astrophysical accelerators and beam dumps
10. Extragalactic propagation of cosmic rays
11. Ultra-high-energy energy cosmic rays
12. Astrophysical gamma rays and neutrinos
13. Neutrino astronomy
14. Gamma-ray astronomy

lecture 8
Radio detection of extensive air showers

Gaisser chapter 16

16 Extensive air showers

16.1 Basic features of air showers
16.2 The Heitler–Matthews splitting model
16.3 Muons in air showers
16.4 Nuclei and the superposition model
16.5 Elongation rate theorem
16.6 Shower universality and cross section measurement
16.7 Particle detector arrays
16.8 Atmospheric Cherenkov light detectors
16.9 Fluorescence telescopes
16.10 Radio signal detection

First radio detection of air showers 1965

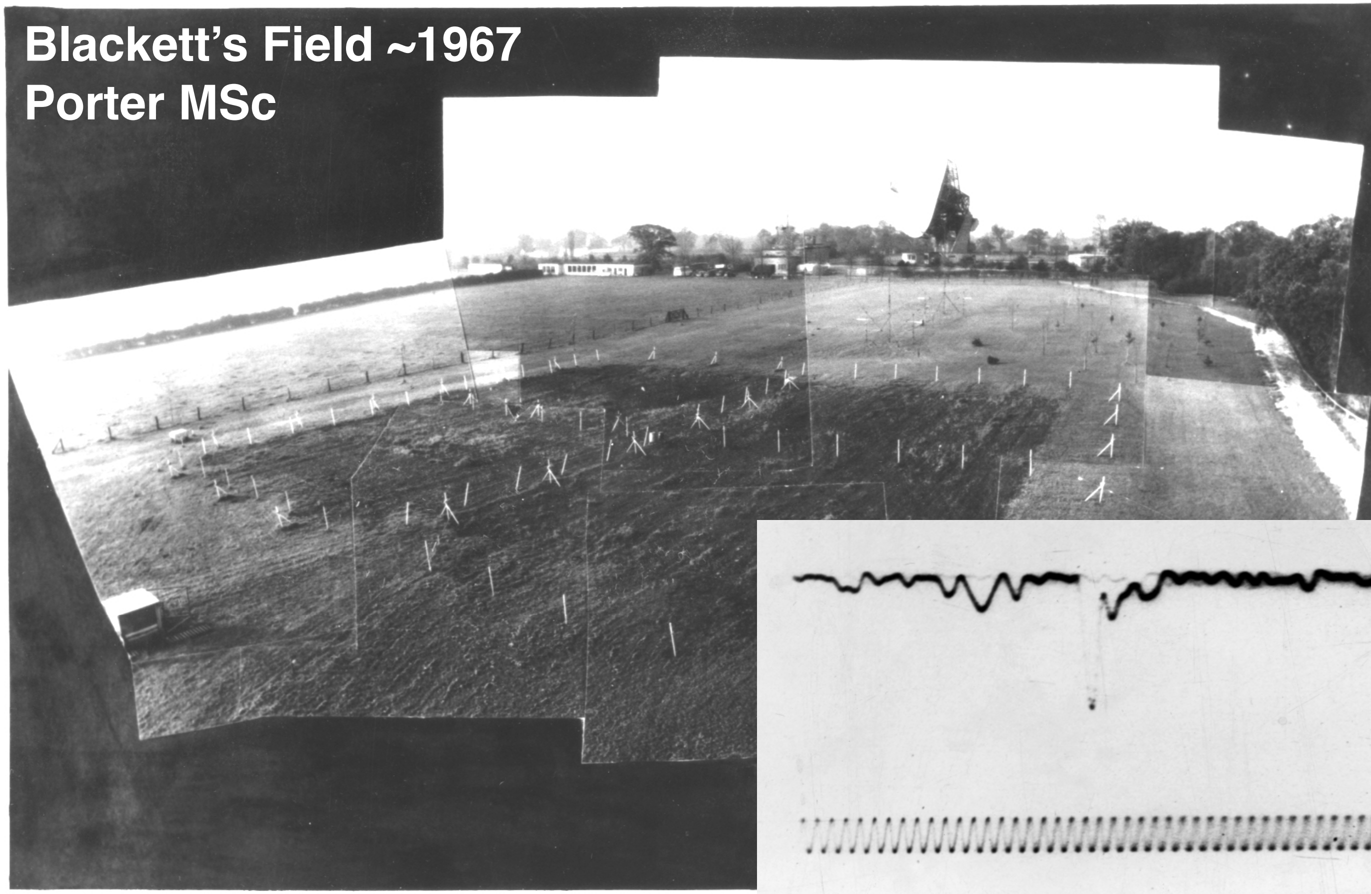

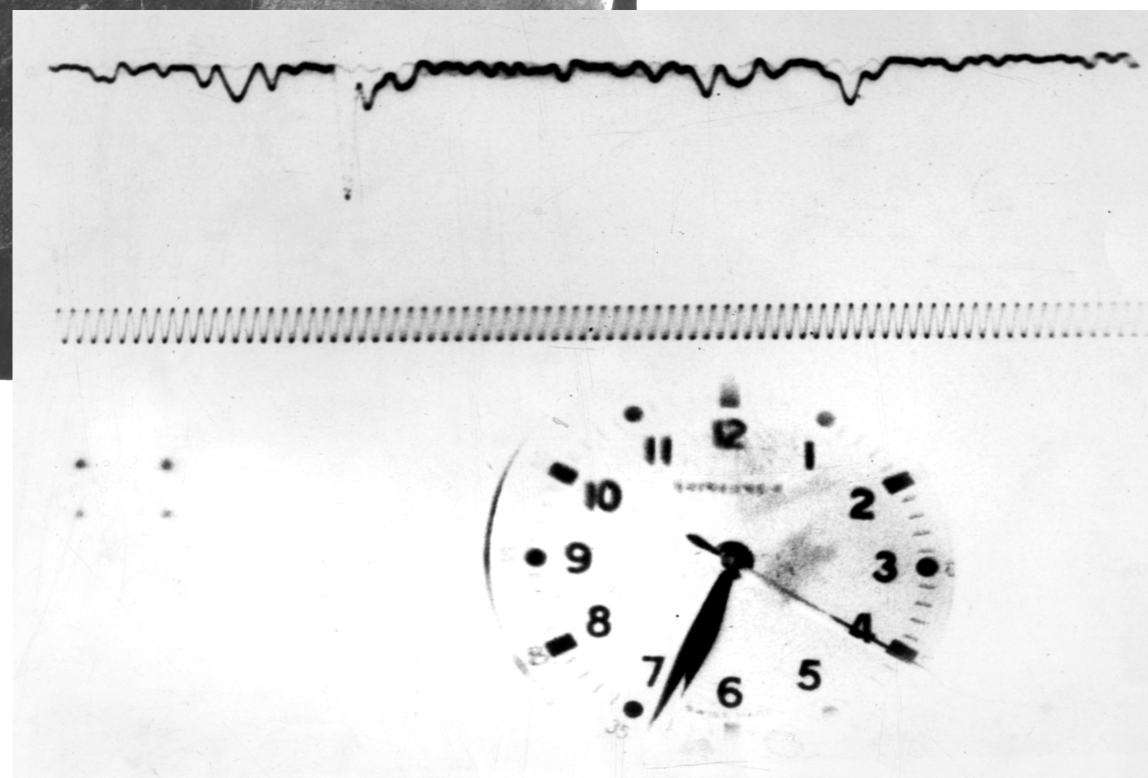

Jelley et al Nature 1965
R. A. Porter MSc Thesis 1967

Haverah Park (Leeds) Allan 1971

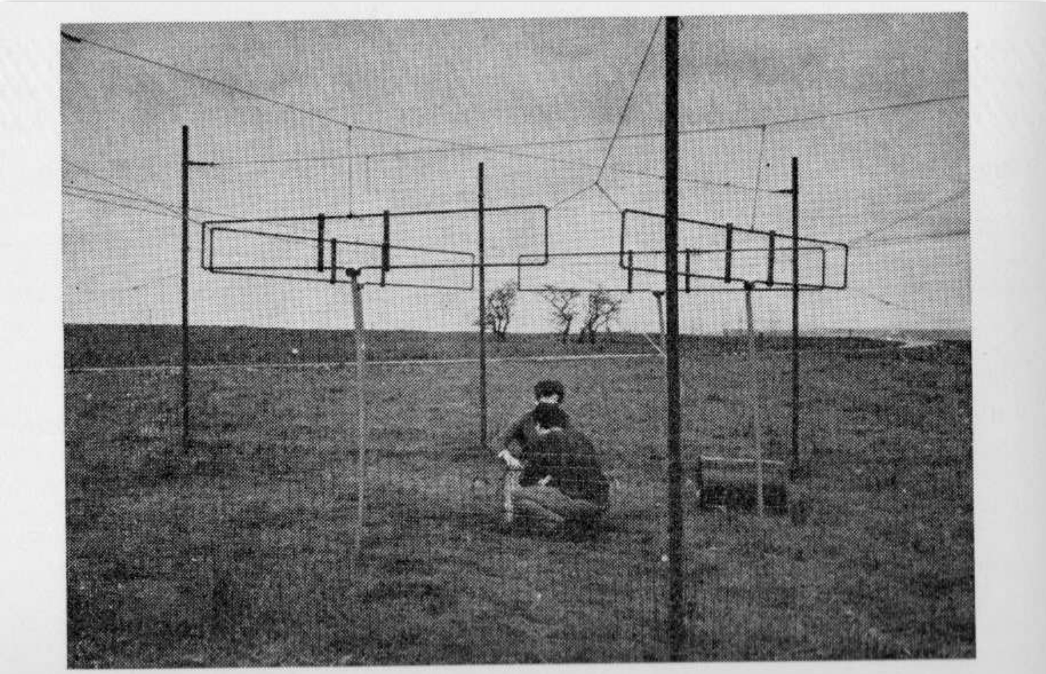

Recent receiving antennas (44 MHz) forming part of the Haverah Park Extensive Air Shower Array.

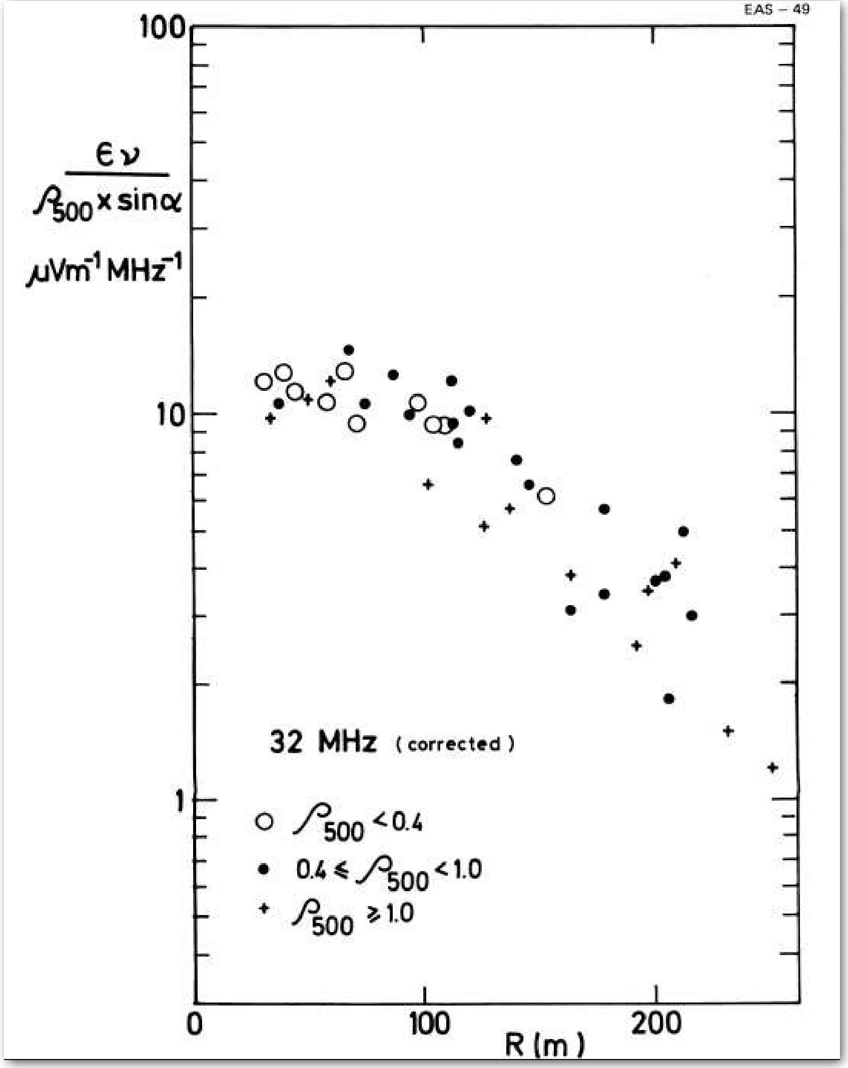

$$\varepsilon_\nu = 2\left(\frac{E_p}{10^{17}}\right)\left(\frac{\sin\alpha\cos\theta}{\sin 45\cos 30}\right)\exp\left(\frac{-r}{r_0}\right)\left(\frac{\nu}{50}\right)^{-1} \quad \mu\mathrm{V/m/MHz}$$

$r_0 = 110$ m at ν=55 MHz. α=angle to B, θ=Zenith angle

H.R. Allan, Prog. Element. Part. Cosmic Ray Phys (1971) 169

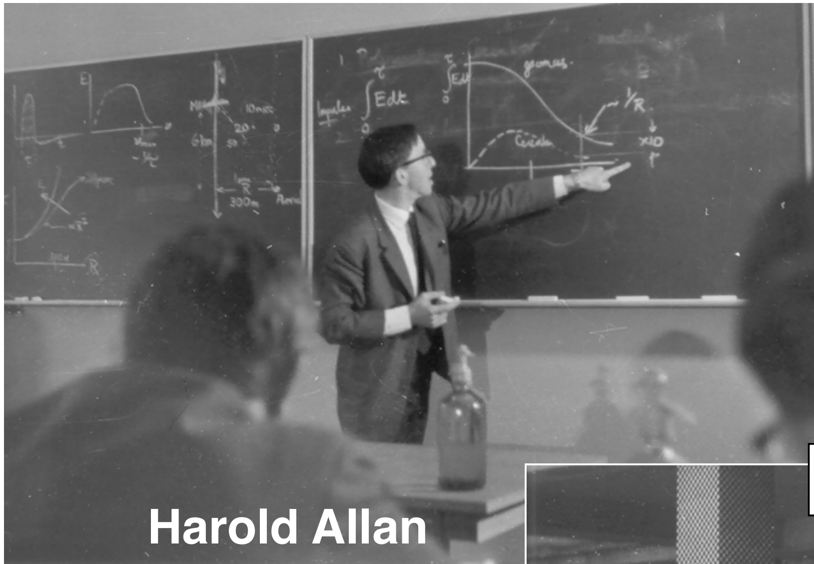

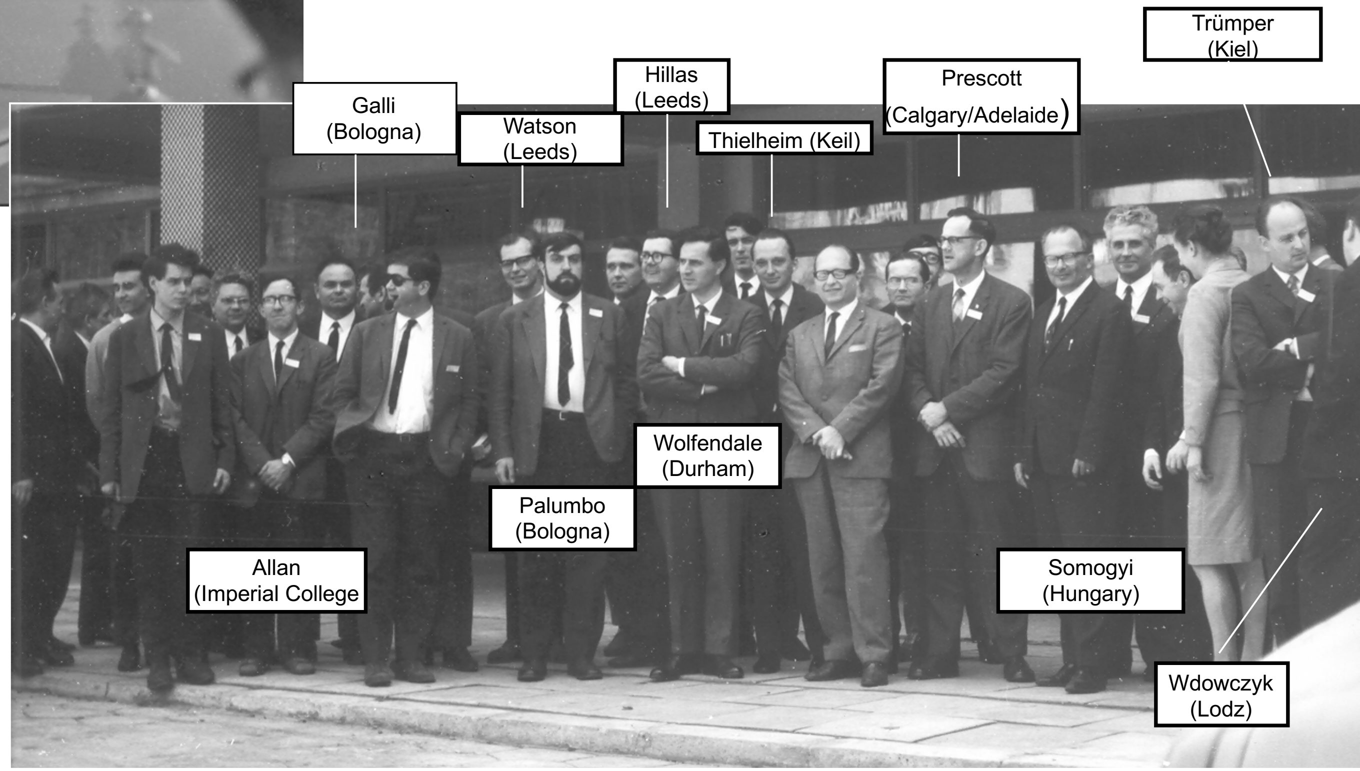

First European Symposium on High Energy Interactions and Extensive Air Shower: Lodz, Poland April 1968

33RD INTERNATIONAL COSMIC RAY CONFERENCE, RIO DE JANEIRO 2013
THE ASTROPARTICLE PHYSICS CONFERENCE

ICRC 2013

The renaissance of radio detection of cosmic rays

TIM HUEGE[1]

2018: beyond capabilities of standard installations

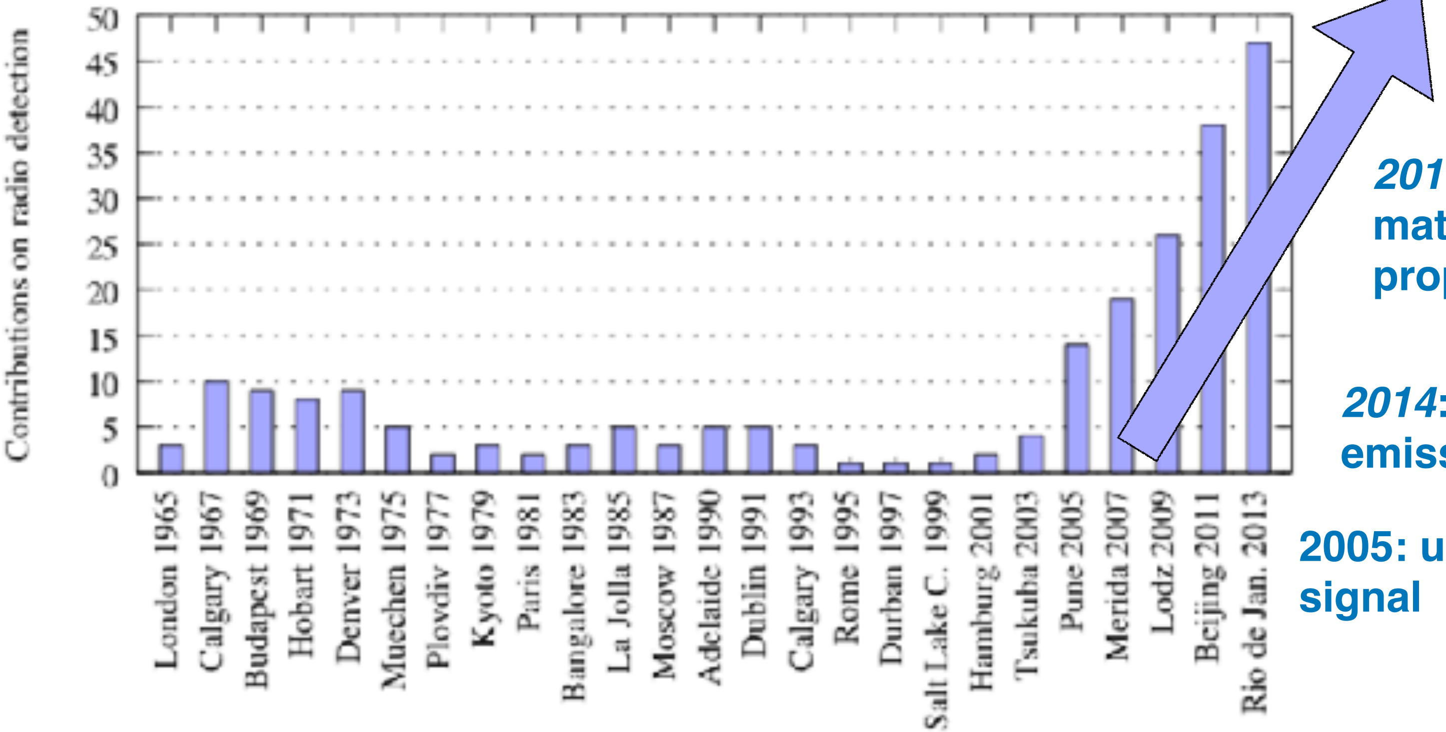

2016: radio technique mature: properties of cosmic rays

2014: understanding the emission processes

2005: understanding the signal

Figure 1: Number of contributions related to radio detection of cosmic rays or neutrinos to the ICRCs since 1965. The field has grown very impressively since the modern activities started around 2003. Data up to 2007 were taken from [11].

Radio Detectors

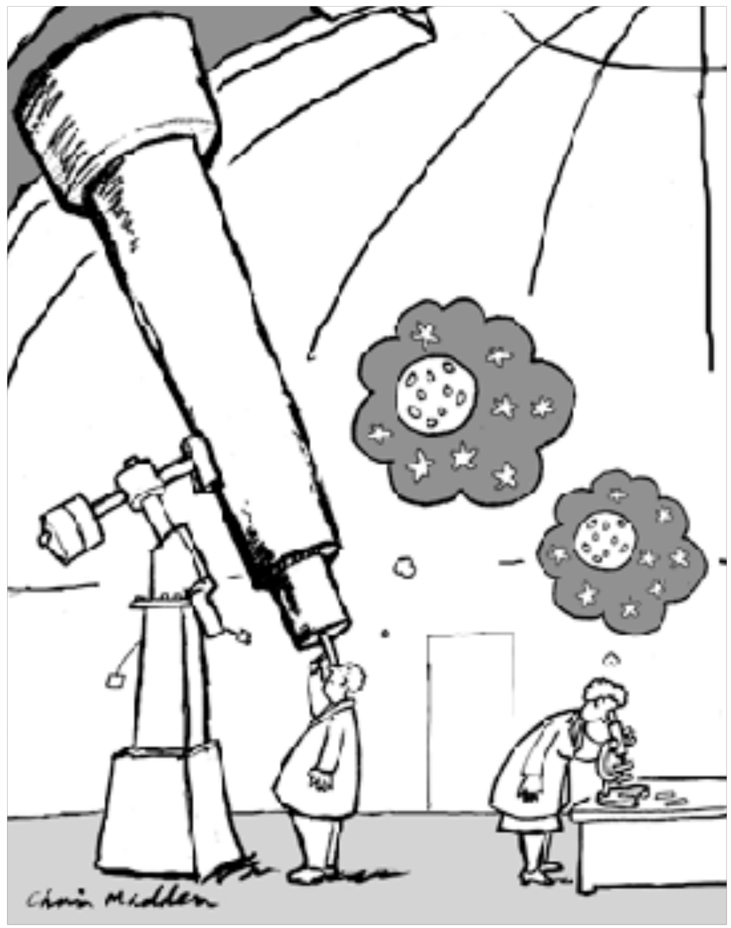

Radio detection of extensive air showers around the world

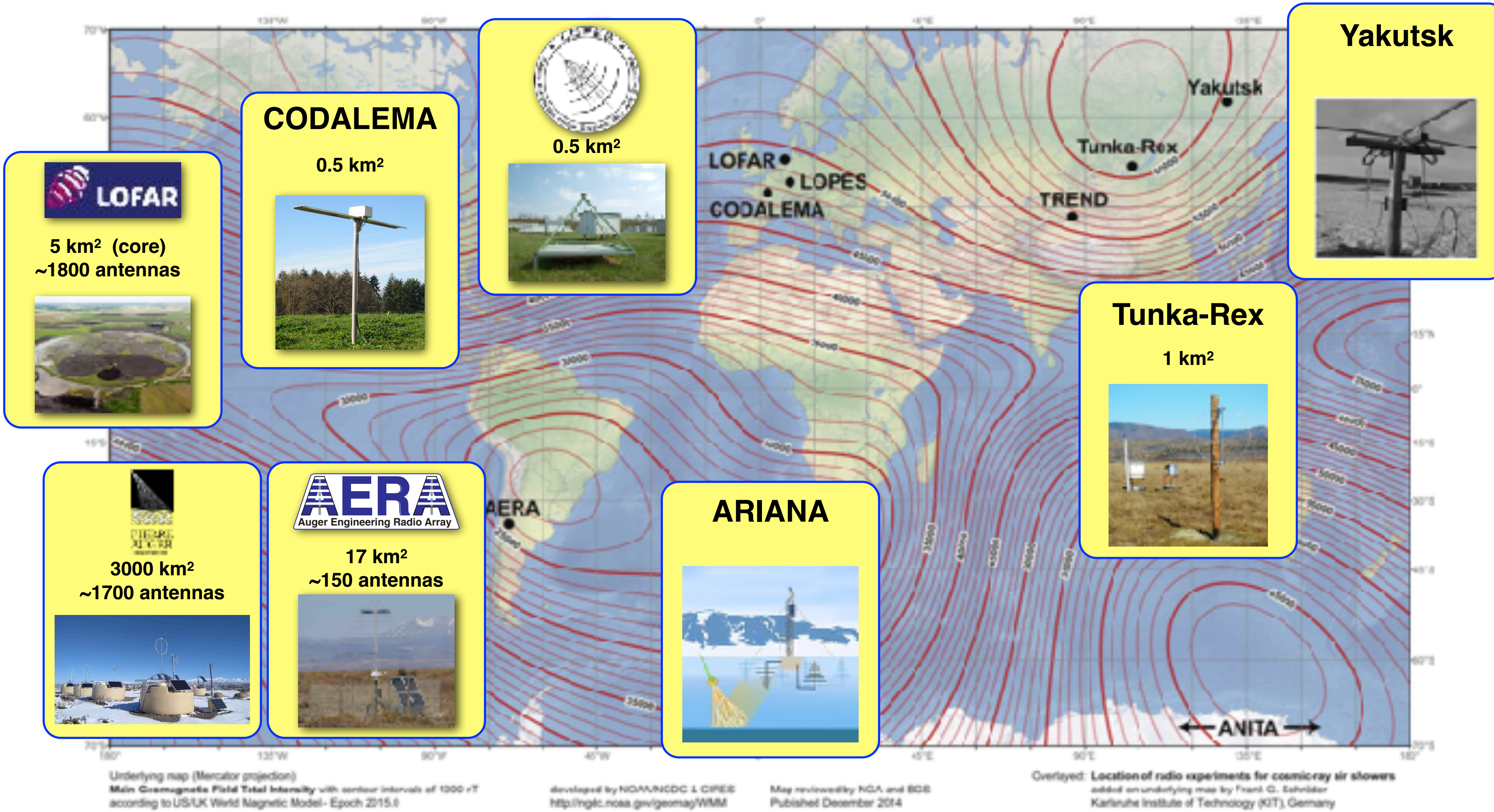

Fig. 21. Map of the total geomagnetic field strengths (world magnetic model [207]) and the location of various radio experiments detecting cosmic-ray air showers.

F.G. Schröder, Prog. Part. Nucl. Phys. 92 (17) 1

LOFAR

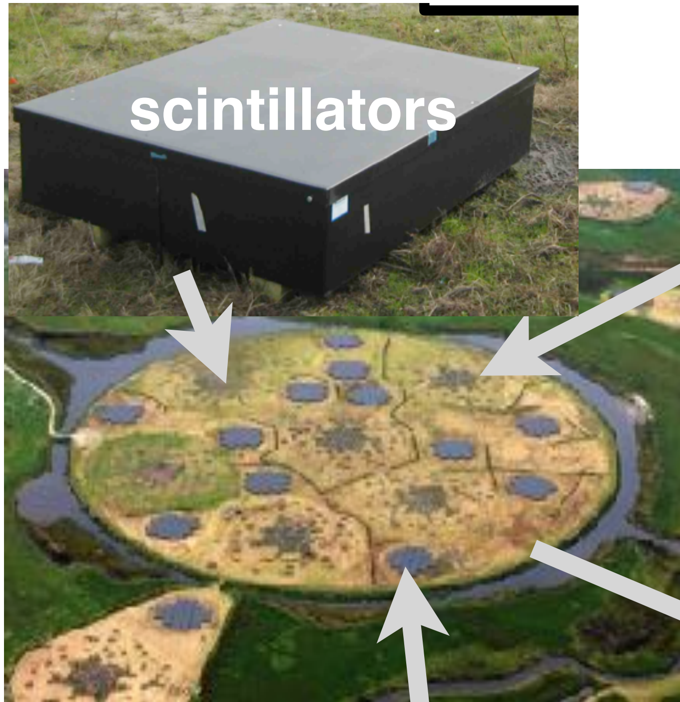

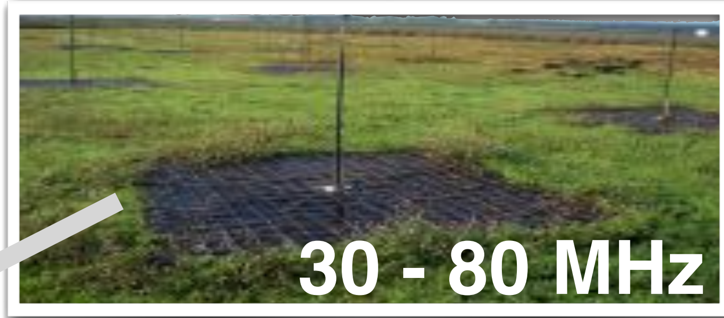

core
23 stations ~5 km²

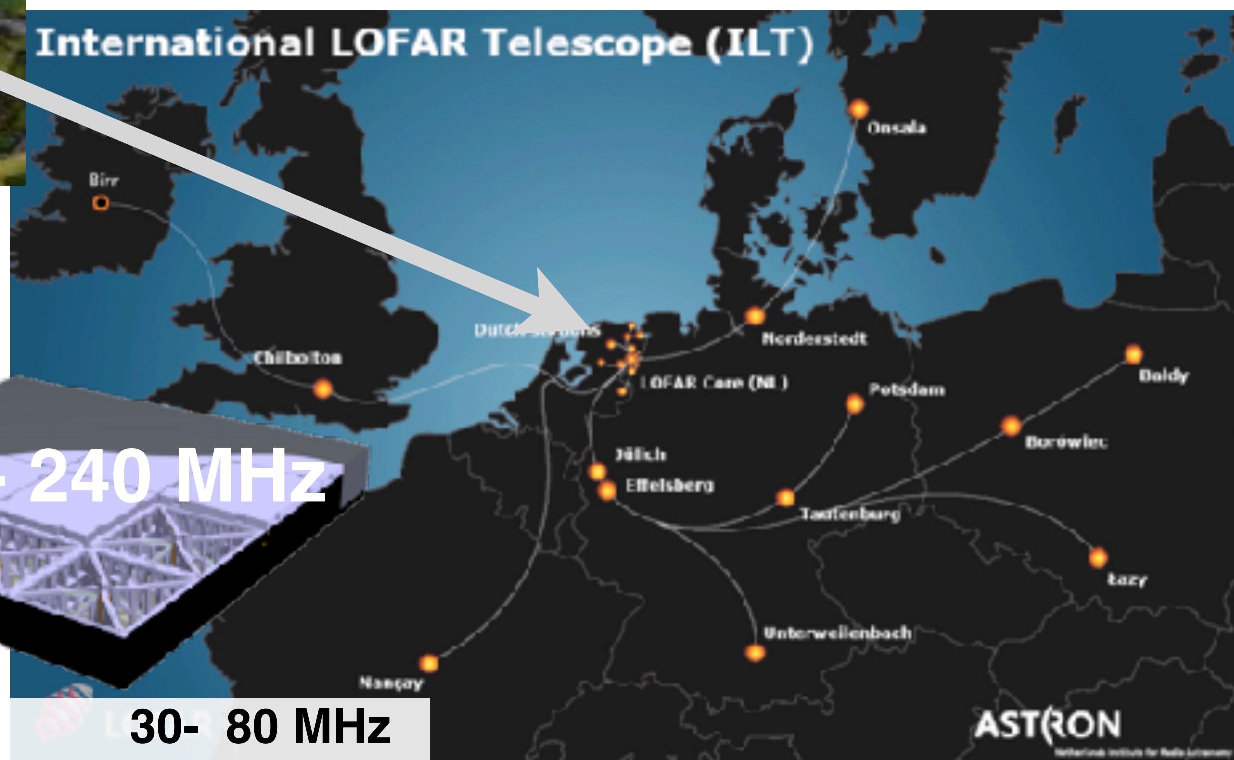

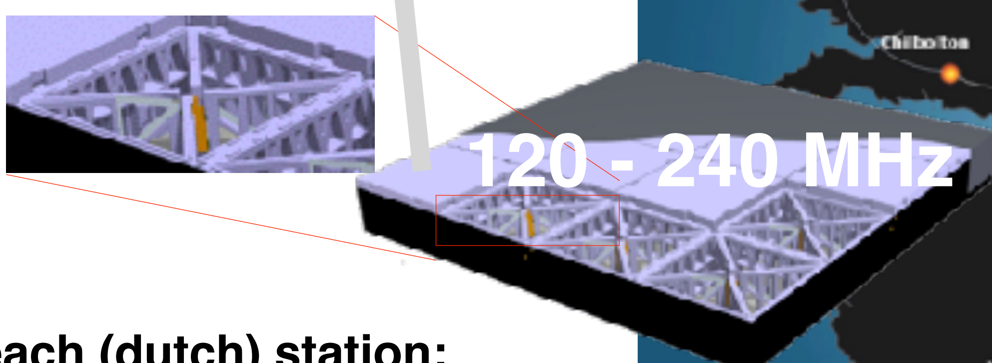

each (dutch) station:
96 low-band antennas 30- 80 MHz
high-band antennas (2x24 tiles) 120-240 MHz

M. van Haarlem et al., A&A 556 (2013) A2

S. Thoudam et al., Nucl. Instr. Meth. A 767 (2014) 339

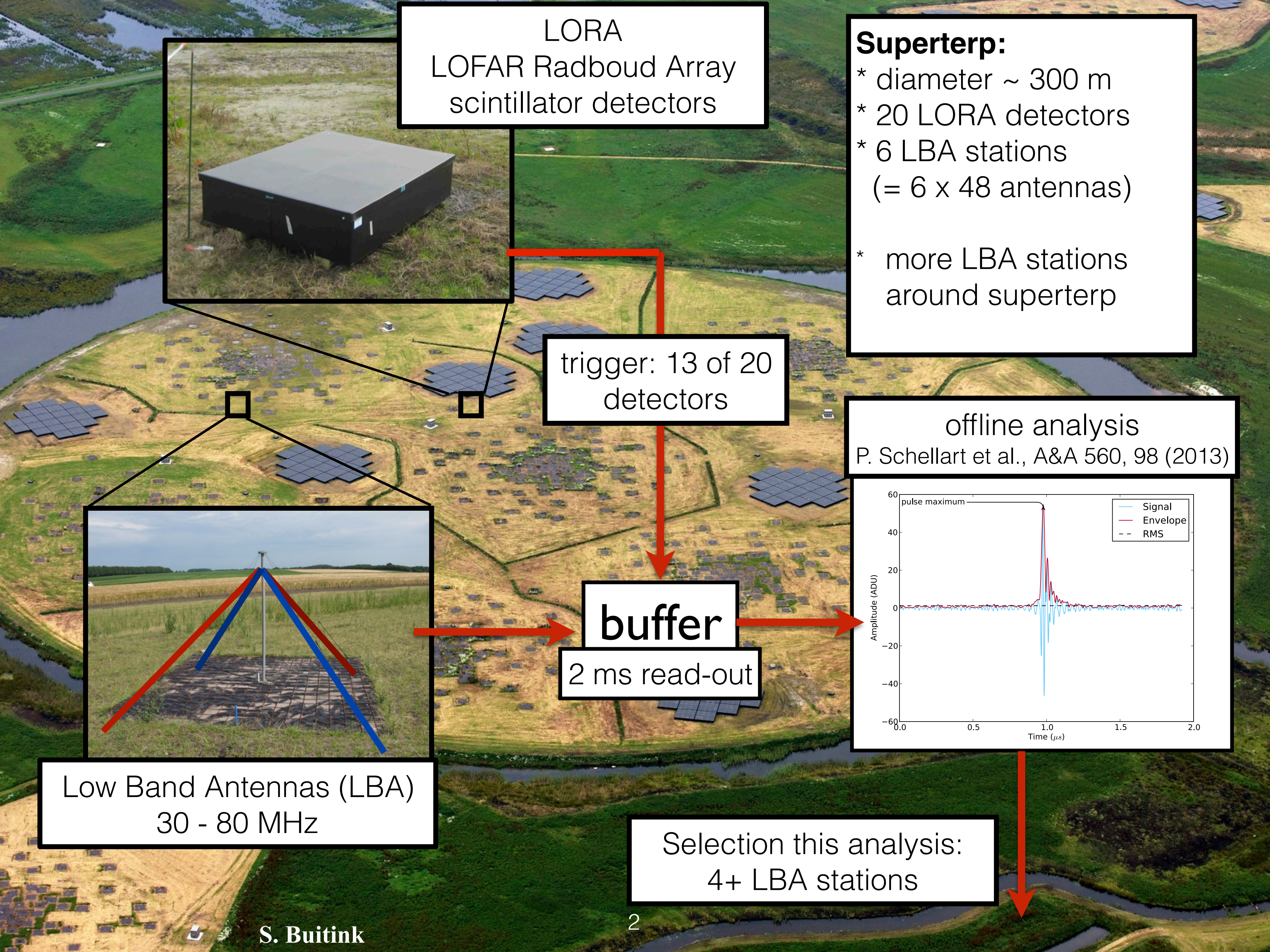
LORA
LOFAR Radboud Array
scintillator detectors
Superterp:
* diameter ~ 300 m
* 20 LORA detectors
* 6 LBA stations
(= 6 x 48 antennas)
* more LBA stations around superterp
trigger: 13 of 20 detectors
offline analysis
P. Schellart et al., A&A 560, 98 (2013)
pulse maximum
Signal
Envelope
RMS
Amplitude (ADU)
Time (μs)
buffer
2 ms read-out
Low Band Antennas (LBA)
30 - 80 MHz
Selection this analysis:
4+ LBA stations

LOFAR core

23 stations ~5 km^2

~150 antennas

~17 km^2

30-80 MHz

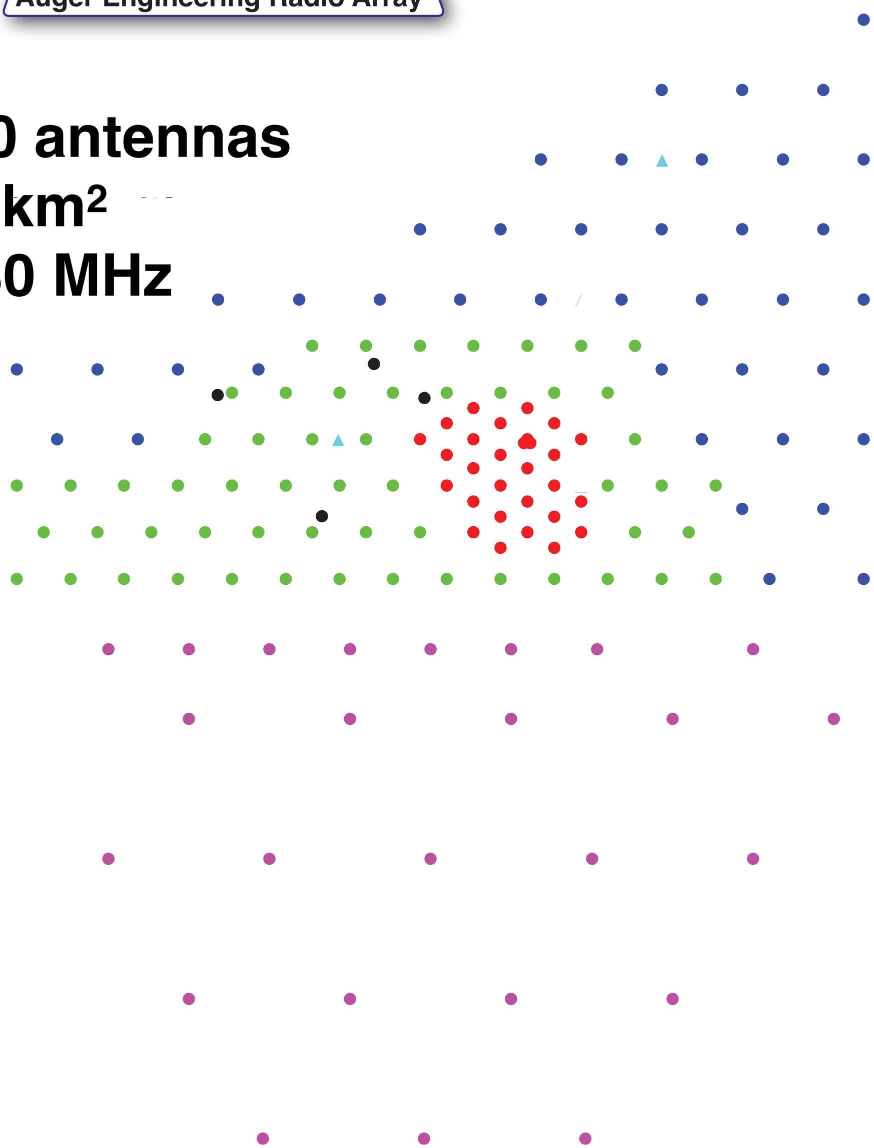

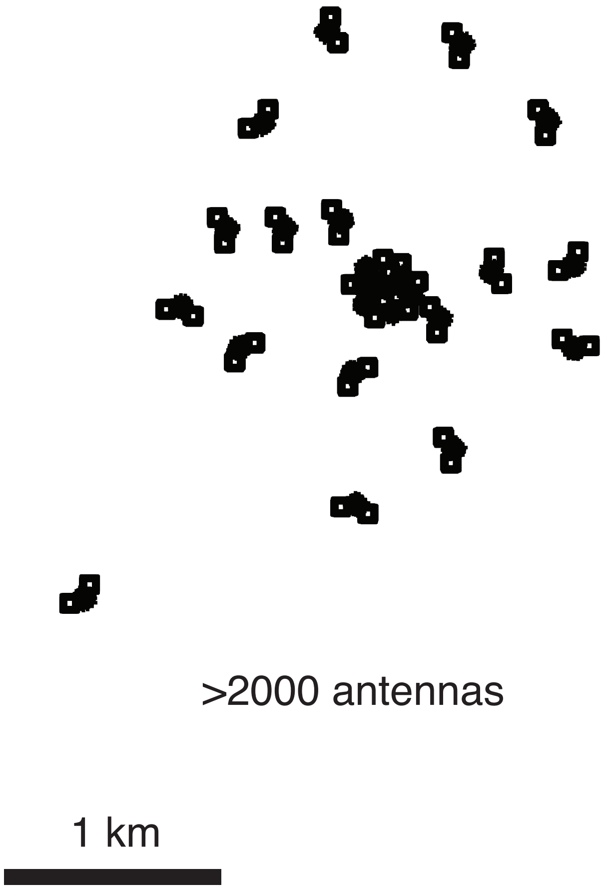

>2000 antennas

PIERRE AUGER

AERA
Auger Engineering Radio Array

~150 antennas
~17 km²
30-80 MHz

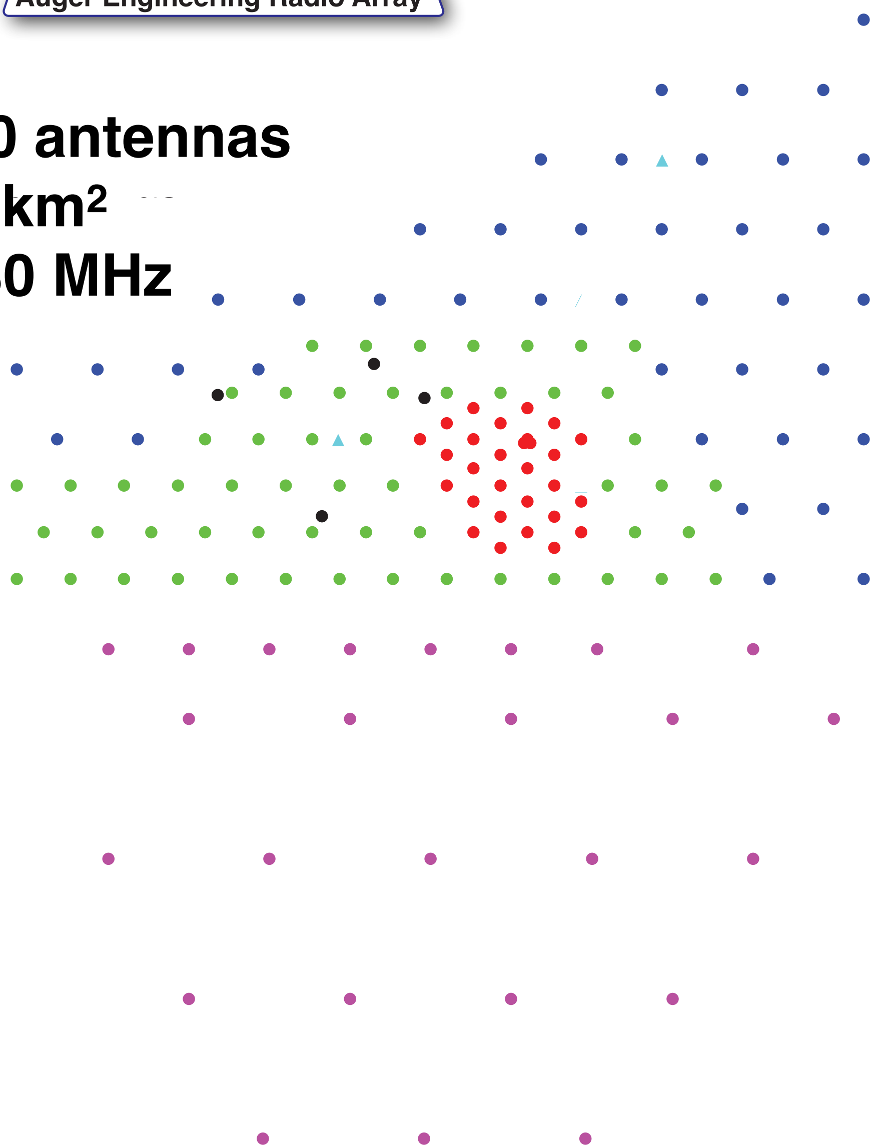

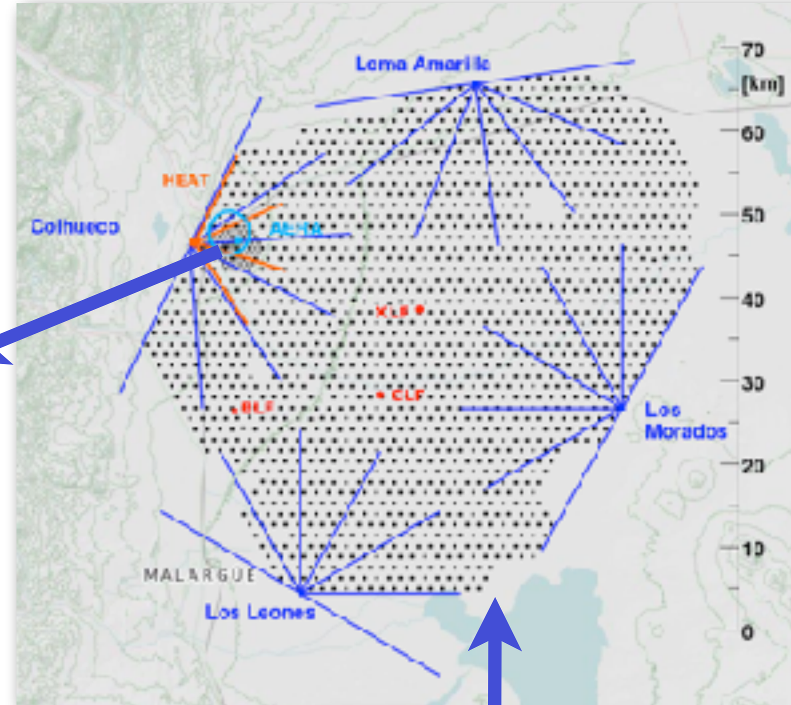

AERA
Auger Engineering Radio Array

~150 antennas
~17 km²
30-80 MHz

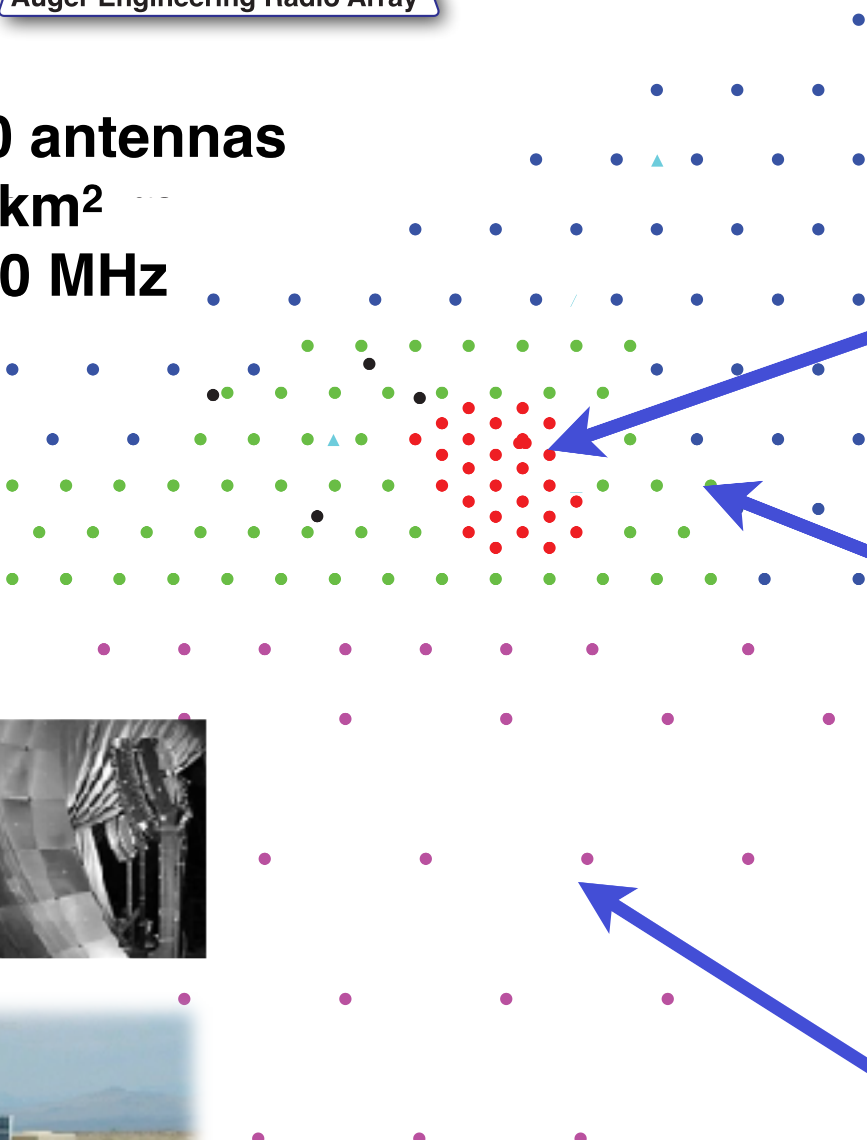

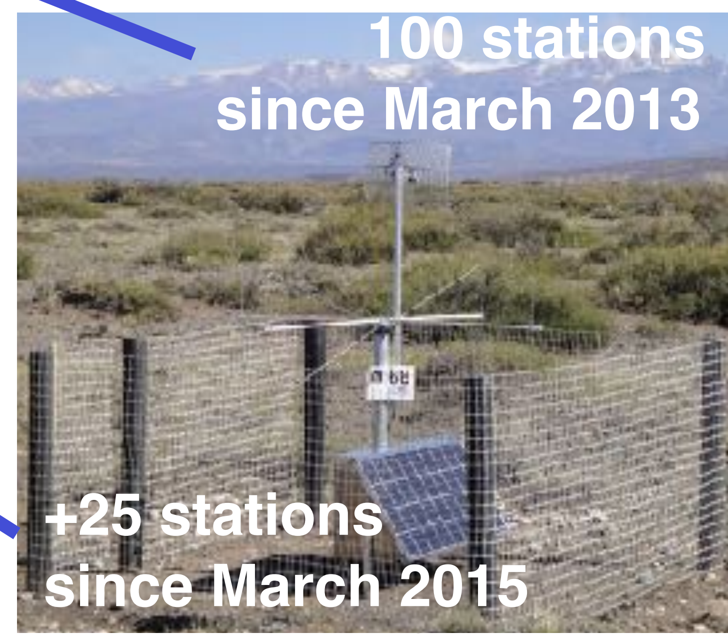

A measured air shower

angular difference particles - radio

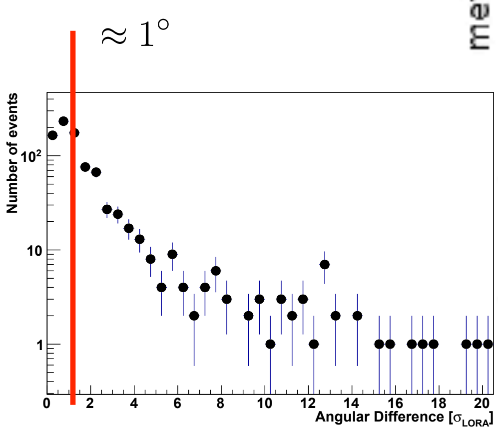

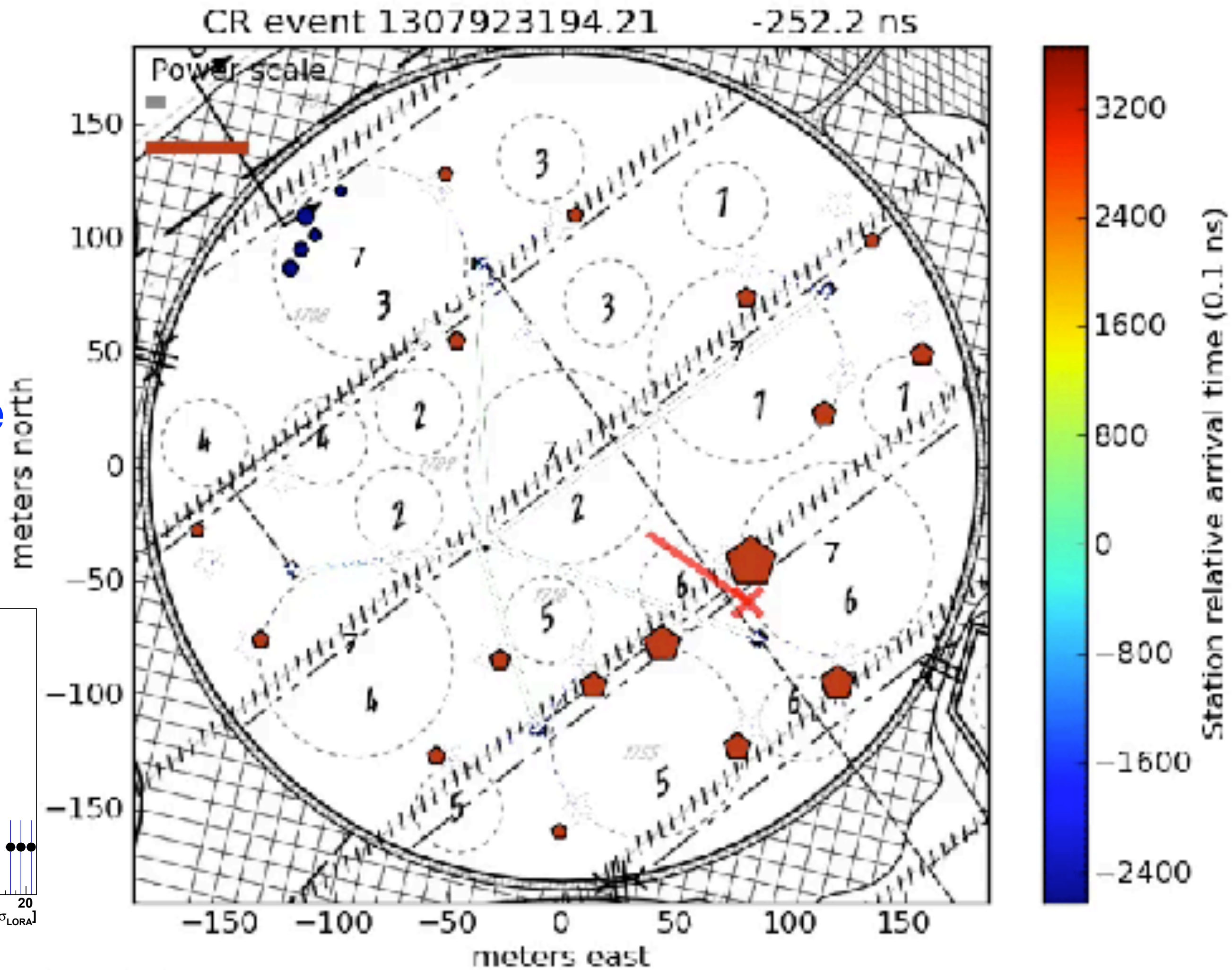

Circles: LOFAR antennas, Pentagons: LORA particle detectors, size denotes signal strength

LOFAR Signal Chain

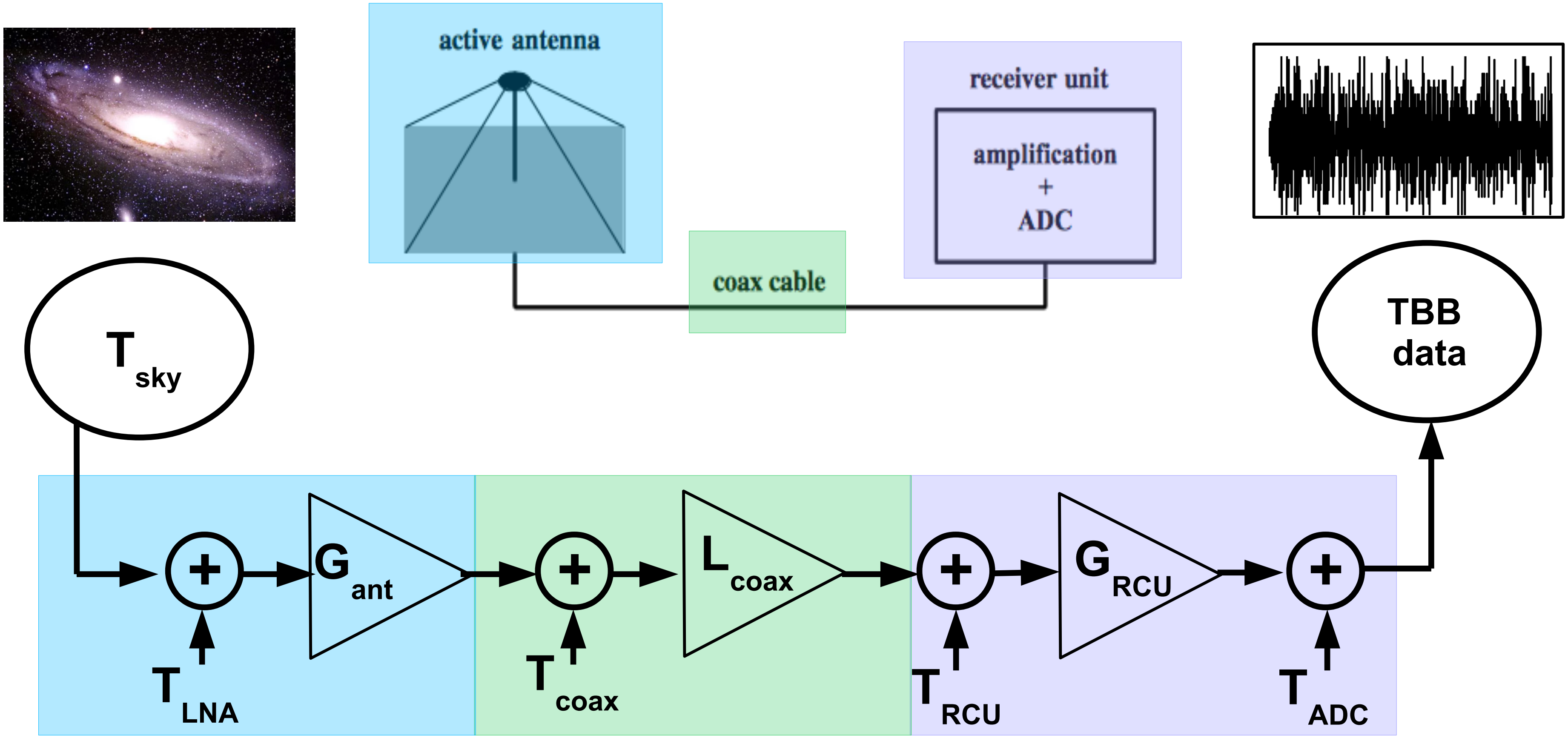

G_{ant} , L_{coax} , G_{RCU} → **Freq. Dependent losses and gains**

T_{LNA} , T_{coax} , T_{RCU} , T_{ADC} → **Constant noise values**

7

K. Mulrey, ARENA 2018

Calibration Results

$$\mathbf{C^2}(\nu) = \mathbf{A}(\nu)\mathbf{L}_{\mathrm{coax}}(\nu)\mathbf{G}_{\mathrm{RCU}}(\nu)\mathbf{S}$$

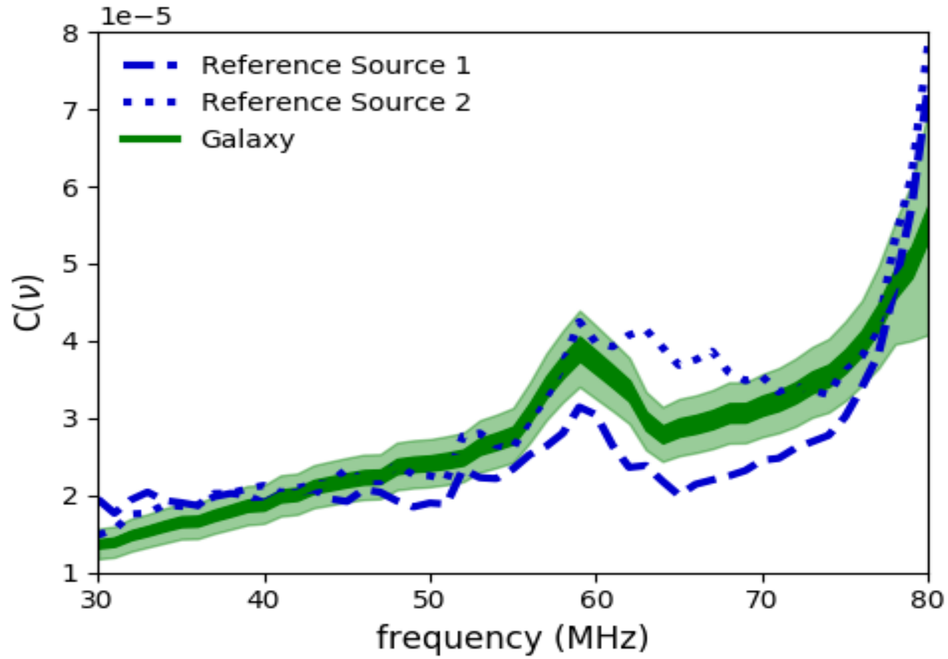

Uncertainty	Percentage
event-to-event fluctuation	4
galaxy model	12
electronic noise < 77 MHz	5-6
electronic noise > 77 MHz	10-20
total < 77 MHz	**14**

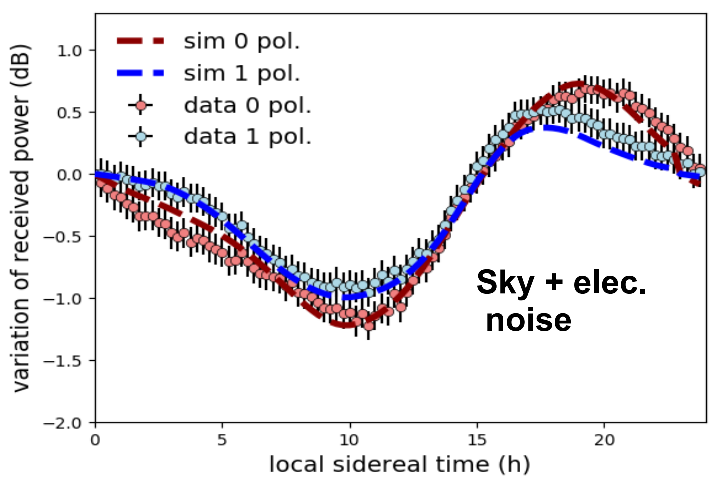

- Galaxy model now limits systematic uncertainties
- Uncertainties from electronic noise are found by comparing resulting calibration constants for different antennas

12

Timing calibration

Use beacon broadcasting at 4 different frequencies to measure relative time shifts

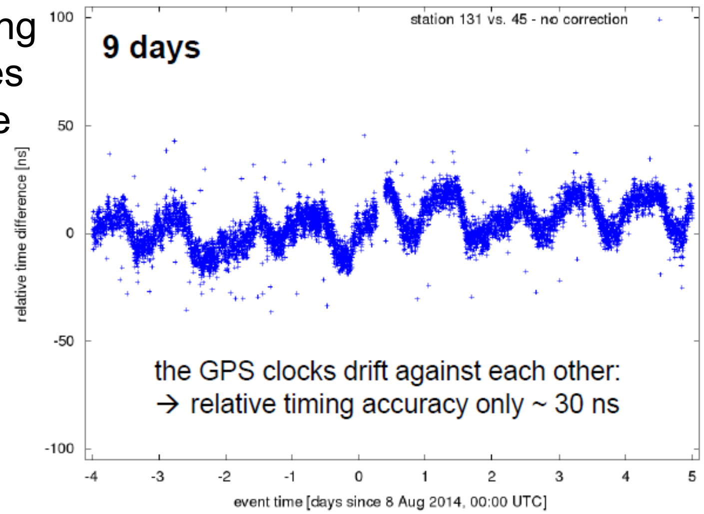

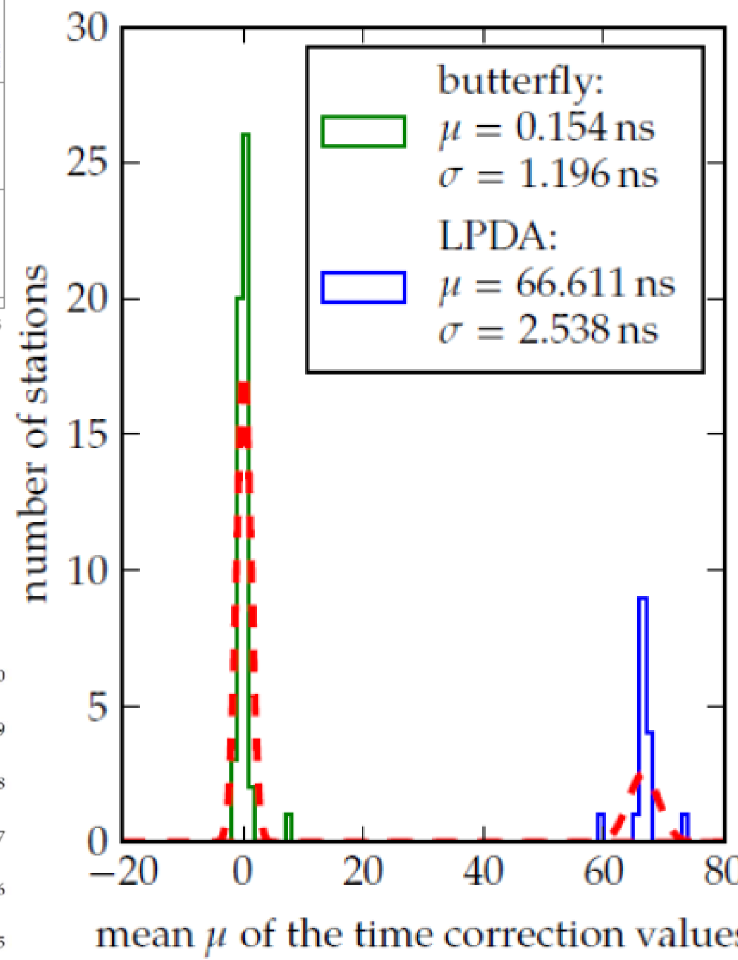

A. Aab et al., JINST 11 (2016) no.01, P01018

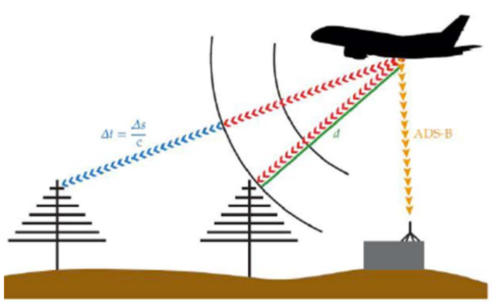

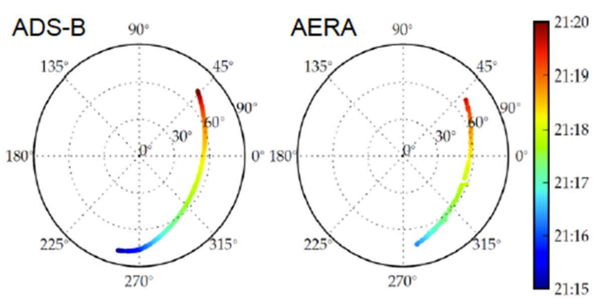

Radiation Processes

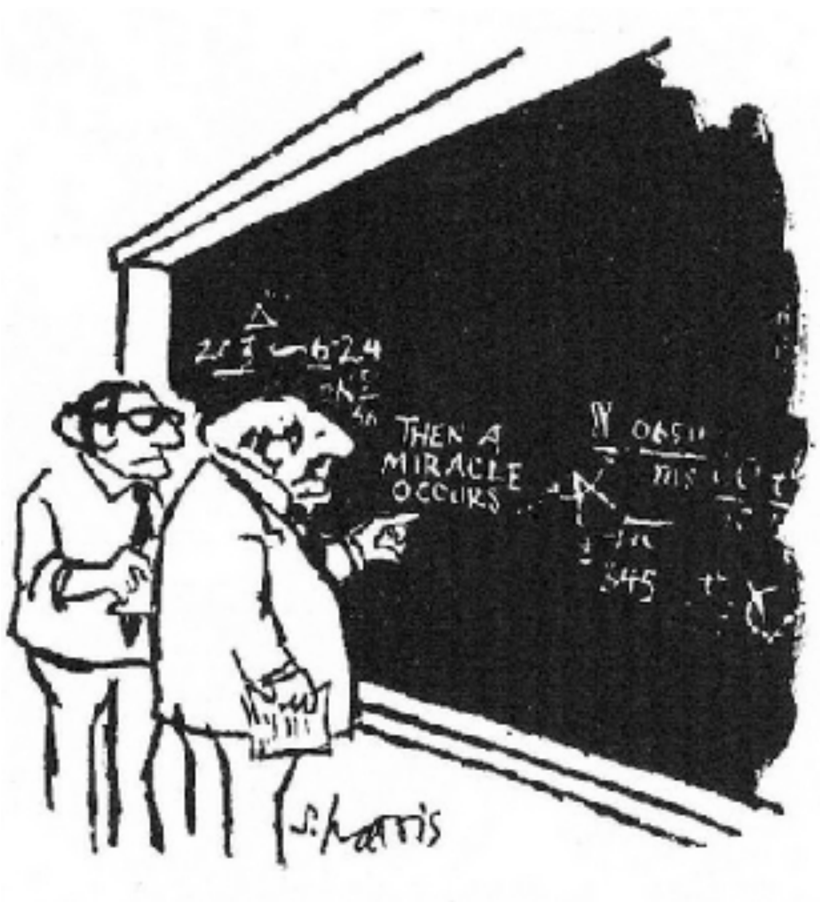

"I think you should be more explicit here in step two."

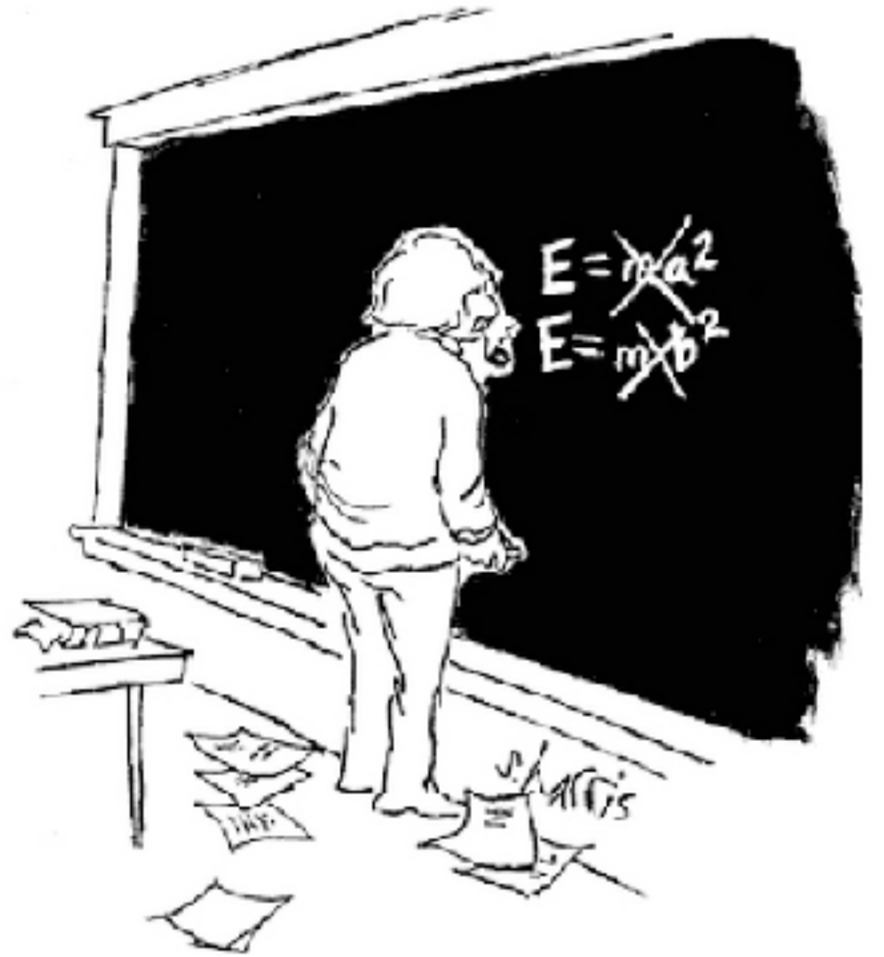

Radio Emission in Air Showers

Mainly: Charge separation in geomagnetic field

$$\vec{E} \propto \vec{v} \times \vec{B}$$

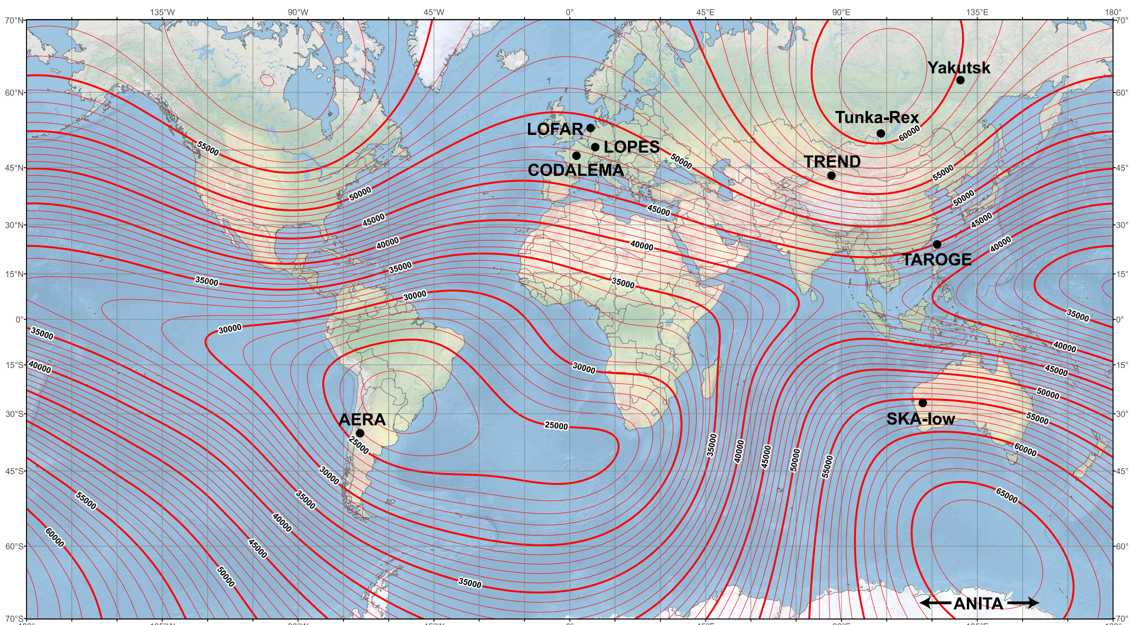

Underlying map (Mercator projection):
Main Geomagnetic Field Total Intensity with contour intervals of 1000 nT according to US/UK World Magnetic Model - Epoch 2015.0
developed by NOAA/NGDC & CIRES http://ngdc.noaa.gov/geomag/WMM
Map reviewed by NGA and BGS Published December 2014
Overlayed: **Location of radio experiments for cosmic-ray air showers** added on underlying map by Frank G. Schröder Karlsruhe Institute of Technology (KIT), Germany

F. Schröder, Prog. Part. Nucl. Phys. 93 (2017) 1

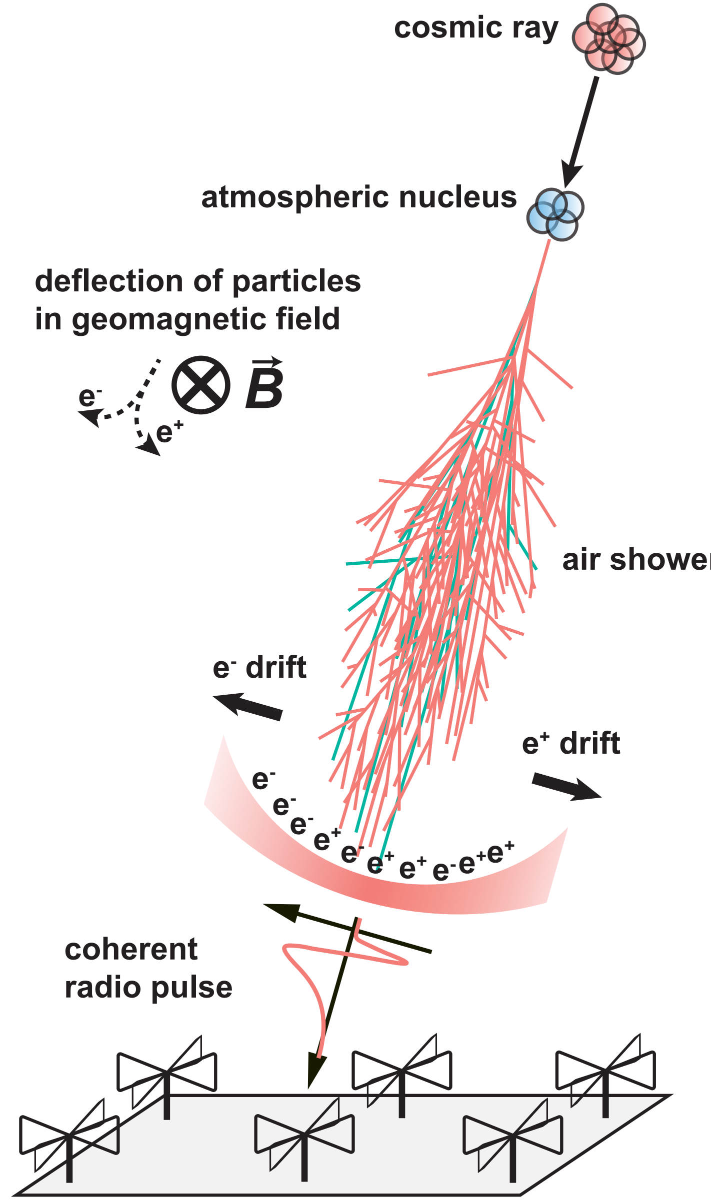

Arrival direction of showers with strong radio signals

north-south asymmetry
v x B effect

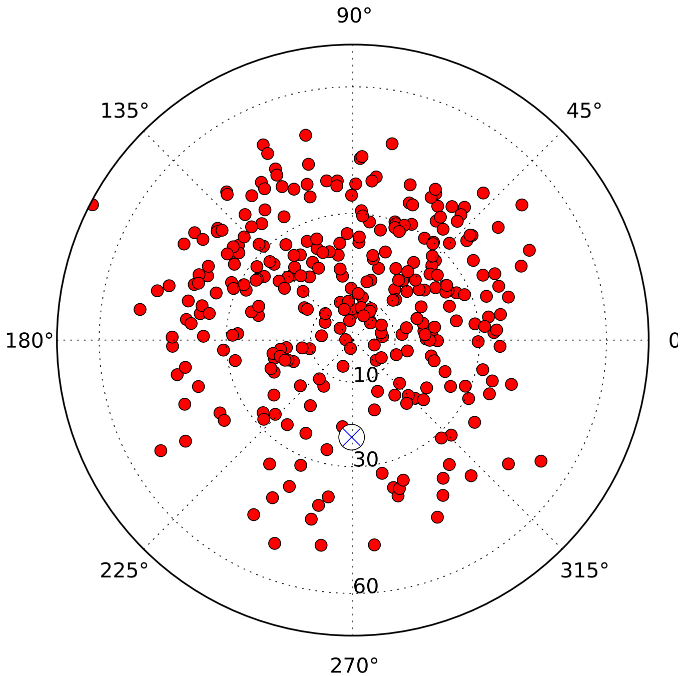

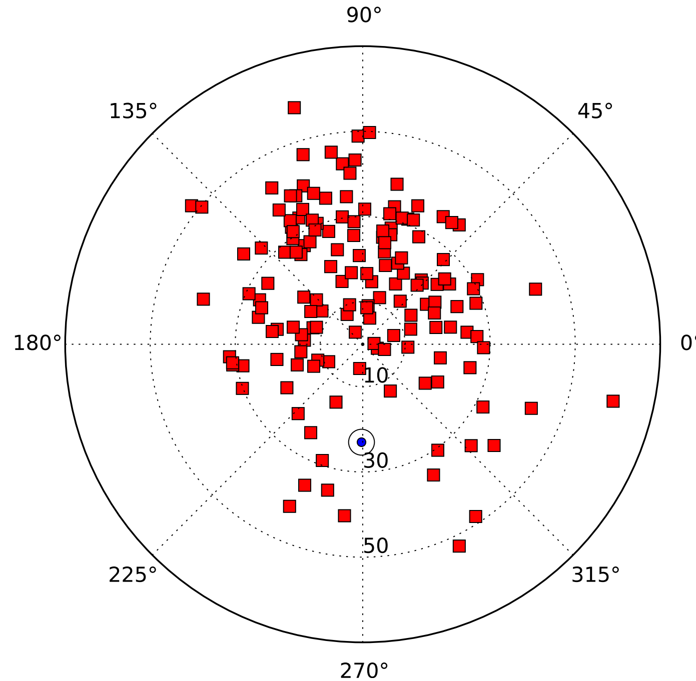

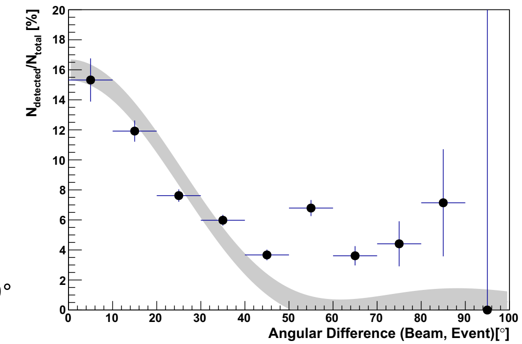

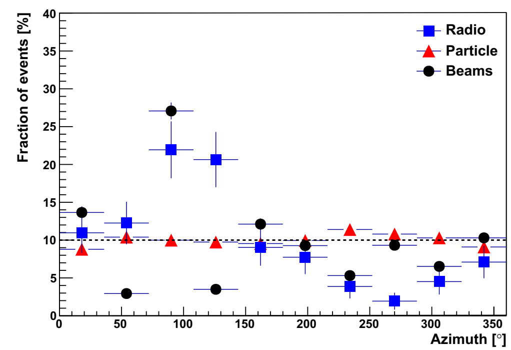

LOFAR

30 - 80 MHz

110 - 190 MHz

A. Nelles et al., Astroparticle Physics 65 (2015) 11

P. Schellart et al., A&A 560 (2013) A98

Arrival direction of showers with strong radio signals

north-south asymmetry
v x B effect

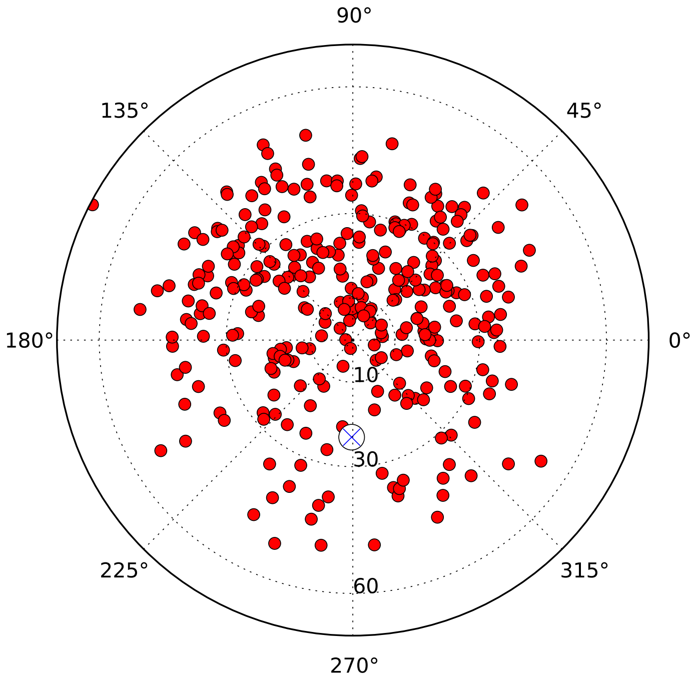

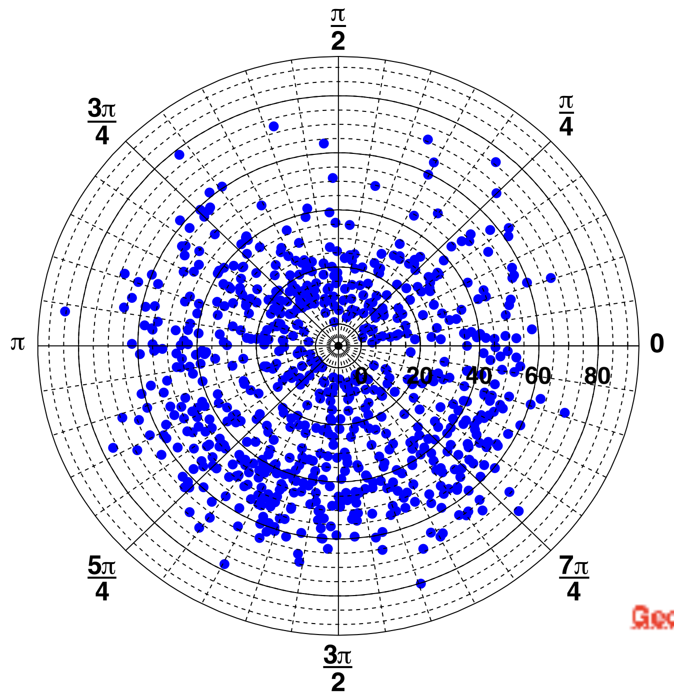

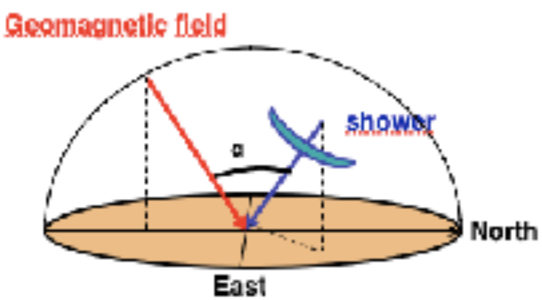

LOFAR

Auger Engineering Radio Array

30 - 80 MHz

P. Schellart et al., A&A 560 (2013) A98

Geomagnetic effect

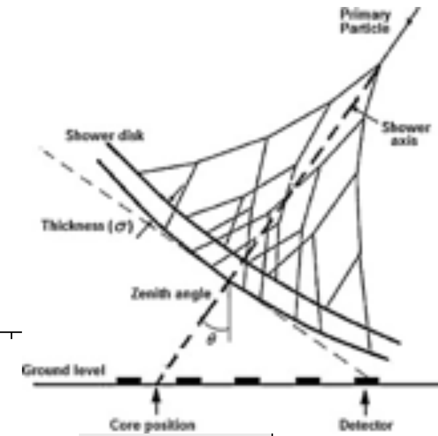

T. Huege / Physics Reports 620 (2016) 1–52

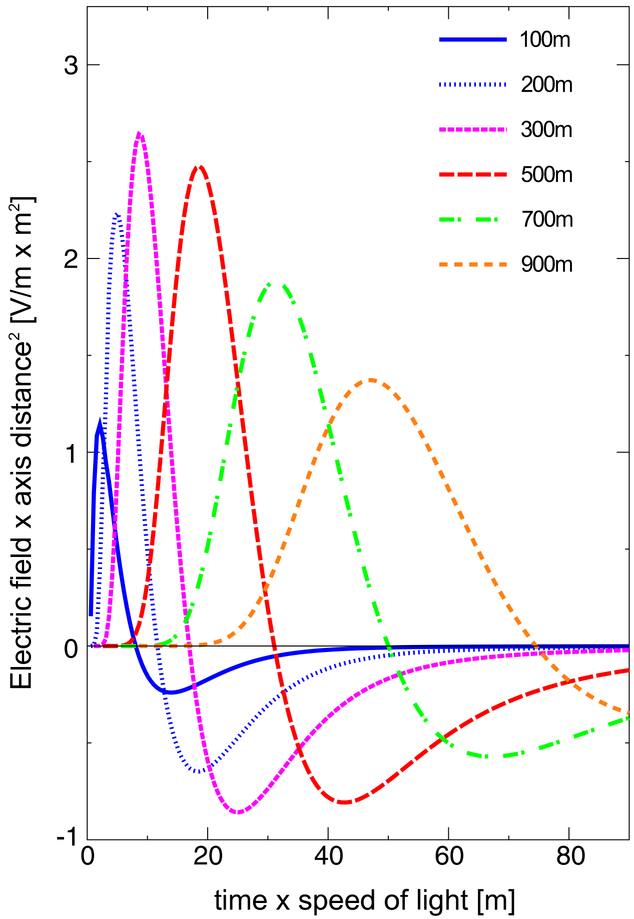

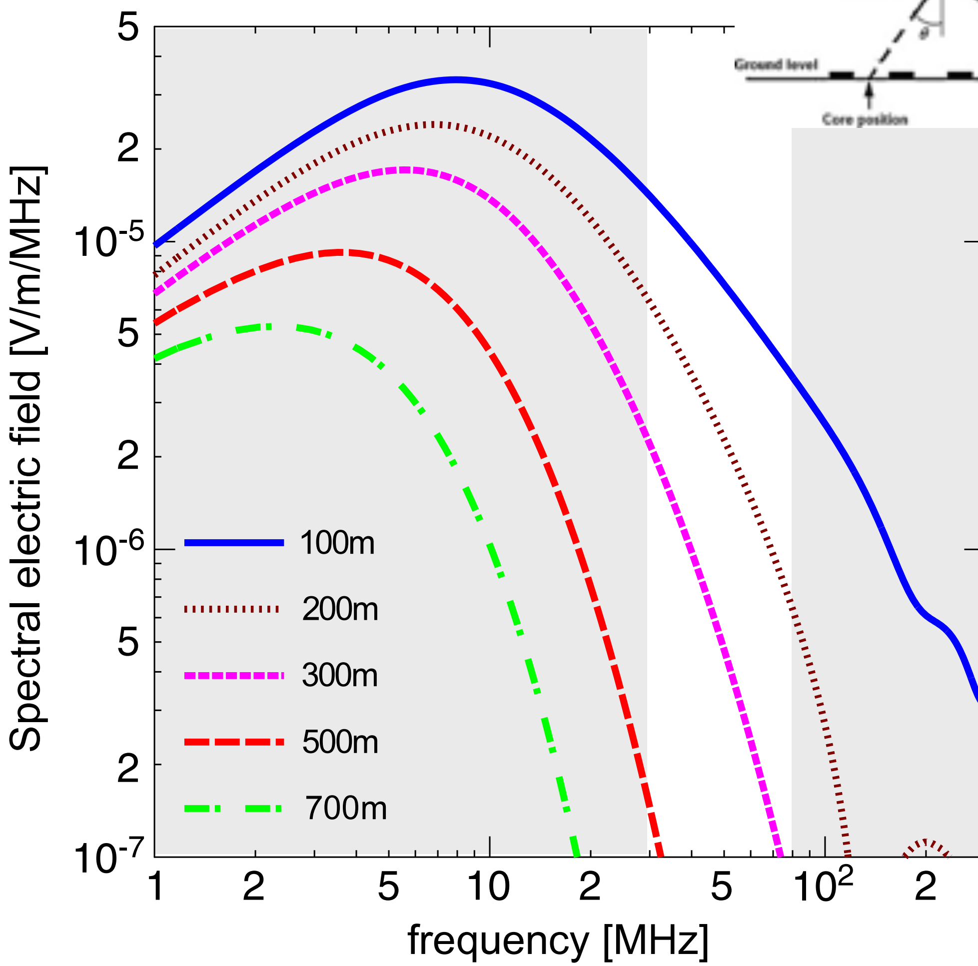

Fig. 4. Radio pulses (top) arising from the time-variation of the geomagnetically induced transverse currents in a 10^{17} eV air shower as observed at various observer distances from the shower axis and their corresponding frequency spectra (bottom). Refractive index effects are not included.
Source: Adapted from [18].

Radio Emission in Air Showers

- **Mainly: Charge separation in geomagnetic field**
  $\vec{E} \propto \vec{v} \times \vec{B}$

Theory predicts additional mechanisms:

- **excess of electrons in shower: charge excess**
- **superposition of emission due to Cherenkov effects in atmosphere**

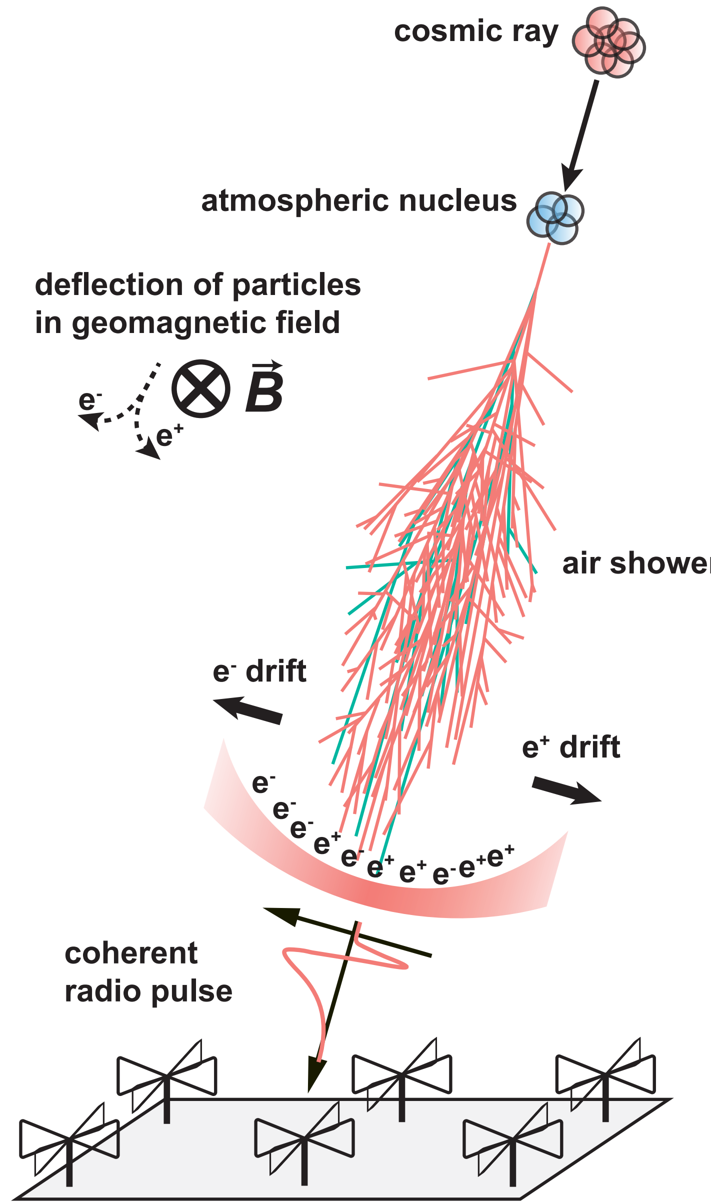

polarization of radio signal

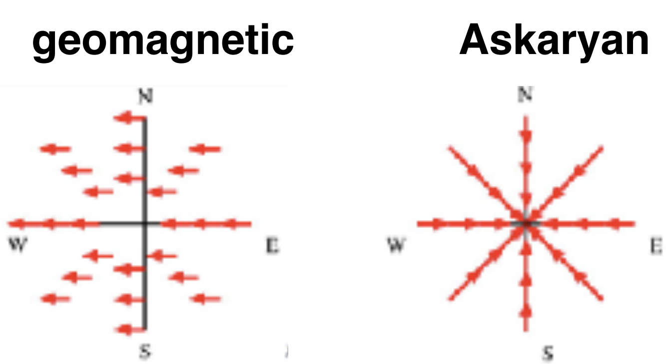

Polarization footprint
of an individual air shower

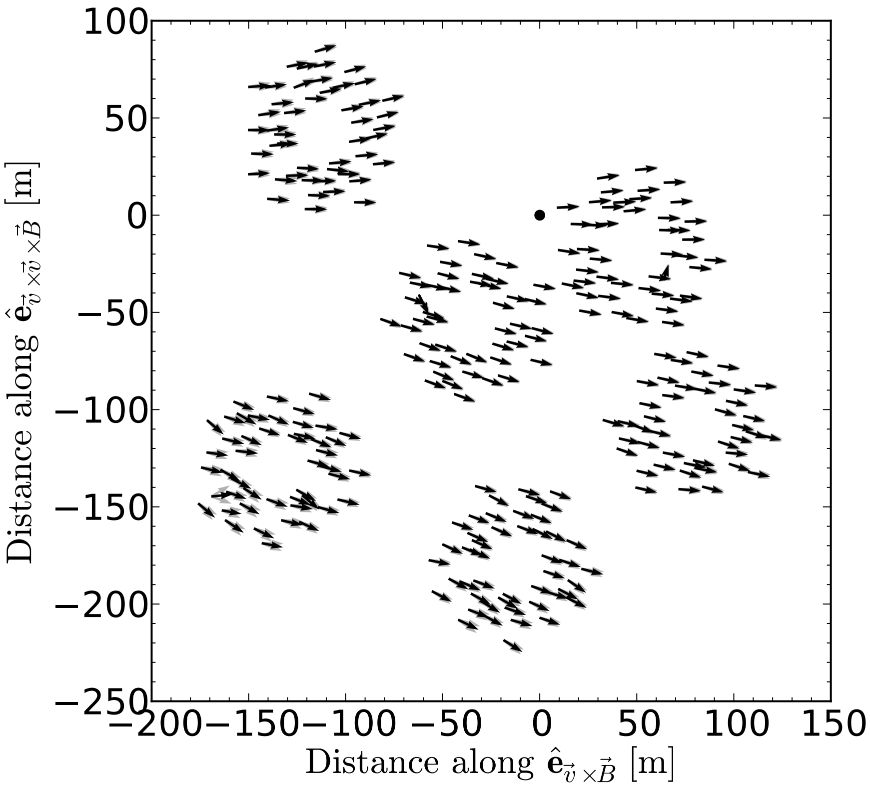

geomagnetic

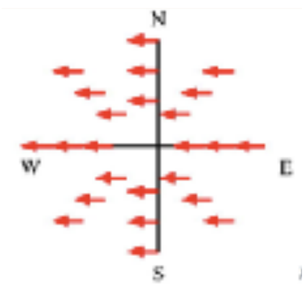

Askaryan

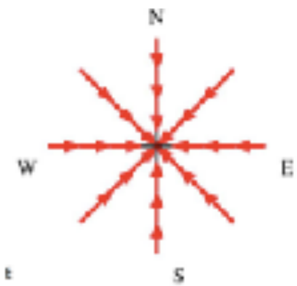

LOFAR

P. Schellart et al., JCAP 10 (2014) 014

Charge excess fraction

$$a = \frac{\text{Askaryan}}{\text{geomagnetic}}$$

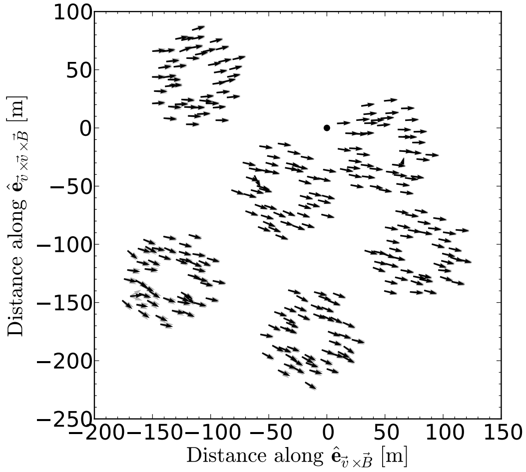

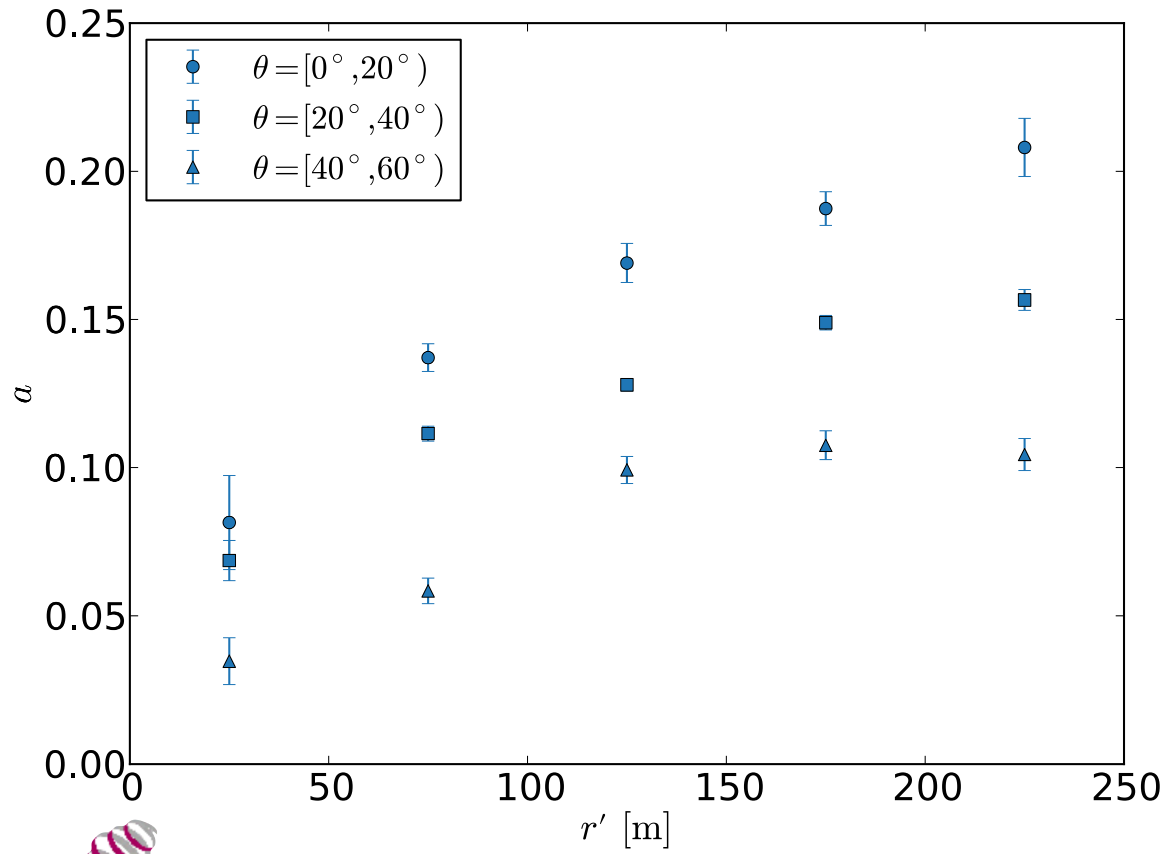

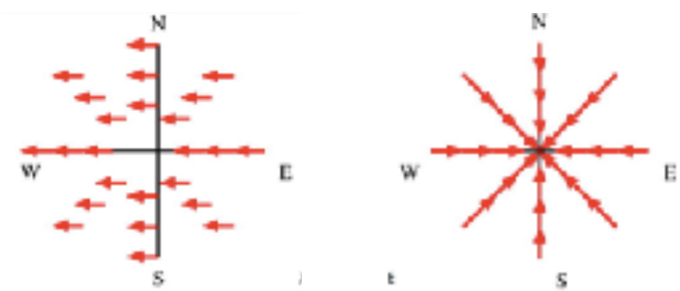

LOFAR

P. Schellart et al., JCAP 10 (2014) 014

Charge excess fraction

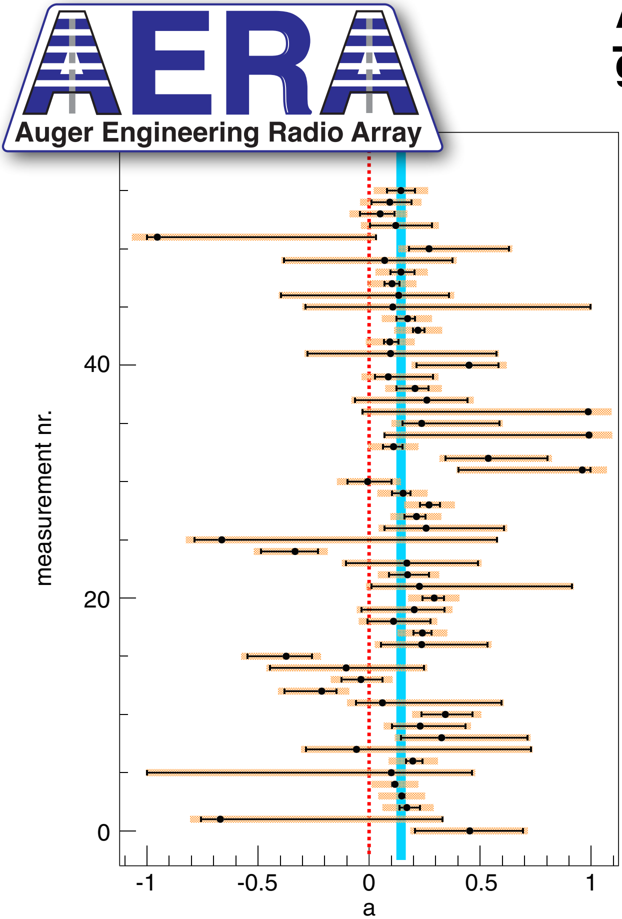

Askaryan
geomagnetic

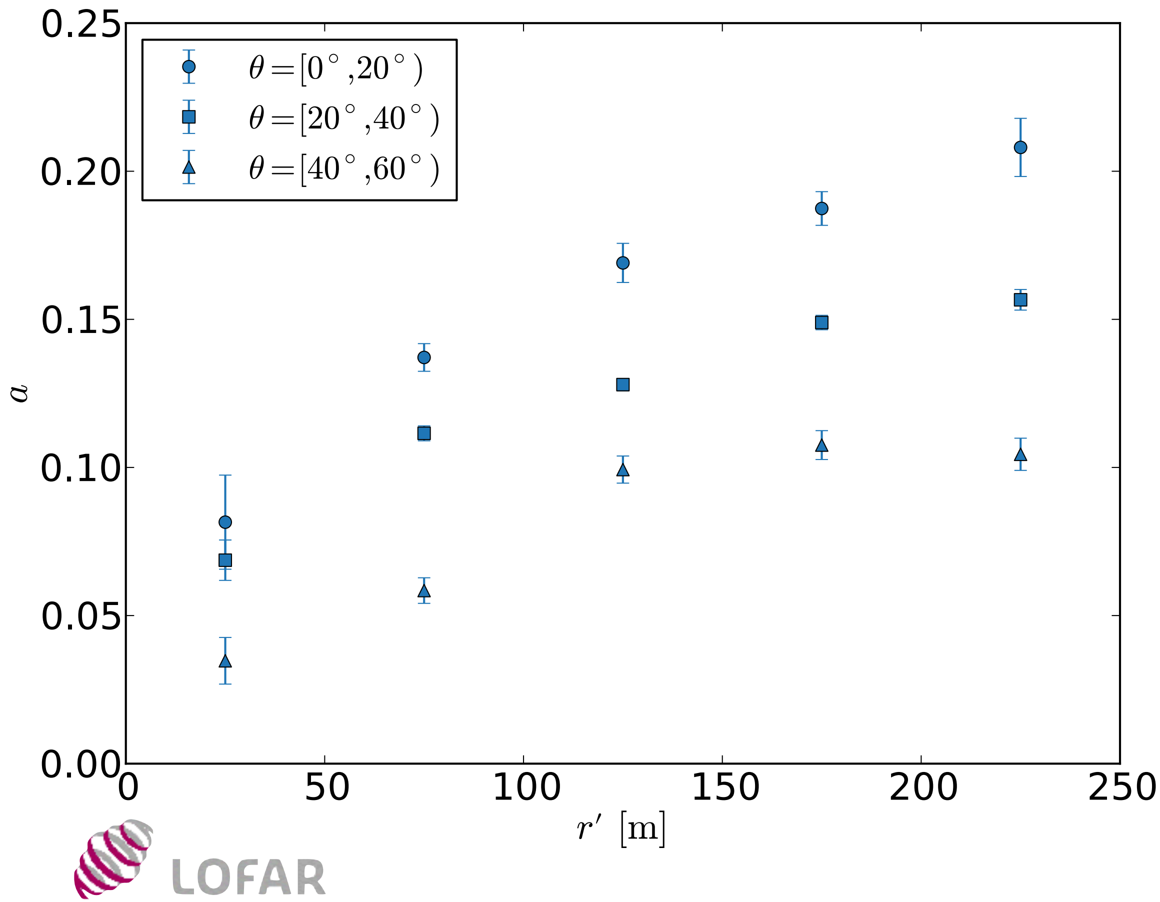

A. Aab, PRD 89 (2014) 052002

P. Schellart et al., JCAP 10 (2014) 014

Footprint of radio emission on the ground

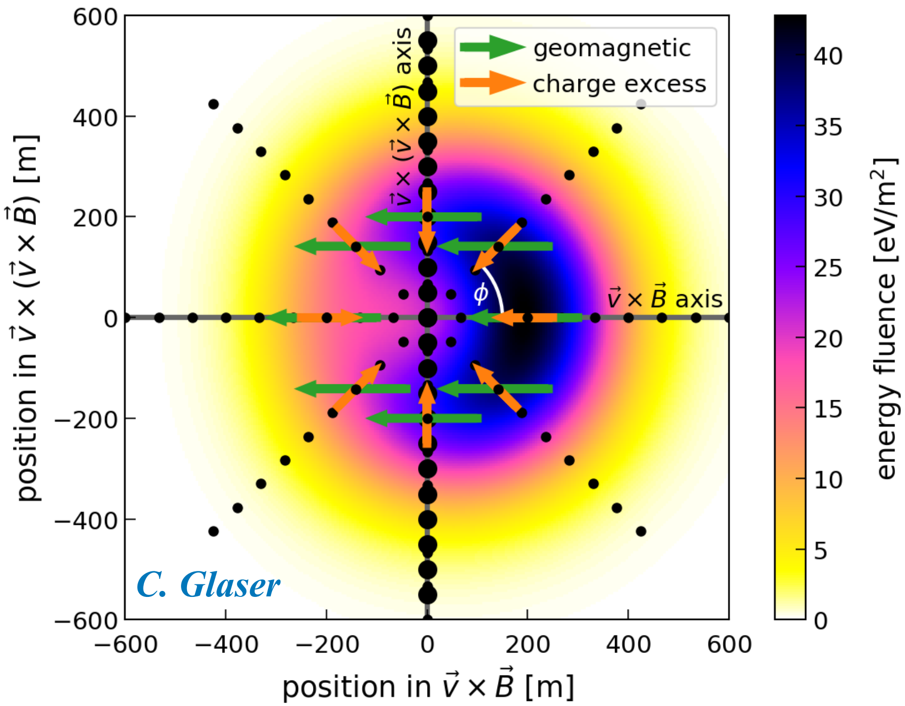

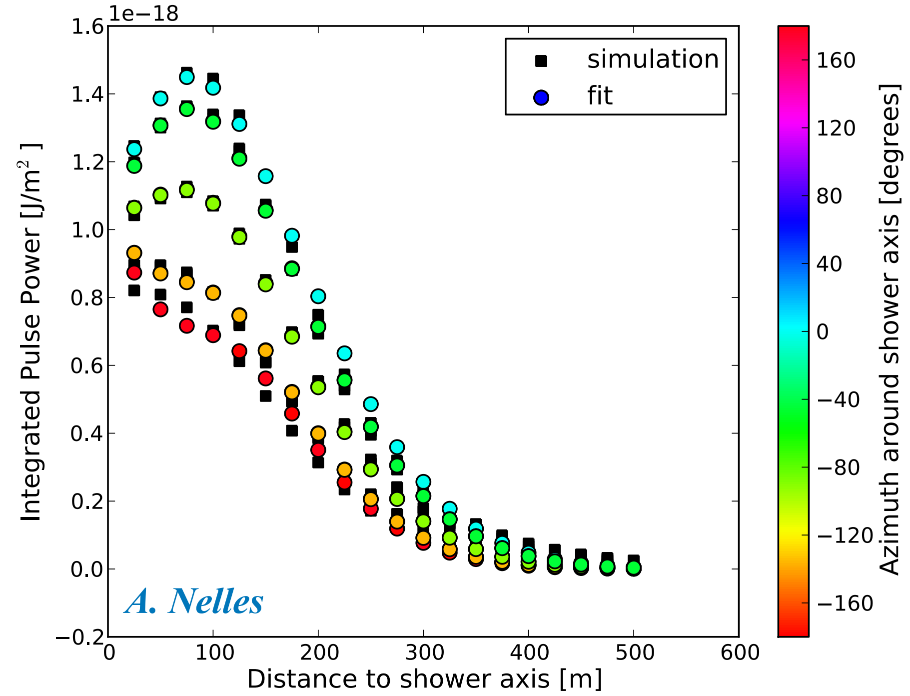

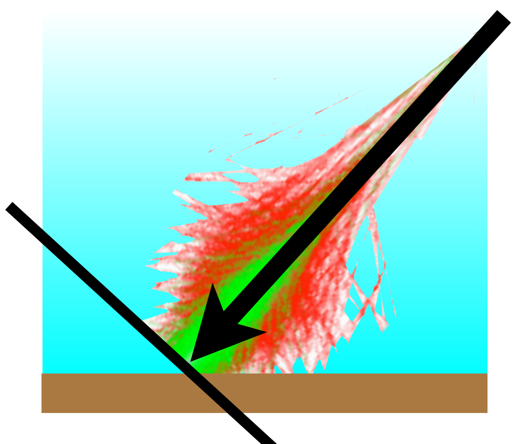

Lateral distribution of radio signals

not rotationally symmetric —> fit two Gaussian functions

v x (v x B)

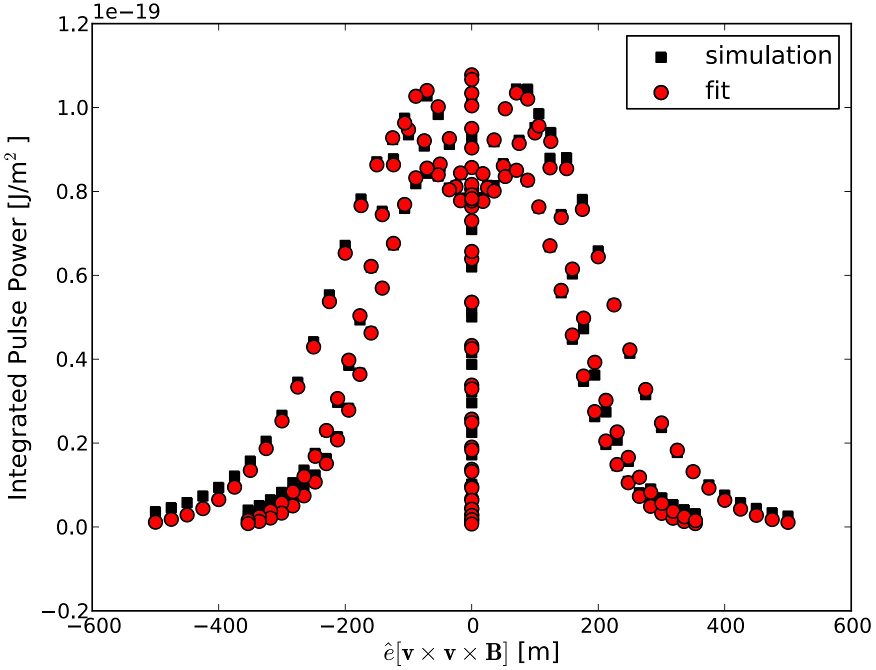

v x B

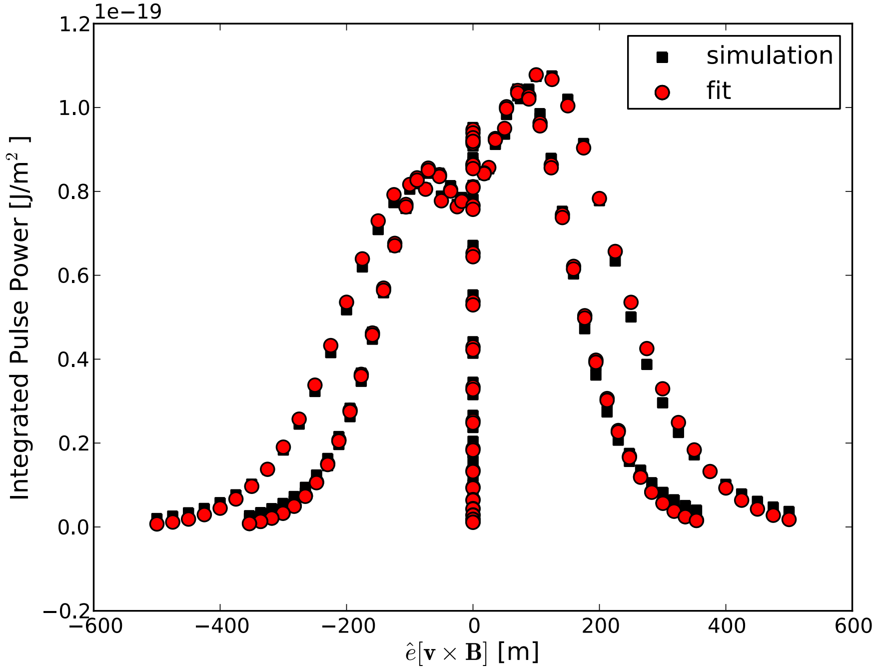

$$P(x',y') = A_+ \cdot \exp\left(\frac{-[(x'-X_+)^2+(y'-Y_+)^2]}{\sigma_+^2}\right) - A_- \cdot \exp\left(\frac{-[(x'-X_-)^2+(y'-Y_-)^2]}{\sigma_-^2}\right) + O$$

A. Nelles et al., Astropart. Phys. 60 (2015) 13

Properties of incoming cosmic ray

- direction
- energy
- type

Direction

Shape of Shower Front

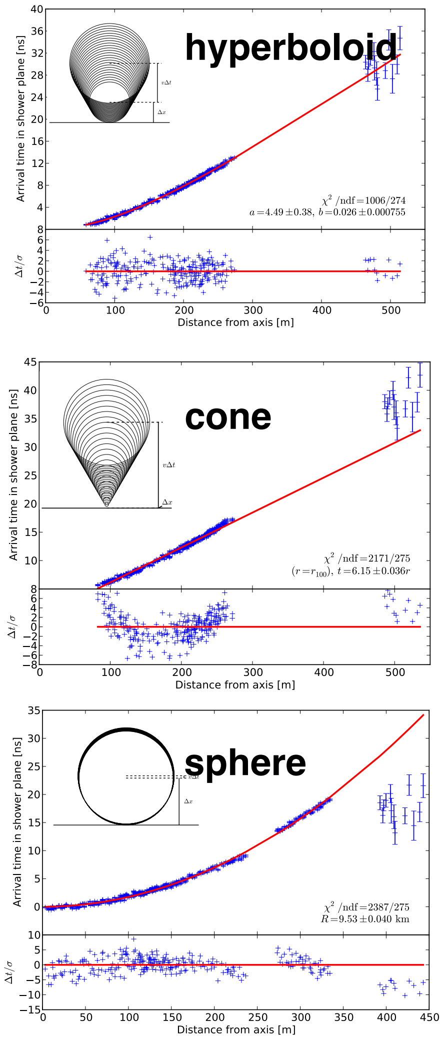

fit quality

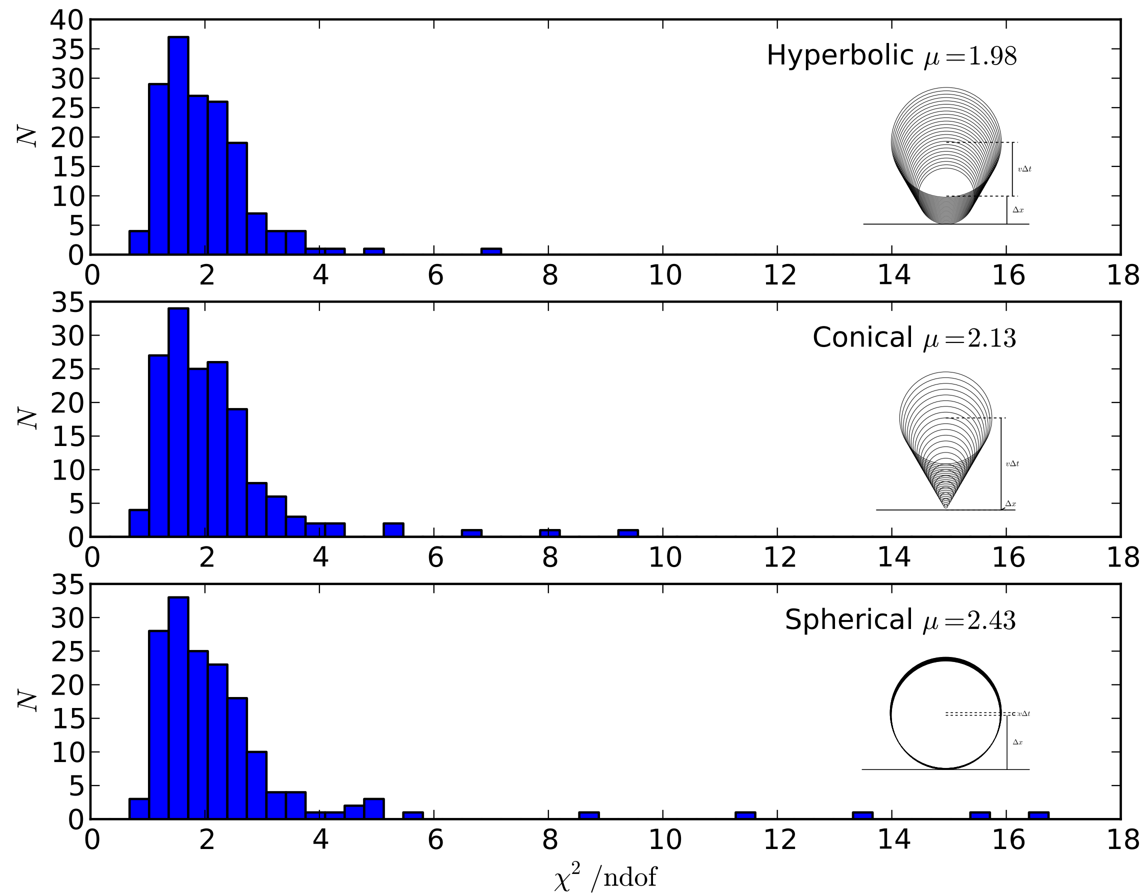

A. Corstanje et al., Astropart. Phys. 61 (2015) 22

Shape of Shower Front

LOFAR

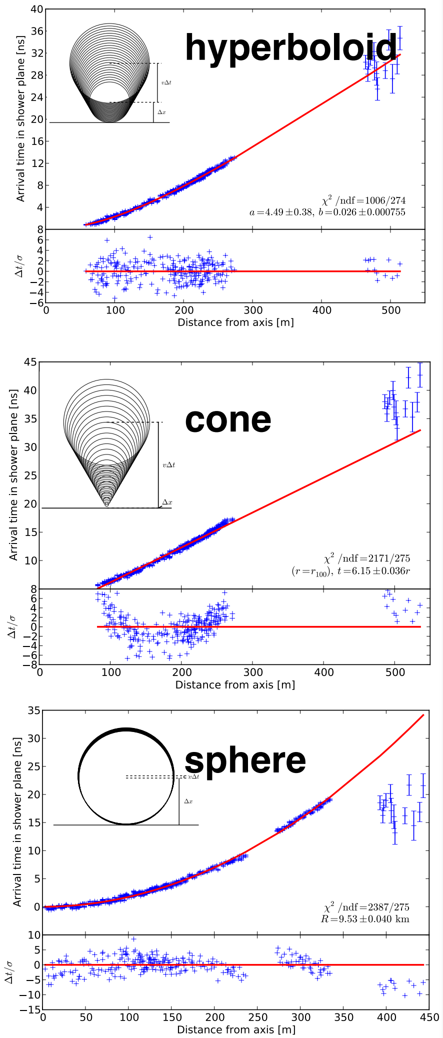

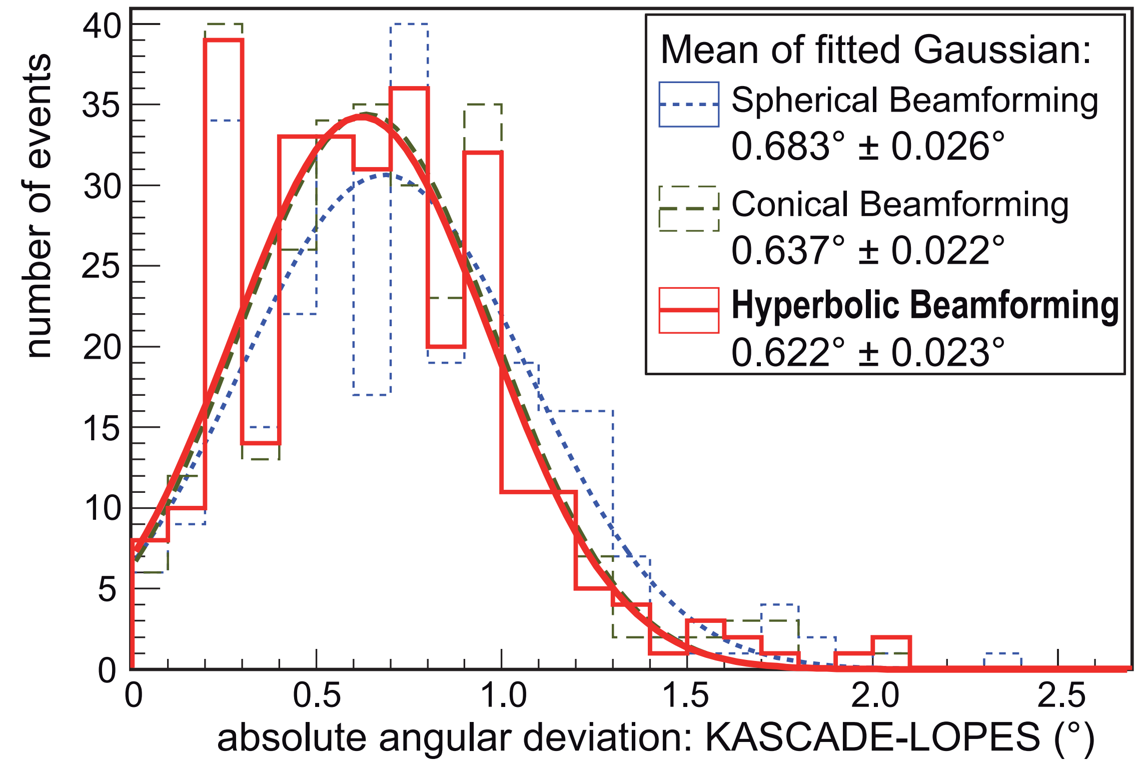

W.D. Apel et al., JCAP 1409 (2014) no.09, 025

A. Corstanje et al., Astropart. Phys. 61 (2015) 22

Accuracy of Shower Direction

angular difference between..

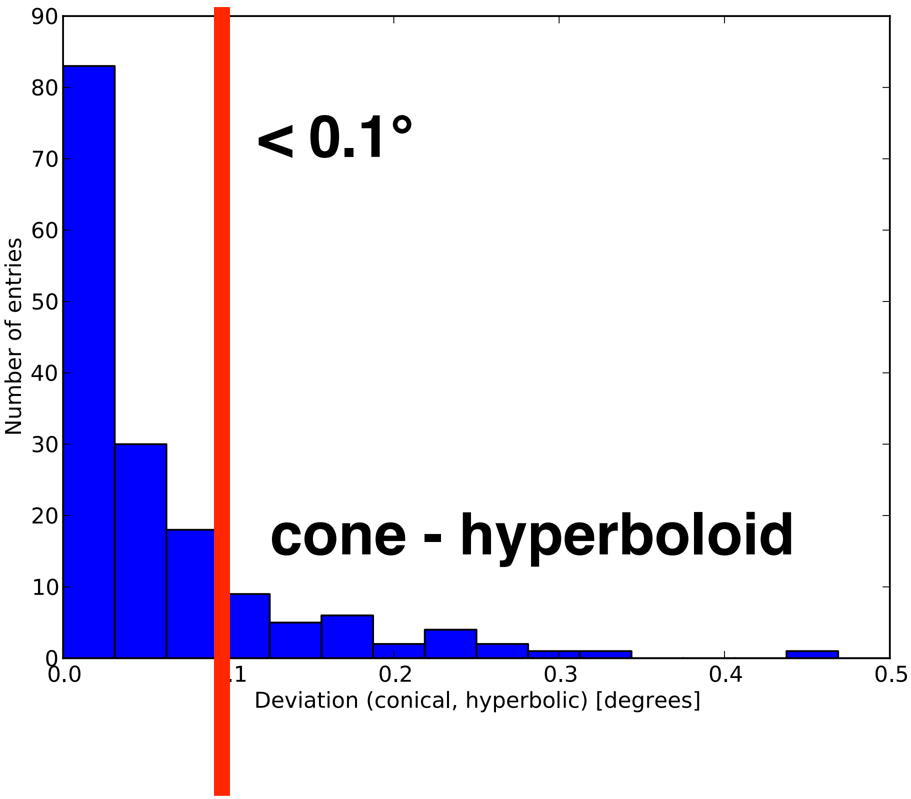

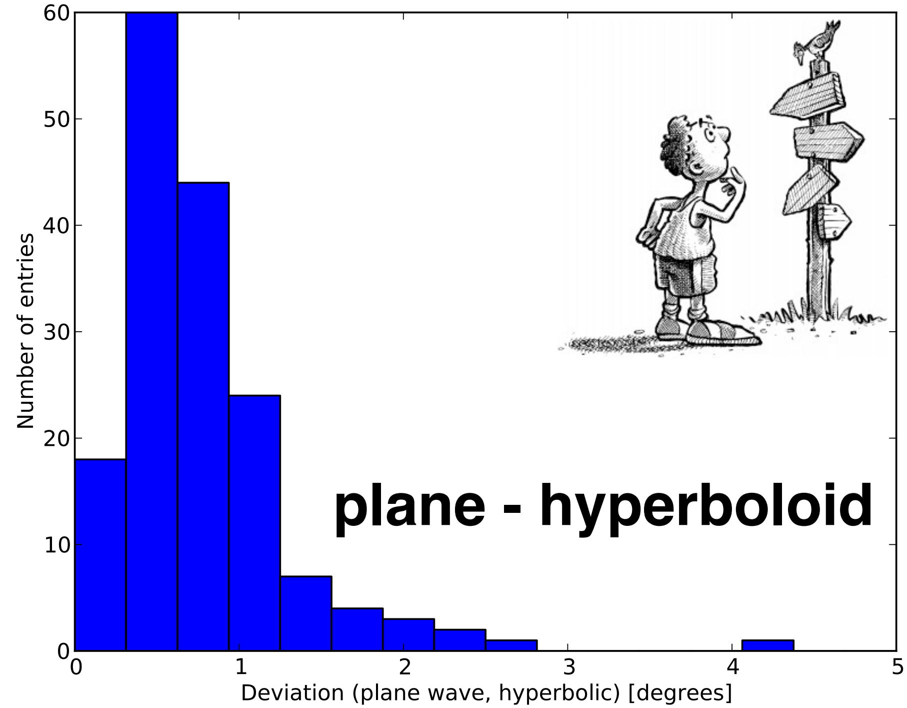

LOFAR

A. Corstanje et al., Astropart. Phys. 61 (2015) 22

Energy

Energy of primary particle

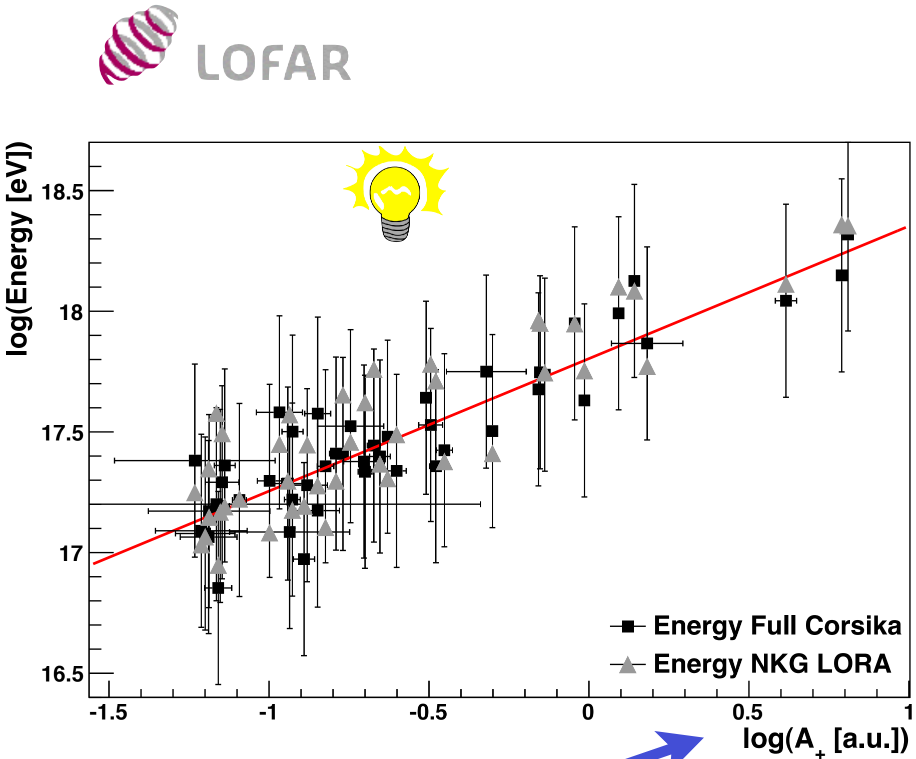

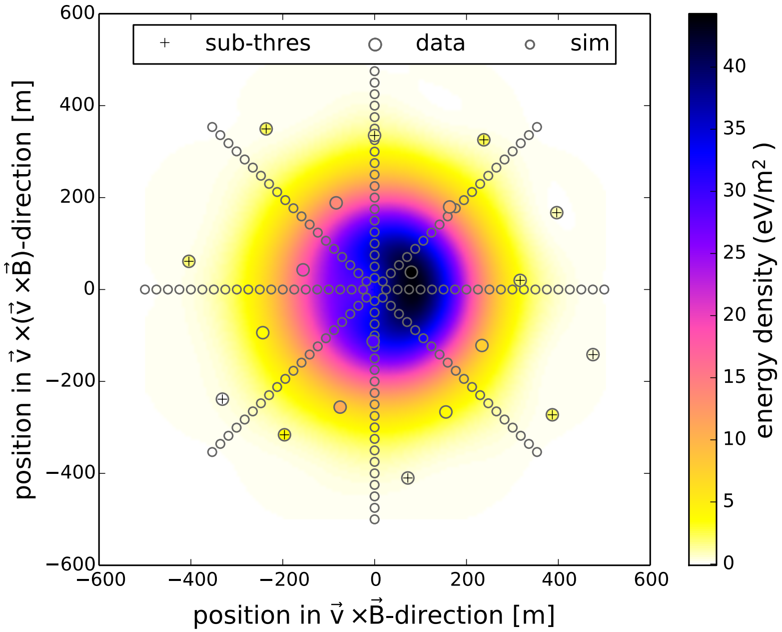

$$P(x', y') = A_+ \cdot \exp\left(\frac{-[(x' - X_+)^2 + (y' - Y_+)^2]}{\sigma_+^2}\right) - A_- \cdot \exp\left(\frac{-[(x' - X_-)^2 + (y' - Y_-)^2]}{\sigma_-^2}\right) + O$$

A. Nelles et al., JCAP 05 (2015) 018

Measurement of the Radiation Energy in the Radio Signal of Extensive Air Showers as a Universal Estimator of Cosmic-Ray Energy

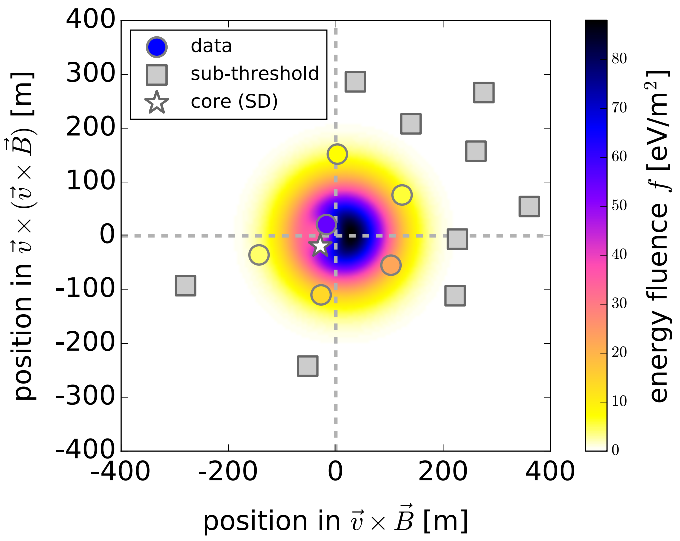

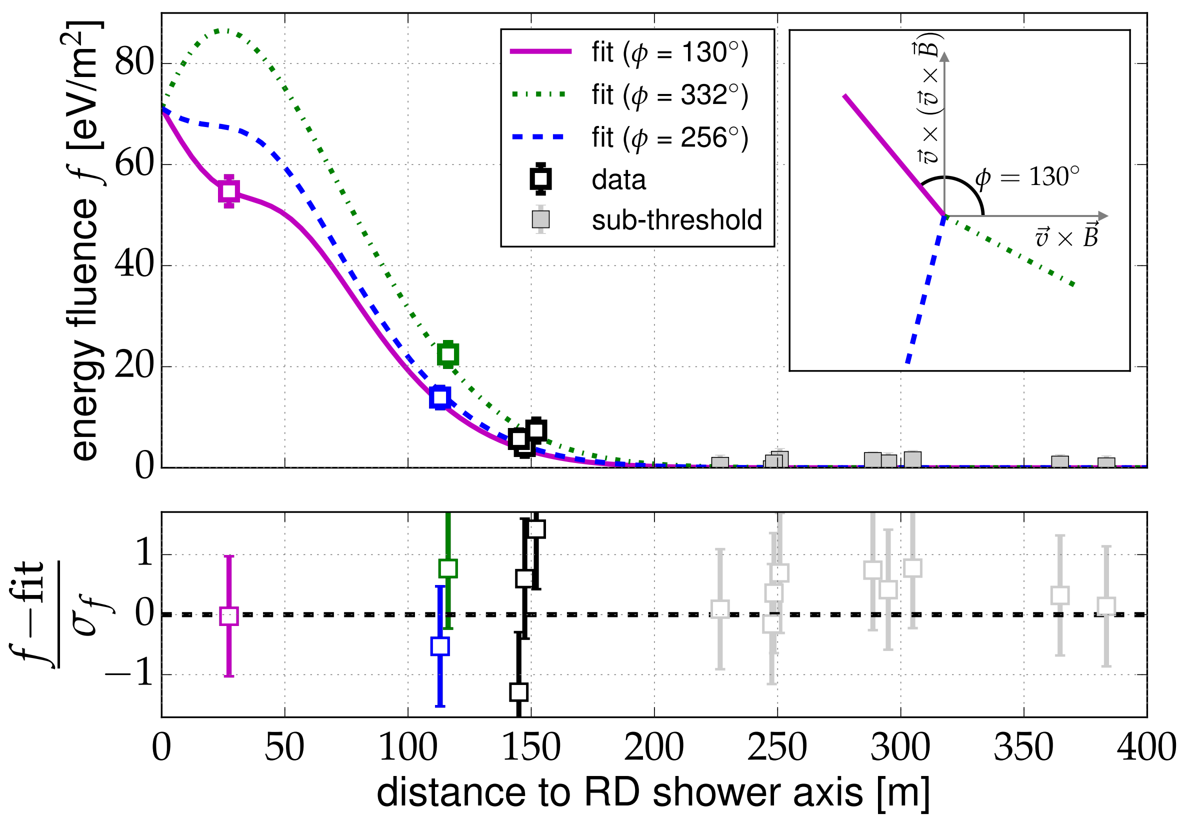

A. Aab et al., PRL 116 (2016) no.24, 241101

Measurement of the Radiation Energy in the Radio Signal of Extensive Air Showers as a Universal Estimator of Cosmic-Ray Energy

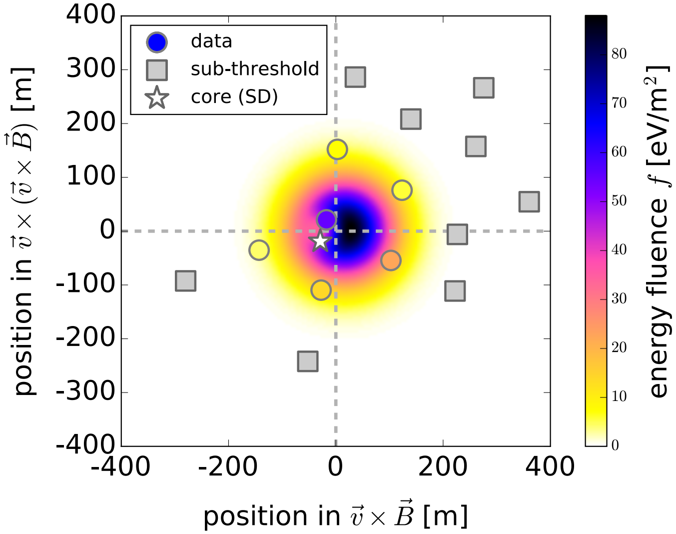

$E_{30\text{-}80}$ MHz = 15.8 MeV @ 10^{18} eV

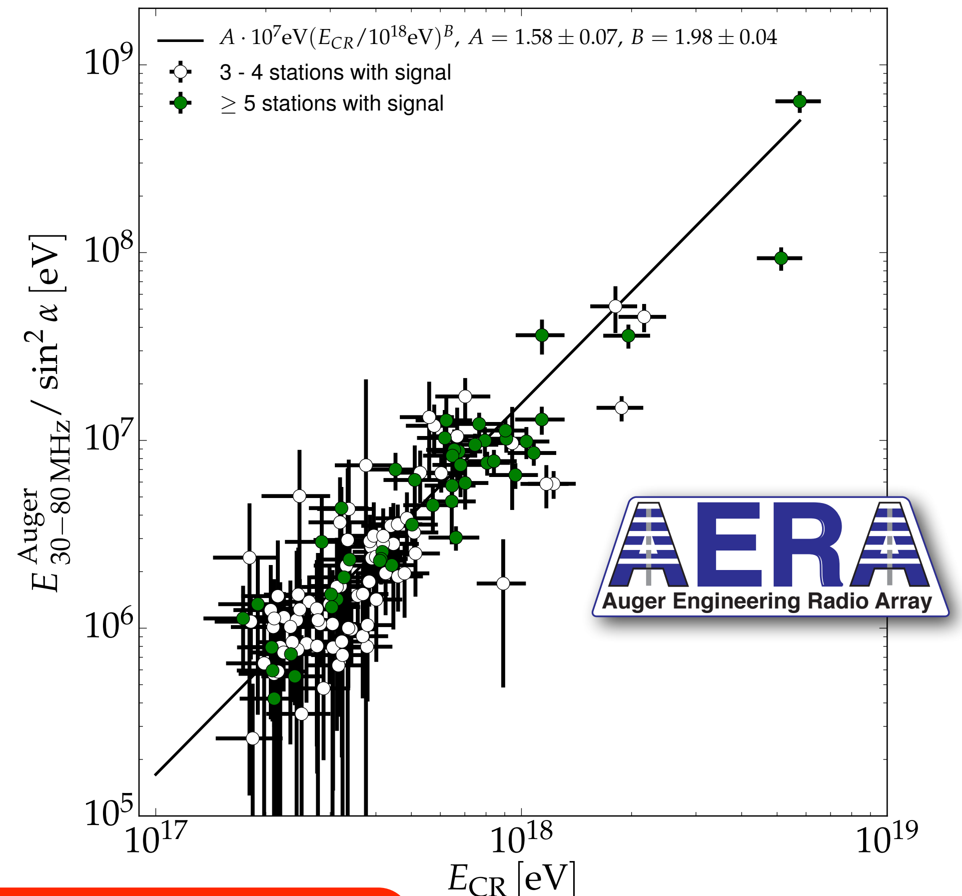

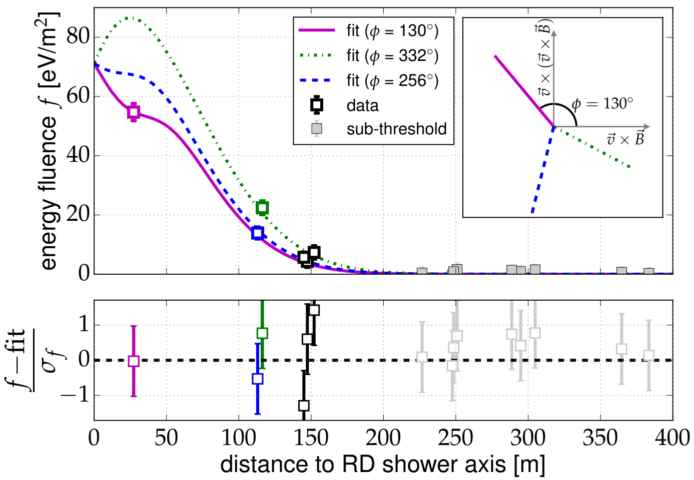

$$E_{30\text{-}80\ \text{MHz}} = (15.8 \pm 0.7(\text{stat}) \pm 6.7(\text{syst})\ \text{MeV}) \times \left(\sin\alpha \frac{E_{CR}}{10^{18}\ \text{eV}} \frac{B_{Earth}}{0.24\ \text{G}}\right)^2$$

A. Aab et al., PRL 116 (2016) no.24, 241101

Energy Estimation of Cosmic Rays with the Engineering Radio Array of the Pierre Auger Observatory

$E_{30\text{-}80}$ MHz = 15.8 MeV @ 10^{18} eV

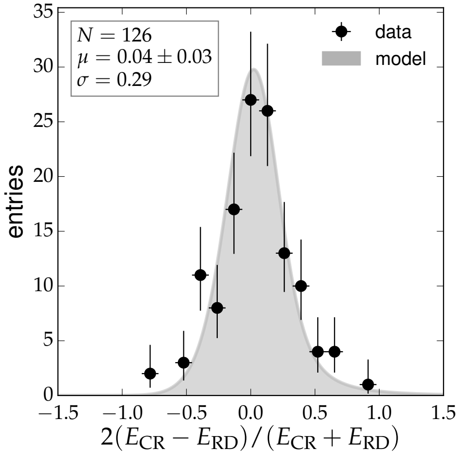

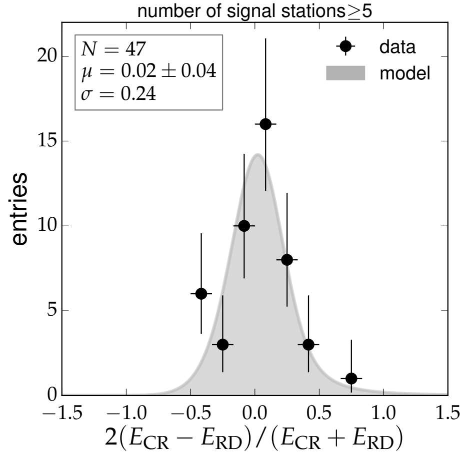

$$\sigma \approx 24\%$$

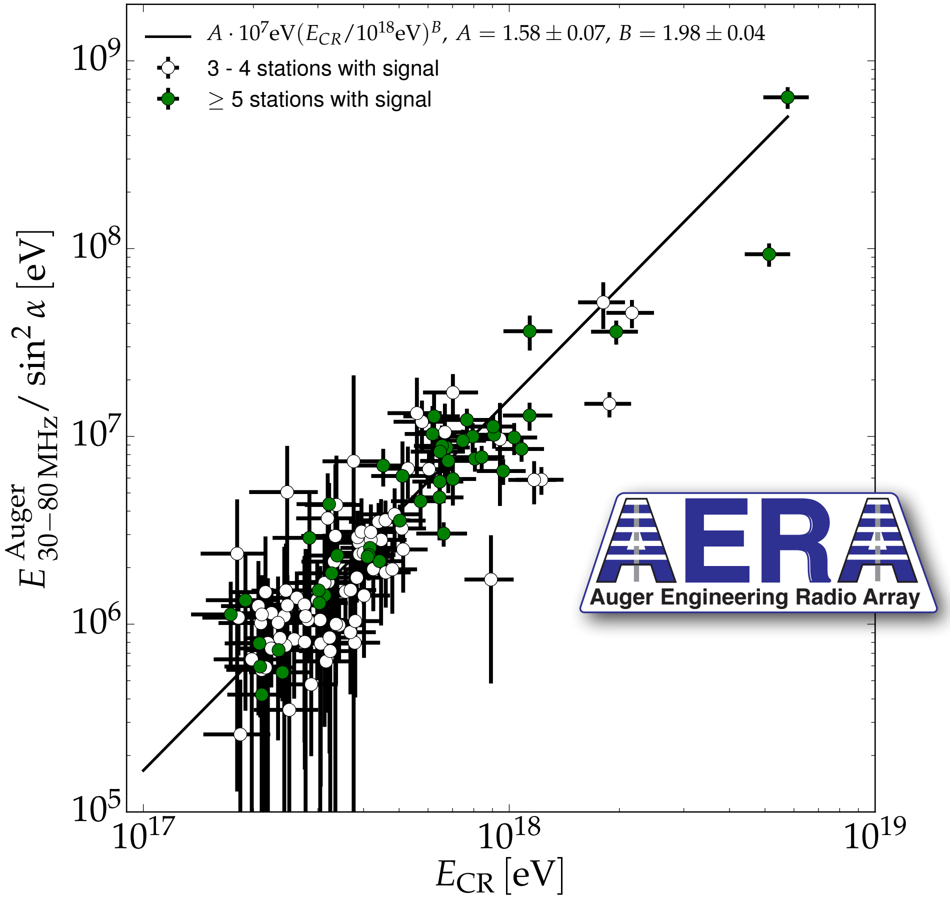

A. Aab et al., PRD 93 (2016) no.12, 122005

A. Aab et al., PRL 116 (2016) no.24, 241101

Cosmic-ray energy (Cherenkov) vs radio signal

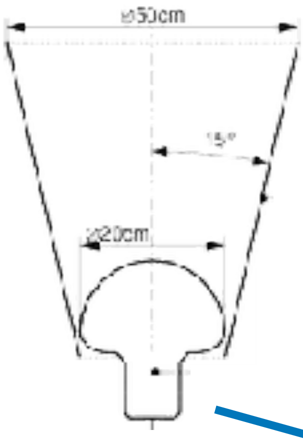

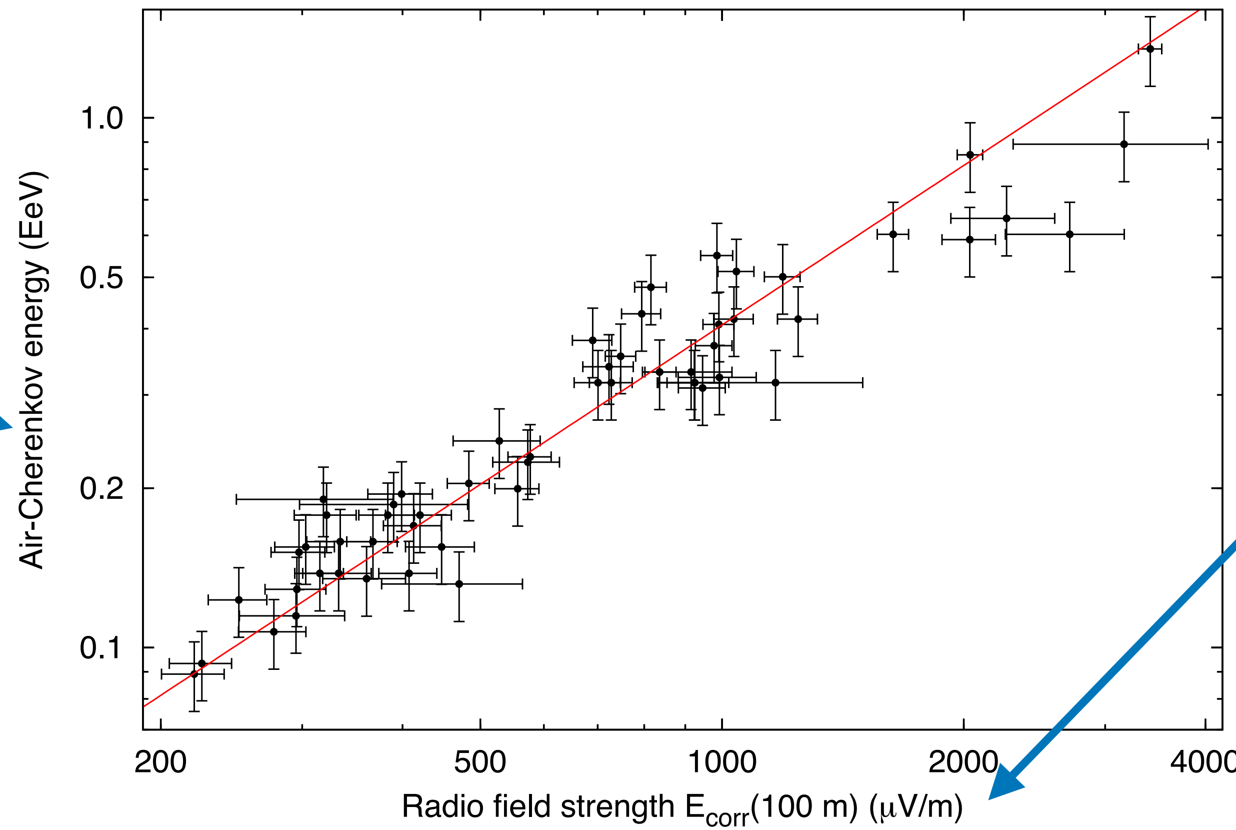

Fig. 3. Correlation of the energy measured with the air-Cherenkov array and an energy estimator based on the radio amplitude at 100 m measured with Tunka-Rex. The line indicates a linear correlation.

F.G. Schröder et al., JPS Conf. Proc. 9 (2016) 010008

Mass

Properties of primary particle

energy

distance to Xmax

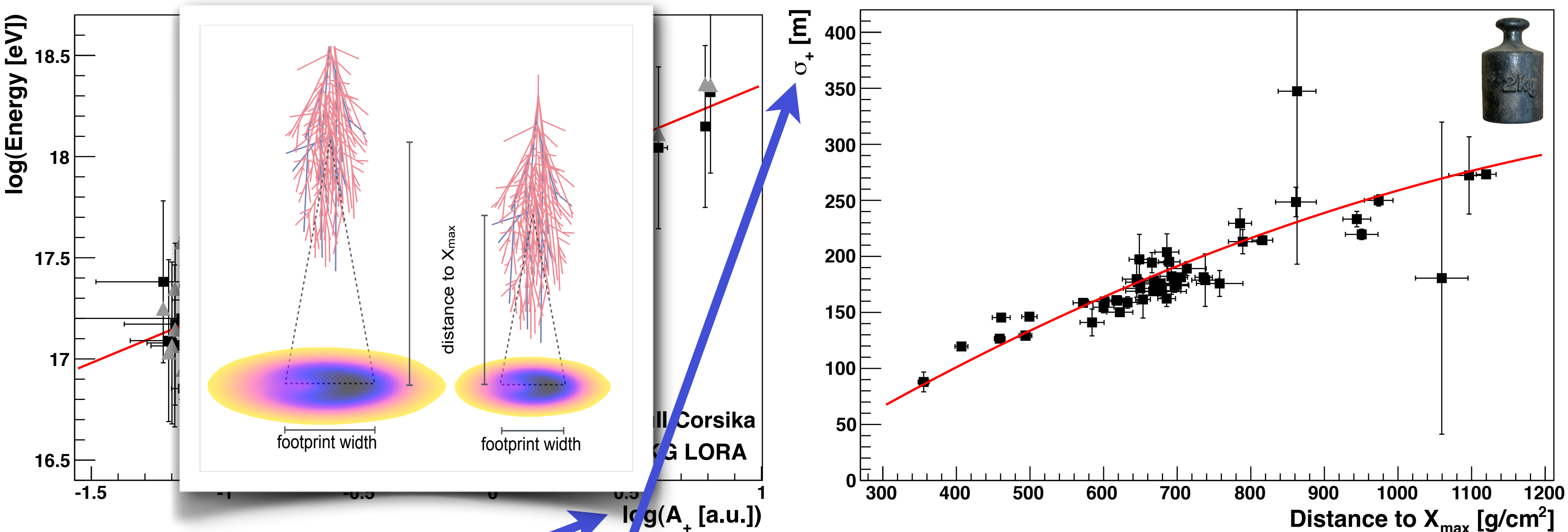

$$P(x', y') = A_+ \cdot \exp\left(\frac{-[(x'-X_+)^2 + (y'-Y_+)^2]}{\sigma_+^2}\right) - A_- \cdot \exp\left(\frac{-[(x'-X_-)^2 + (y'-Y_-)^2]}{\sigma_-^2}\right) + O$$

LOFAR

A. Nelles et al., JCAP 05 (2015) 018

Measurement of particle mass

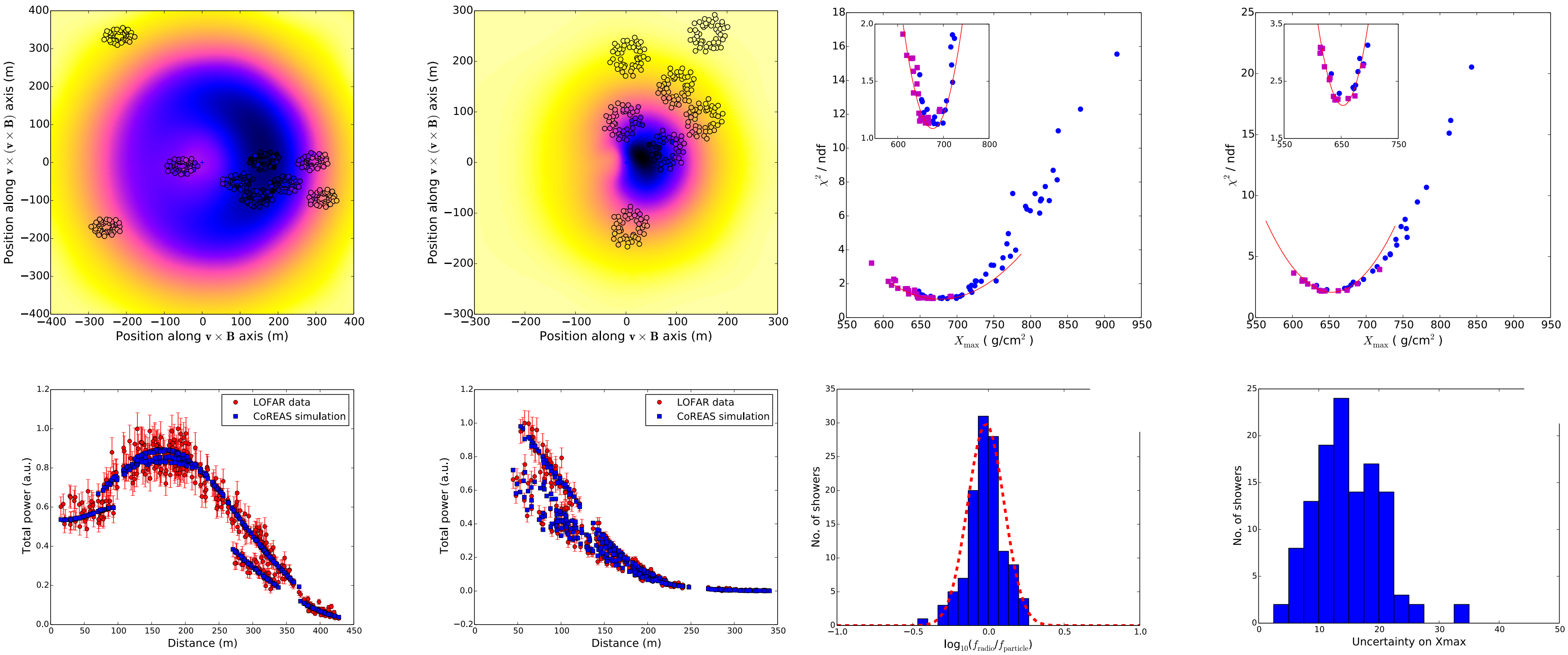

$\sigma_E \approx 32\%$

$\sigma_{X_{max}} \approx 17 \text{ g/cm}^2$

S. Buitink et al., PRD 90 (2014) 082003

Depth of the shower maximum

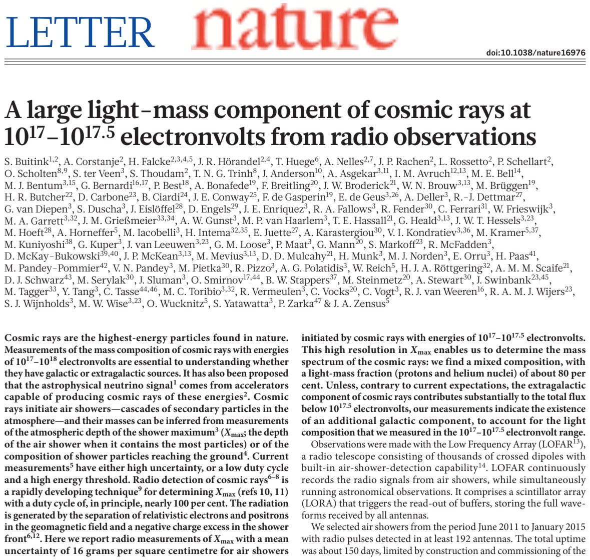

LETTER nature
doi:10.1038/nature16976

A large light-mass component of cosmic rays at 10^{17}–$10^{17.5}$ electronvolts from radio observations

S. Buitink[1,2], A. Corstanje[2], H. Falcke[2,3,4,5], J. R. Hörandel[2,4], T. Huege[6], A. Nelles[2,7], J. P. Rachen[2], L. Rossetto[2], P. Schellart[2], O. Scholten[8,9], S. ter Veen[3], S. Thoudam[2], T. N. G. Trinh[8], J. Anderson[10], A. Asgekar[3,11], I. M. Avruch[12,13], M. E. Bell[14], M. J. Bentum[3,15], G. Bernardi[16,17], P. Best[18], A. Bonafede[19], F. Breitling[20], J. W. Broderick[21], W. N. Brouw[3,13], M. Brüggen[19], H. R. Butcher[22], D. Carbone[23], B. Ciardi[24], J. E. Conway[25], F. de Gasperin[19], E. de Geus[3,26], A. Deller[3], R.-J. Dettmar[27], G. van Diepen[3], S. Duscha[3], J. Eislöffel[28], D. Engels[29], J. E. Enriquez[3], R. A. Fallows[3], R. Fender[30], C. Ferrari[31], W. Frieswijk[3], M. A. Garrett[3,32], J. M. Grießmeier[33,34], A. W. Gunst[3], M. P. van Haarlem[3], T. E. Hassall[21], G. Heald[3,13], J. W. T. Hessels[3,23], M. Hoeft[28], A. Horneffer[5], M. Iacobelli[3], H. Intema[32,35], E. Juette[27], A. Karastergiou[30], V. I. Kondratiev[3,36], M. Kramer[5,37], M. Kuniyoshi[38], G. Kuper[3], J. van Leeuwen[3,23], G. M. Loose[3], P. Maat[3], G. Mann[20], S. Markoff[23], R. McFadden[3], D. McKay-Bukowski[39,40], J. P. McKean[3,13], M. Mevius[3,13], D. D. Mulcahy[21], H. Munk[3], M. J. Norden[3], E. Orru[3], H. Paas[41], M. Pandey-Pommier[42], V. N. Pandey[3], M. Pietka[30], R. Pizzo[3], A. G. Polatidis[3], W. Reich[5], H. J. A. Röttgering[32], A. M. M. Scaife[21], D. J. Schwarz[43], M. Serylak[30], J. Sluman[3], O. Smirnov[17,44], B. W. Stappers[37], M. Steinmetz[20], A. Stewart[30], J. Swinbank[23,45], M. Tagger[33], Y. Tang[3], C. Tasse[44,46], M. C. Toribio[3,32], R. Vermeulen[3], C. Vocks[20], C. Vogt[3], R. J. van Weeren[16], R. A. M. J. Wijers[23], S. J. Wijnholds[3], M. W. Wise[3,23], O. Wucknitz[5], S. Yatawatta[3], P. Zarka[47] & J. A. Zensus[5]

Cosmic rays are the highest-energy particles found in nature. Measurements of the mass composition of cosmic rays with energies of 10^{17}–10^{18} electronvolts are essential to understanding whether they have galactic or extragalactic sources. It has also been proposed that the astrophysical neutrino signal[1] comes from accelerators capable of producing cosmic rays of these energies[2]. Cosmic rays initiate air showers—cascades of secondary particles in the atmosphere—and their masses can be inferred from measurements of the atmospheric depth of the shower maximum[3] (X_{max}; the depth of the air shower when it contains the most particles) or of the composition of shower particles reaching the ground[4]. Current measurements[5] have either high uncertainty, or a low duty cycle and a high energy threshold. Radio detection of cosmic rays[6–8] is a rapidly developing technique[9] for determining X_{max} (refs 10, 11) with a duty cycle of, in principle, nearly 100 per cent. The radiation is generated by the separation of relativistic electrons and positrons in the geomagnetic field and a negative charge excess in the shower front[6,12]. Here we report radio measurements of X_{max} with a mean uncertainty of 16 grams per square centimetre for air showers initiated by cosmic rays with energies of 10^{17}–$10^{17.5}$ electronvolts. This high resolution in X_{max} enables us to determine the mass spectrum of the cosmic rays: we find a mixed composition, with a light-mass fraction (protons and helium nuclei) of about 80 per cent. Unless, contrary to current expectations, the extragalactic component of cosmic rays contributes substantially to the total flux below $10^{17.5}$ electronvolts, our measurements indicate the existence of an additional galactic component, to account for the light composition that we measured in the 10^{17}–$10^{17.5}$ electronvolt range.

Observations were made with the Low Frequency Array (LOFAR[13]), a radio telescope consisting of thousands of crossed dipoles with built-in air-shower-detection capability[14]. LOFAR continuously records the radio signals from air showers, while simultaneously running astronomical observations. It comprises a scintillator array (LORA) that triggers the read-out of buffers, storing the full wave-forms received by all antennas.

We selected air showers from the period June 2011 to January 2015 with radio pulses detected in at least 192 antennas. The total uptime was about 150 days, limited by construction and commissioning of the

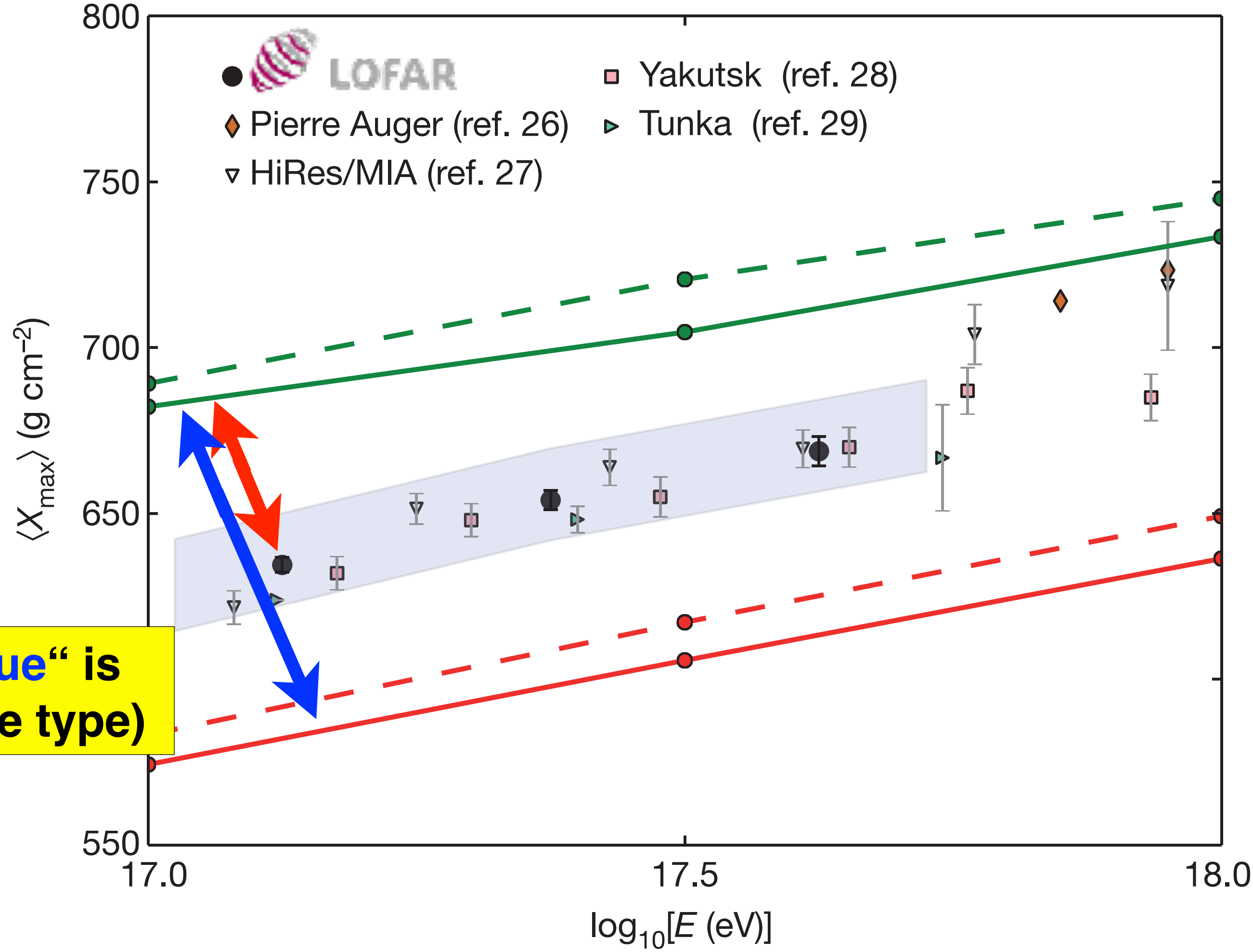

relative distance "red/blue" is measure for ln A (particle type)

S. Buitink et al., Nature 531 (2016) 70

Mean logarithmic mass

$$\ln A = \sum k_i \ln A_i$$

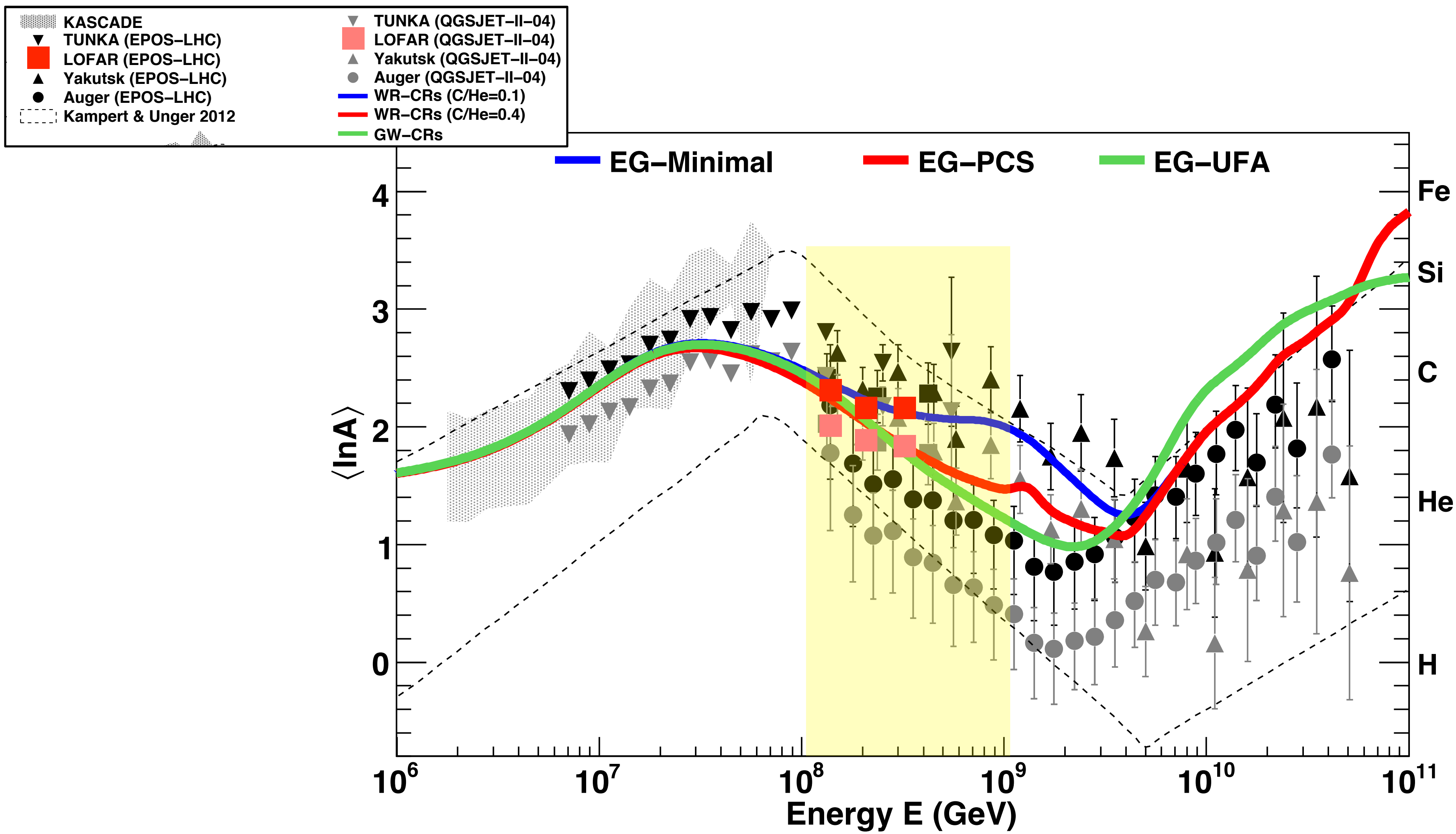

S. Thoudam et al., A&A 595 (2016) A33

Shower maximum: proof by Tunka-Rex

- One of several methods: slope of lateral distribution

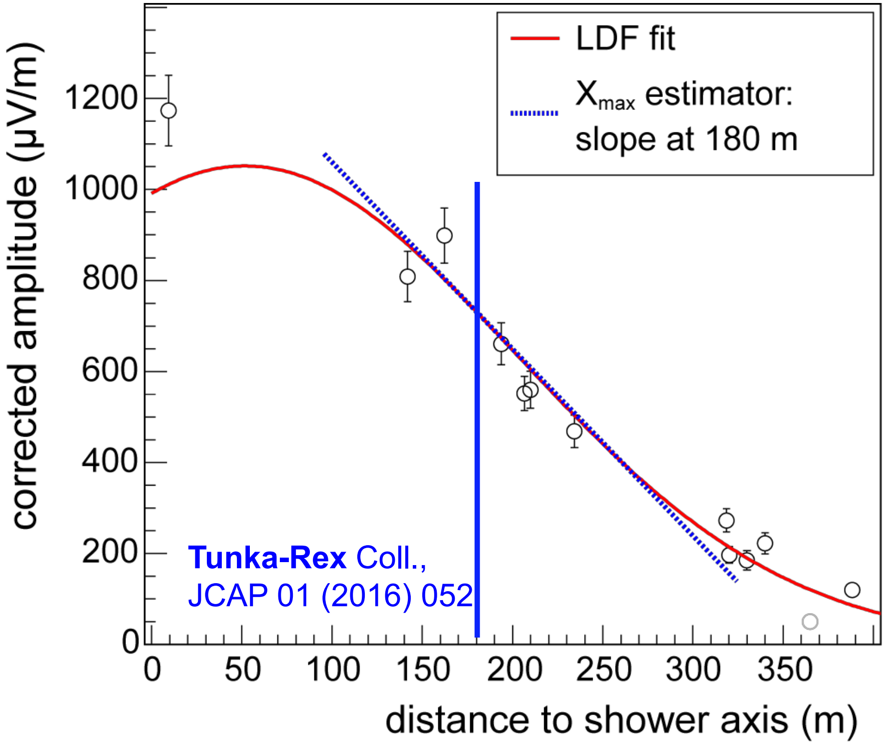

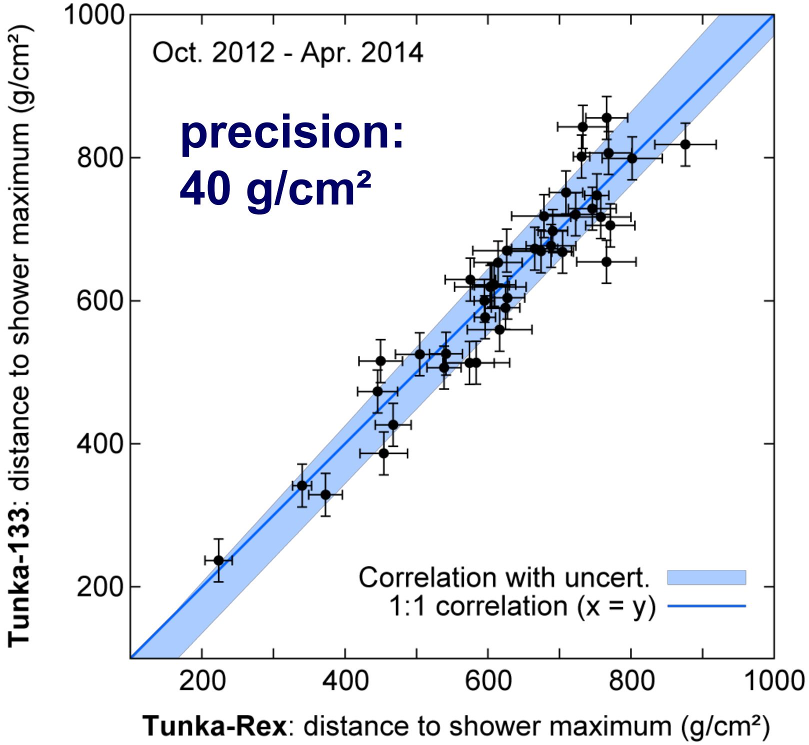

frank.schroeder@kit.edu
Institut für Kernphysik

Introduction: Radio footprint is sensitive to mass

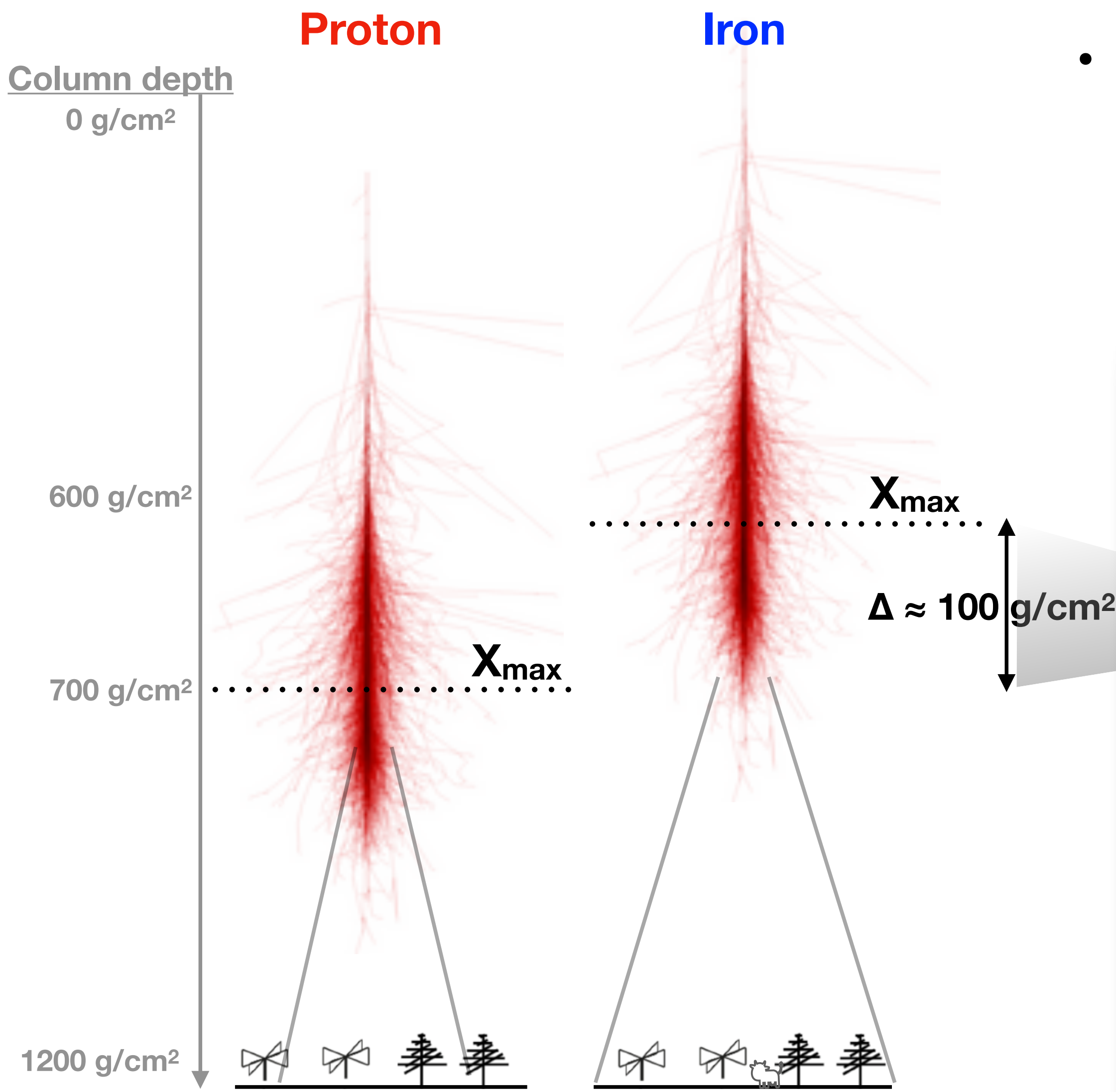

- X_{max} [g/cm²]: *column depth* where *Extensive Air Shower* is maximally developed. —> X_{max} depends on mass (particle type)

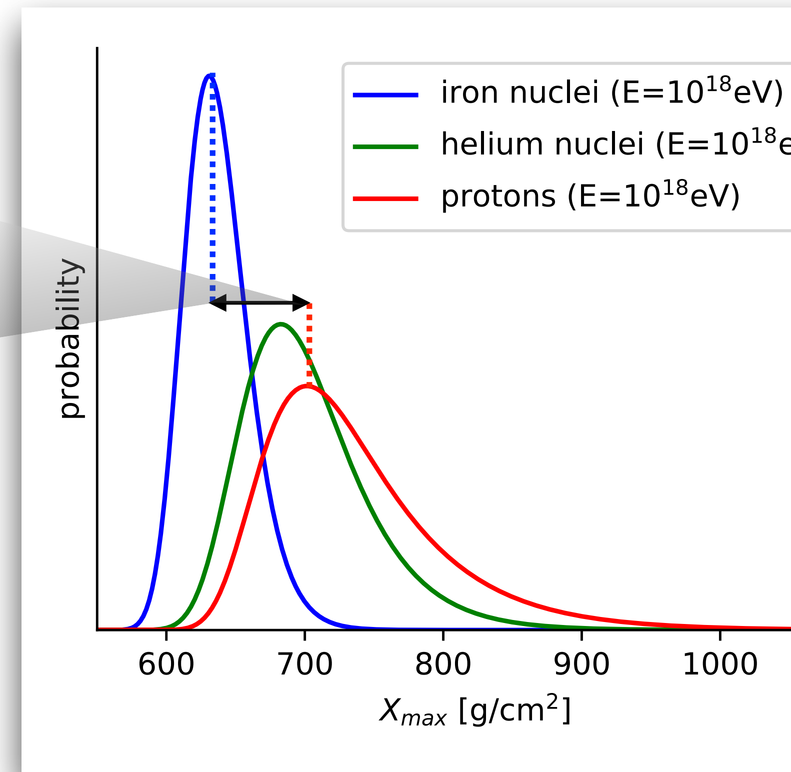

Introduction: Radio footprint is sensitive to mass

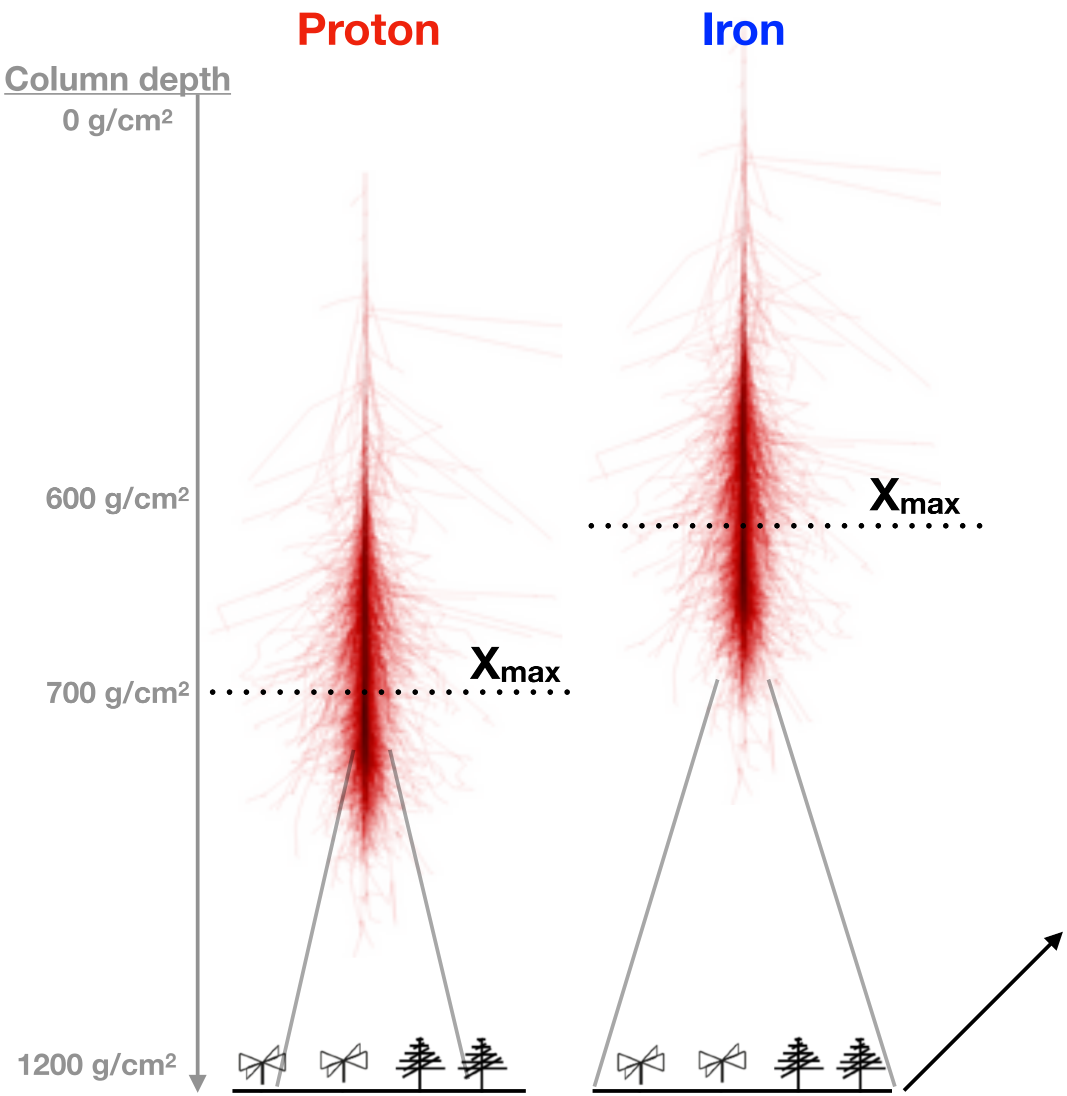

- X_{max} [g/cm²]: *column depth* where *Extensive Air Shower* is maximally developed.
  —> X_{max} depends on mass (particle type)
- Shape of radio footprint changes with X_{max}
  —> Radio footprint is probe for X_{max}.

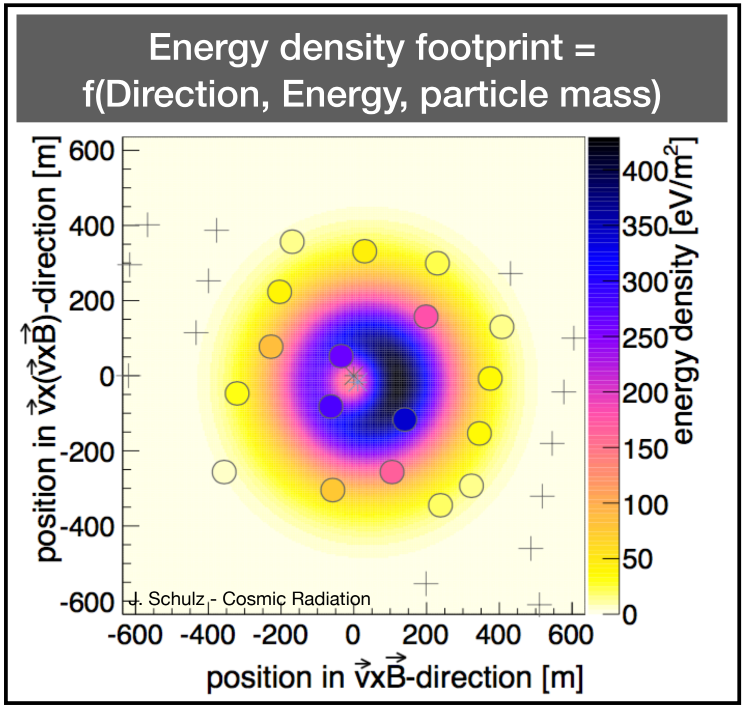

Method: Reconstructing X_{max} from the radio footprint

Radboud University

Reconstruction Air Shower → CORSIKA → Reconstruction Simulations

E, θ, ϕ, … $\{X_{max}\}$

Using same reconstruction code
(includes detector and reconstruction effects)

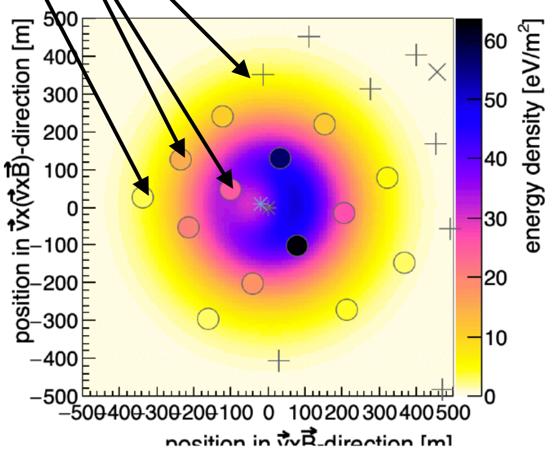

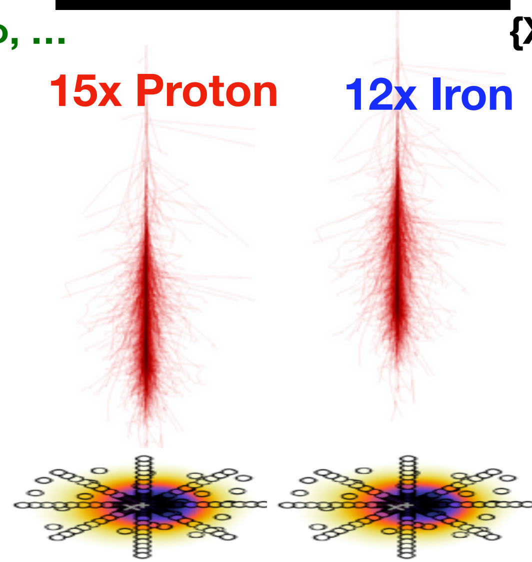

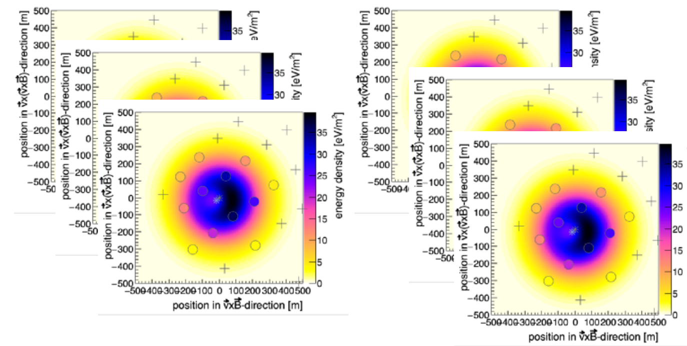

Minimise to find X_{max} of measured shower:

Based on Buitink+(2016)

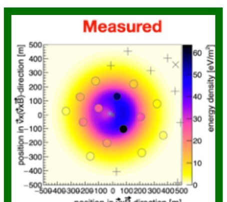

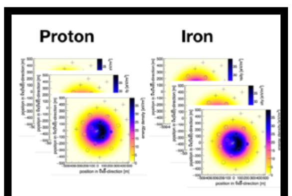

$$\chi^2 = \sum_{\text{AERA Stations}} \left(\frac{u_{data} - S \cdot u_{sim}(\Delta \vec{r}_{\text{core shift}})}{\sigma u_{data}} \right)$$

Minimize $[\,S\,,\,r_{core}\,]$

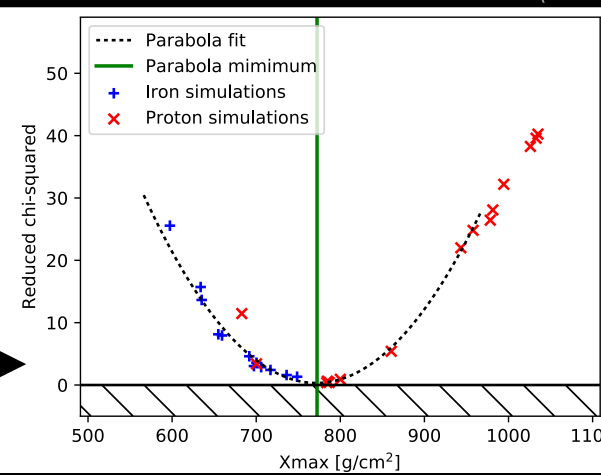

Radbound University

Results: Event-by-event FD vs AERA X_{max}

Histogram of AERA-FD difference

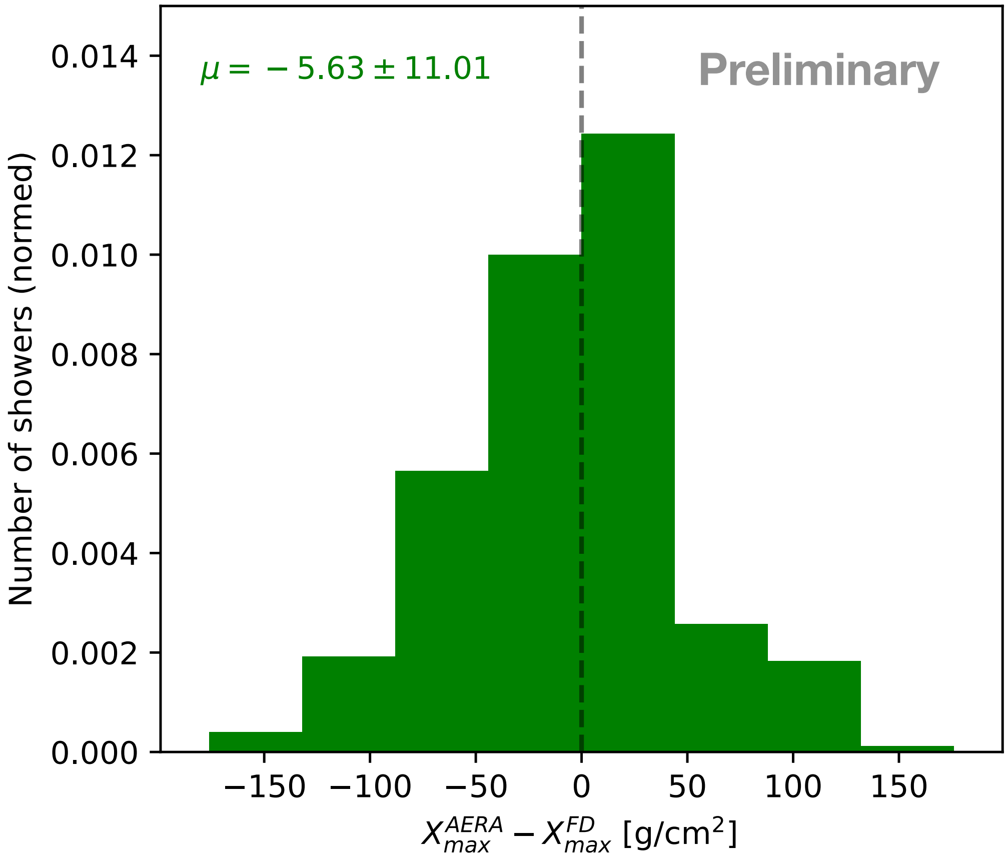

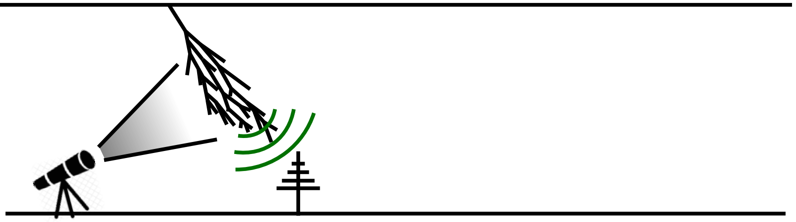

Auger has unique Radio-Fluorescence setup:

- X_{max} of **53** hybrid-showers with AERA and FD; (Are independent observations!)
- No significant bias radio X_{max} w.r.t. fluorescence X_{max}.
- Provides independent checks on:
  - X_{max} reconstruction methods
  - shower physics (probe different aspects)

Results: Resolution of AERA X_{max} method

Radio X_{max} resolution

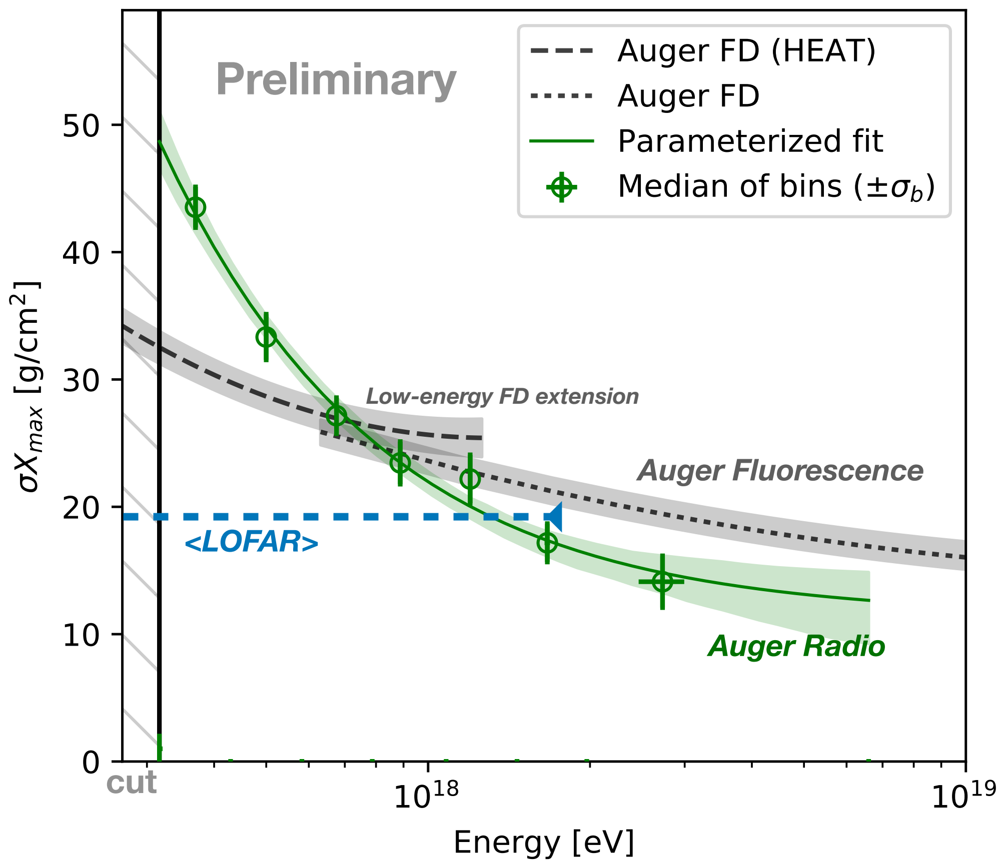

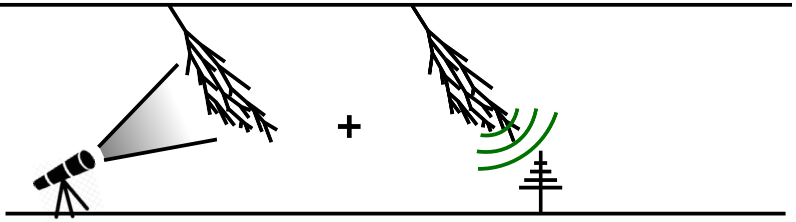

Resolution improves with energy.

- Up to 'better than 15 g/cm² '
- Trend driven by low SNR at low energy.

Resolution competitive with e.g.:

- Auger fluorescence [arXiv:1409.4809]
- LOFAR radio (E=$10^{16.8...18.3}$eV) [arXiv:2103.12549v2]

Side note:
High resolution is crucial for mass composition studies.

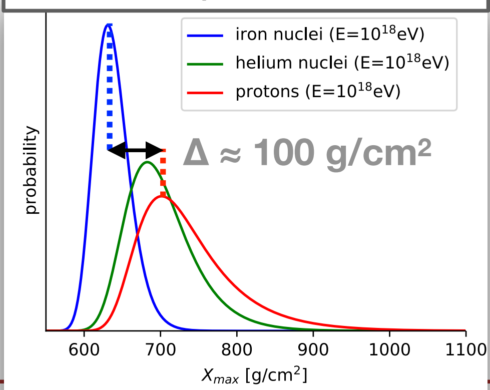

Results: Measured AERA X_{max} distribution

'Mean of X_{max} distribution'

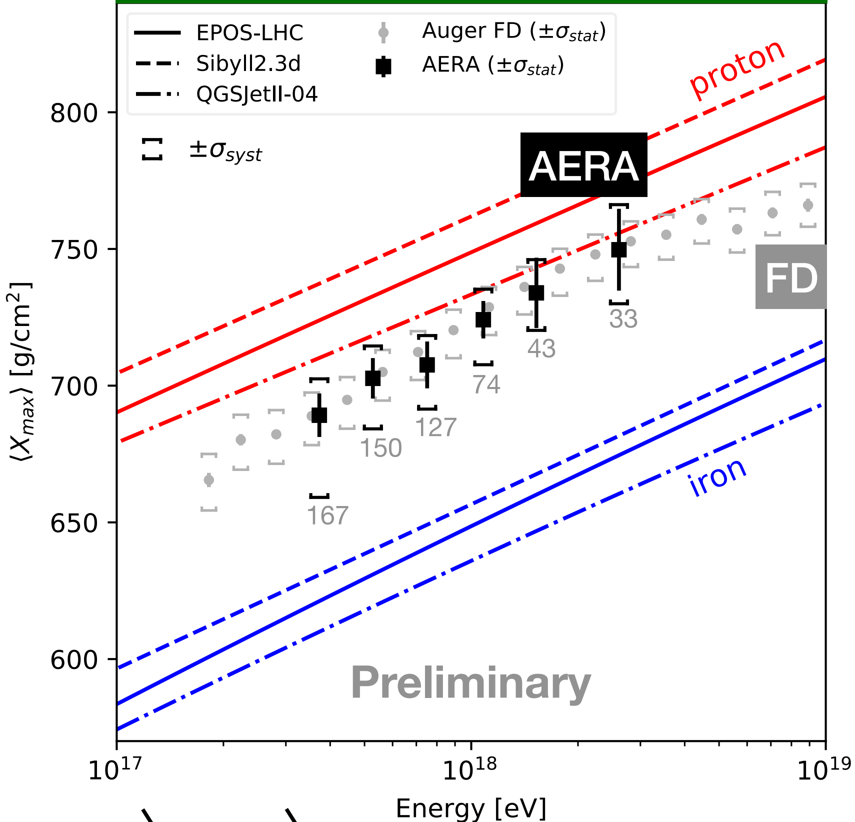

'Width of X_{max} distribution'

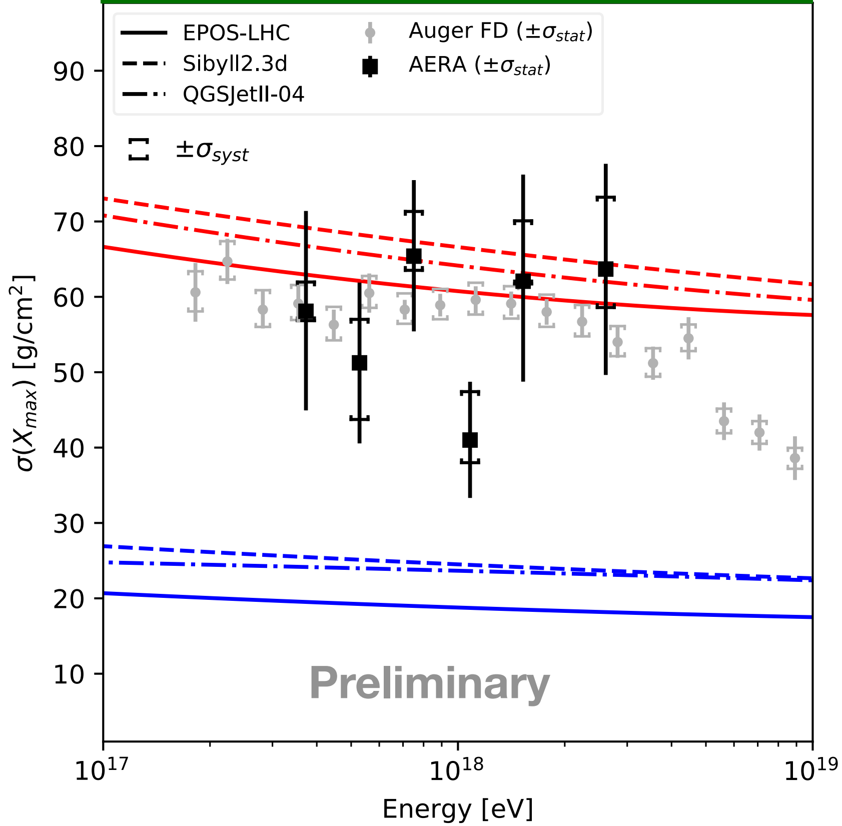

- ~600 showers after quality and anti-bias cuts.
- In agreement with Auger FD in mean, width, and (qualitatively) the X_{max} distribution.
- Light composition (p-He) at E=$10^{17.5}$ eV, seemingly becoming lighter towards E=$10^{18.5}$ eV.

Results: AERA vs other (radio) experiments

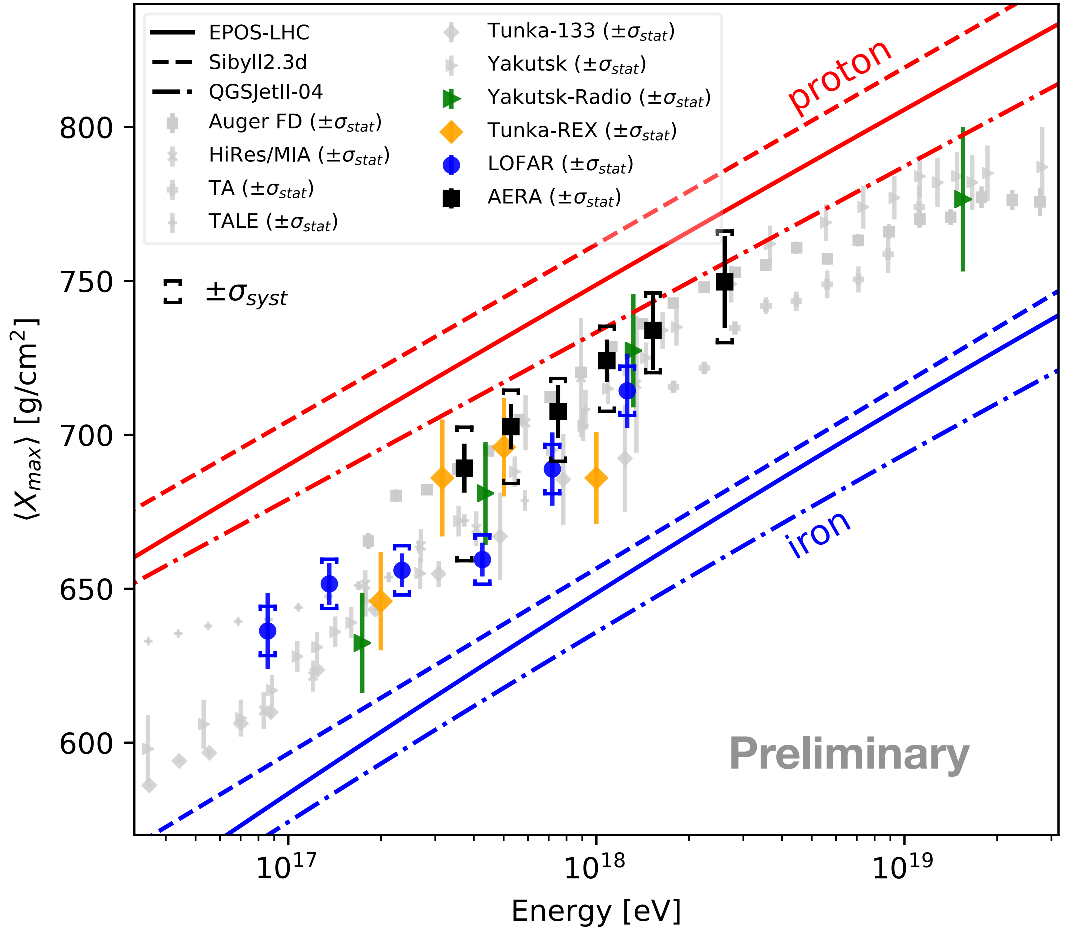

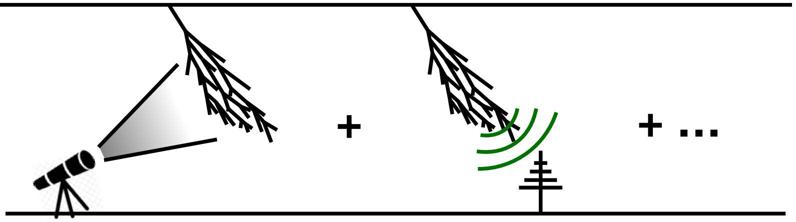

- No general radio-bias w.r.t other techniques (within uncertainties).
- Highlights that systematic uncertainties are key to interpret and compare.
- **LOFAR-AERA** differences are being investigated in a working group

—> come talk to us during coffee and lunch!

Determine the properties of the incoming particle with the radio technique

- direction ~ 0.1° - 0.5°
- energy ~ 20% - 30%
- type (X_{max}) ~ 20 - 40 g/cm²

(depending on detector spacing)

—> radio technique is routinely used to measure properties of cosmic rays


The Future
NEXT EXIT

Concept of ARIANNA

- On ice-shelf: **Ice-water boundary** almost perfect reflector for radio emission
- **Independent antenna stations** can be installed at low costs on the surface
- **Real-time data transfer** via satellite
- Solar and wind power possible
- **High gain antennas** (50 - 1000 MHz) can be used to instrument a large volume
- Array of about 1000 antennas needed

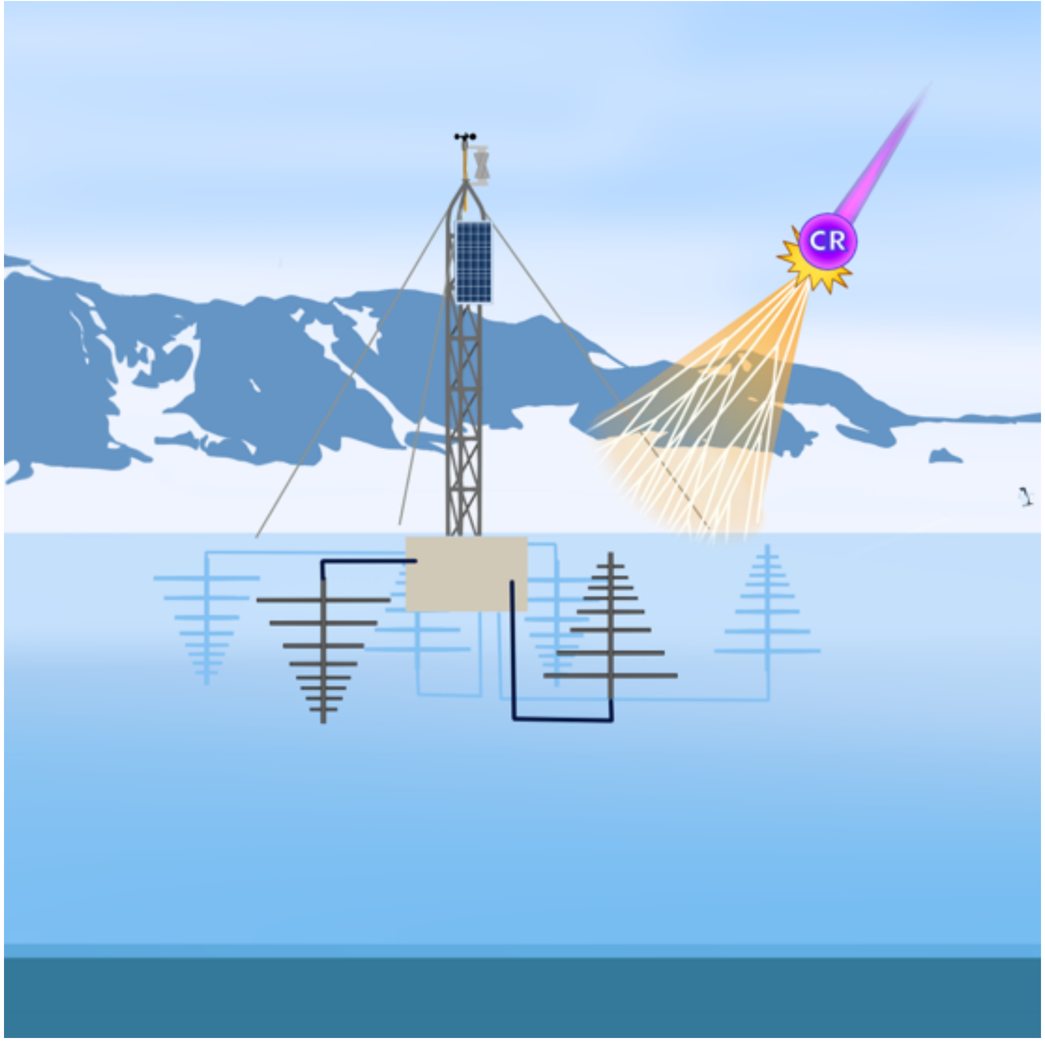

S.W. Barwick et al., Astropart.Phys. 90 (2017) 50

ARIANNA

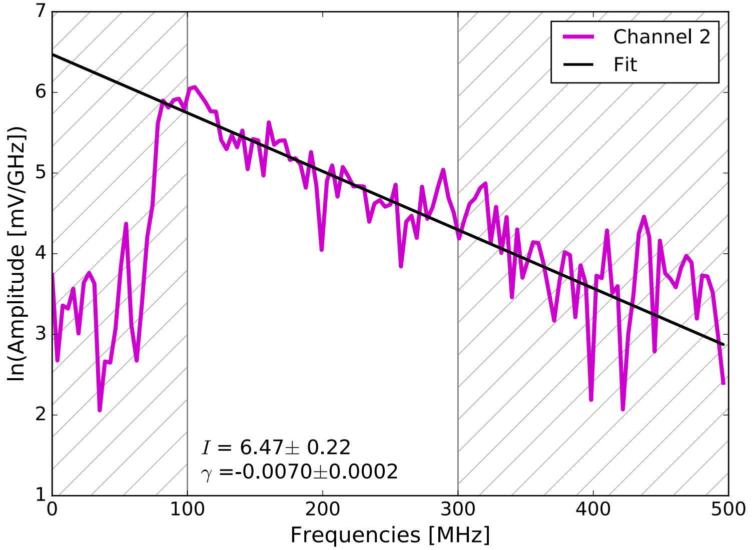

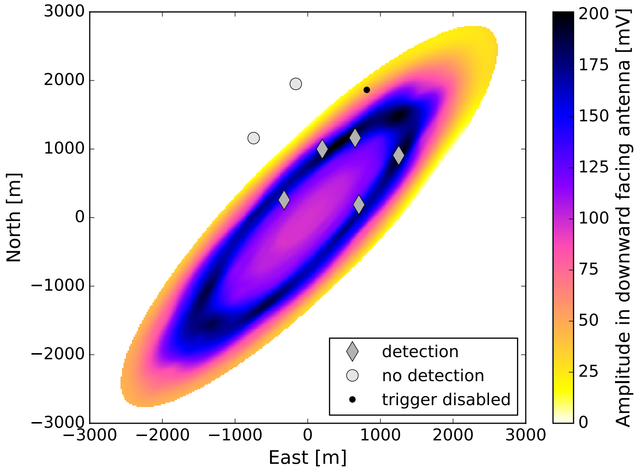

use **slope** **of measured** **frequency spectrum** **to derive** **energy** **and other shower parameters**

full ARIANNA
36 km² x 36 km²
1296 km²

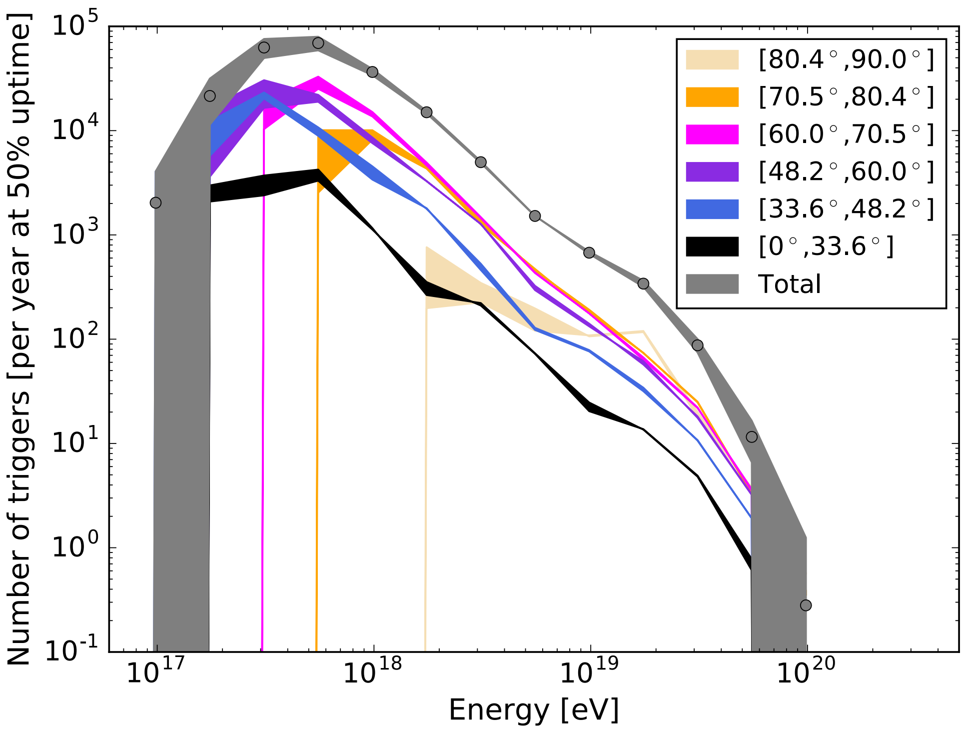

S.W. Barwick et al., Astropart.Phys. 90 (2017) 50

Extension of scintillator array (LORA)

LOFAR

S. Buitink
K. Mulrey

2.5 km

Existing station
New station

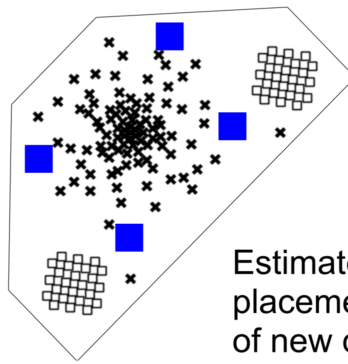

Estimated placement of new detectors

adding 20 scintillator stations in 2018

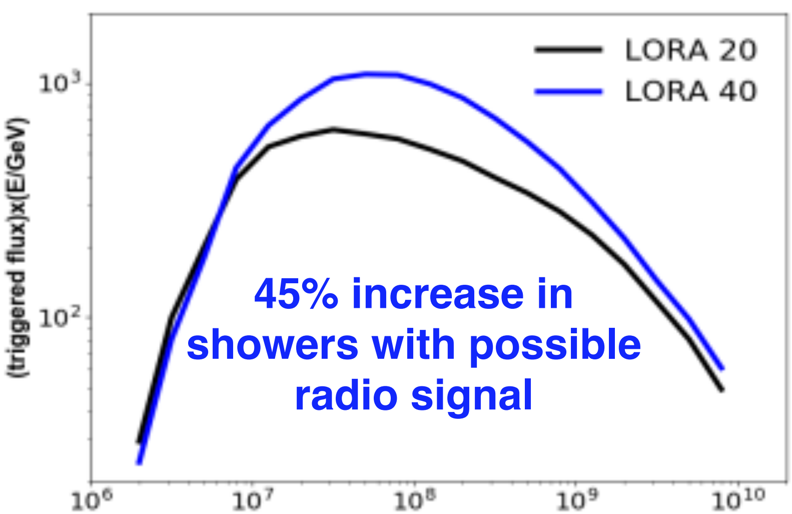

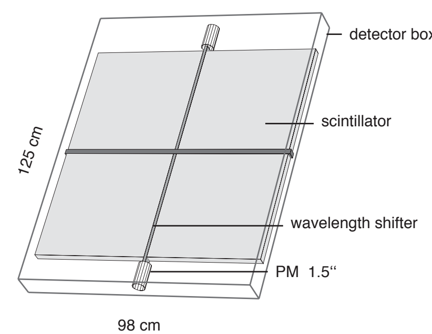

Upgrade of the Pierre Auger Observatory
(astro-)physics of the highest-energy particles in nature

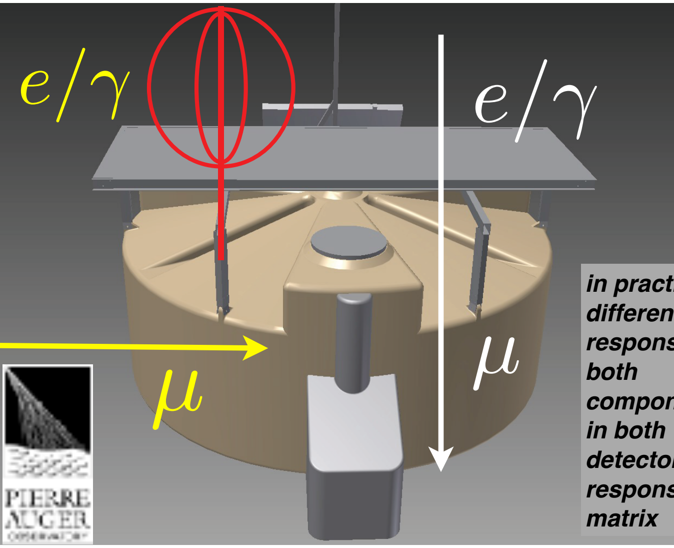

upgrade PAO
- electronics
- scintillator layer
- radio detector

in practice: different response to both components in both detectors: response matrix

Key science questions
- What are the sources and acceleration mechanisms of ultra-high-energy cosmic rays (UHECRs)?
- Do we understand particle acceleration and physics at energies well beyond the LHC (Large Hadron Collider) scale?
- What is the fraction of protons, photons, and neutrinos in cosmic rays at the highest energies?

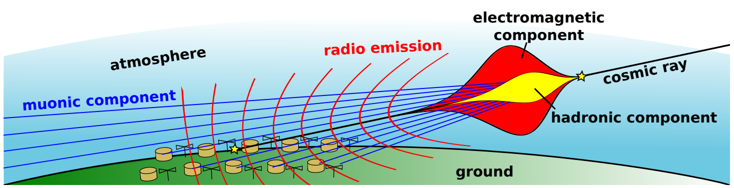

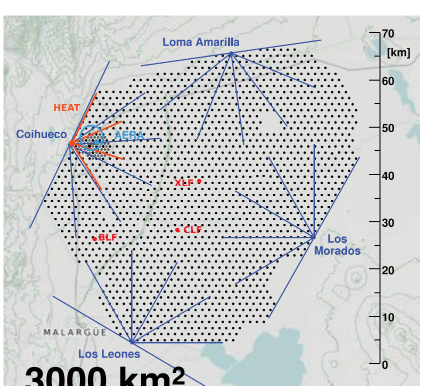

Advanced Grant Hörandel 2018

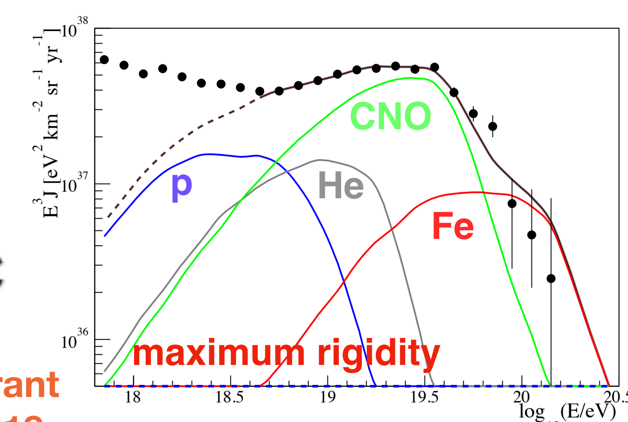

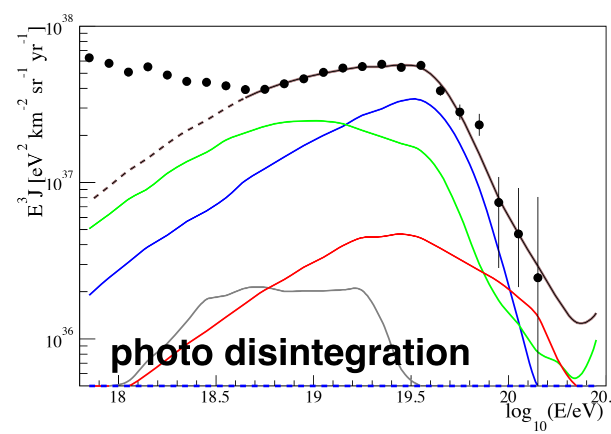

A large radio array at the Pierre Auger Observatory

preparatory work & feasibility

AERA 17 km² --> 3000 km²

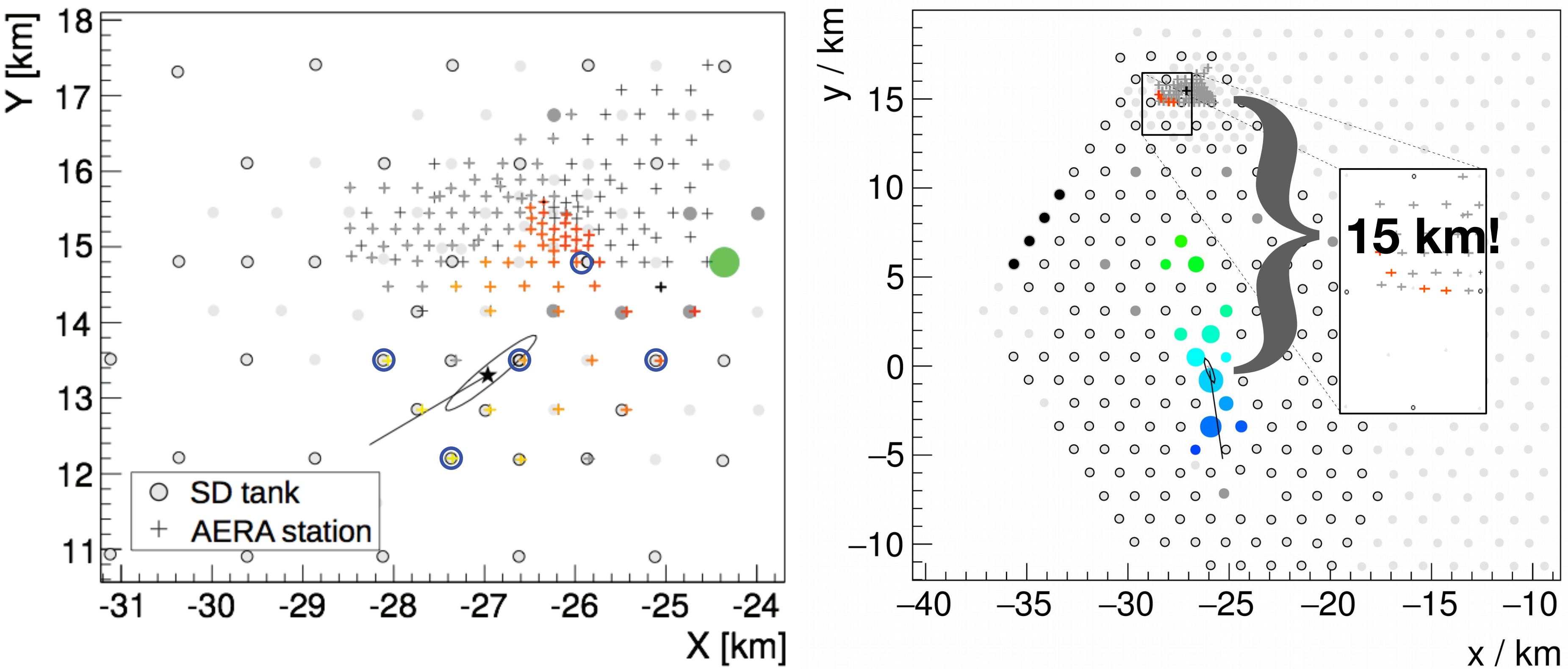

horizontal air showers registered and reconstructed with existing AERA

A. Aab et al., JCAP 10 (2018) 026

Horizontal air showers have large footprints in radio emission

M. Gottowik

AERA 17 km²
--> 3000 km²

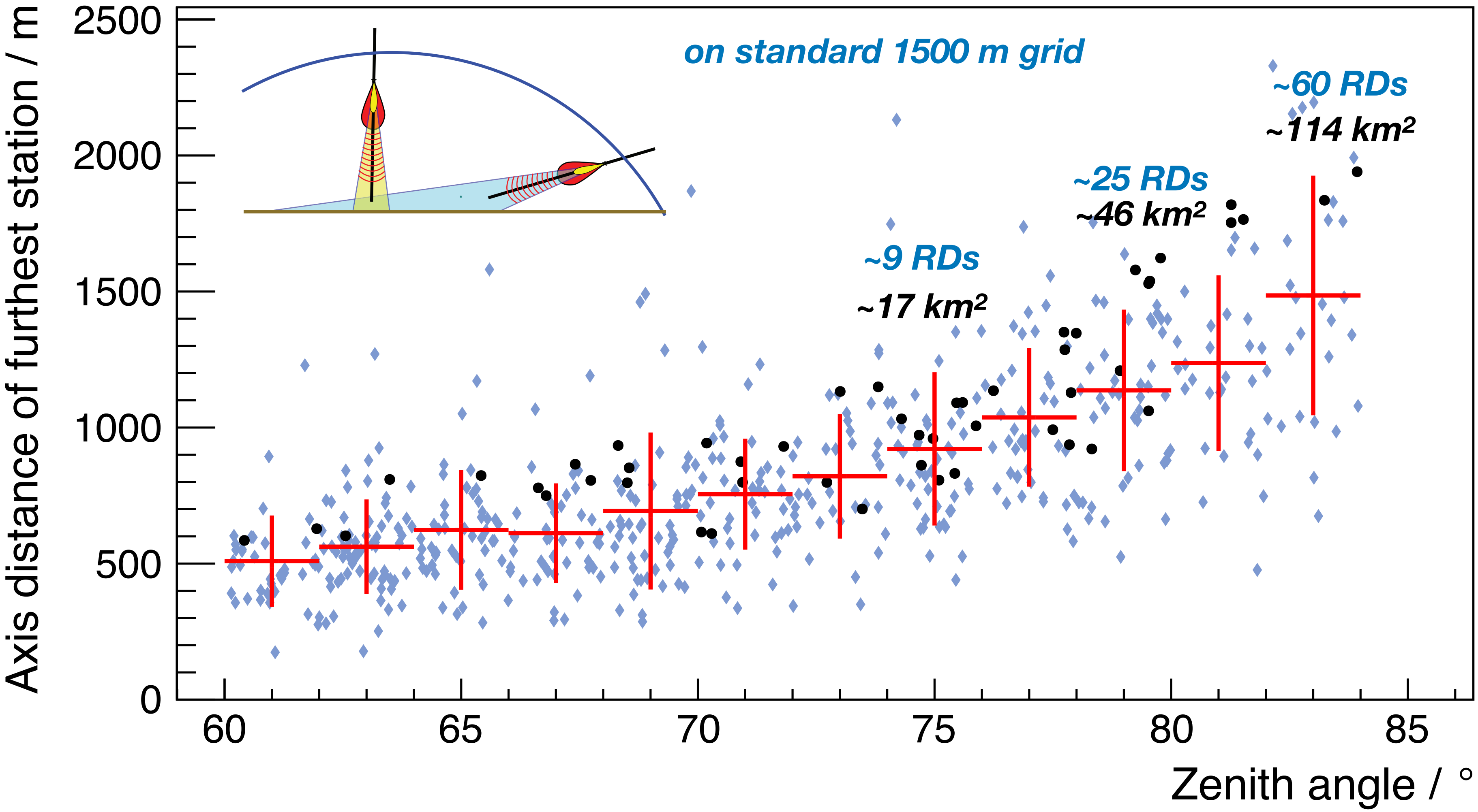

this is MEASURED with the *small* 17km² AERA

A. Aab et al., JCAP 10 (2018) 026

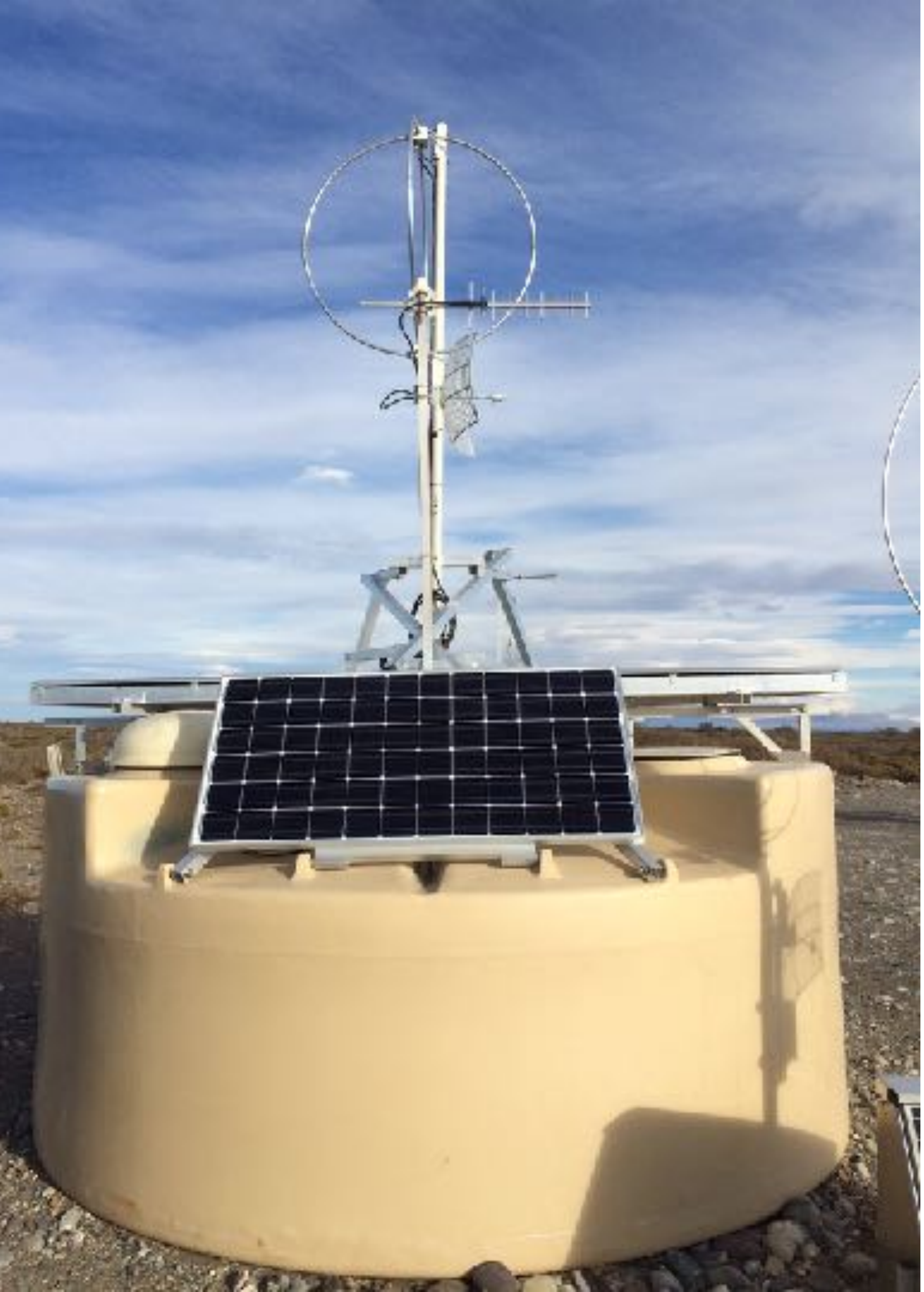

since May 2019 complete prototype at Auger observatory

- new SALLA antenna
- new LNA
- new digitizer/front end coupled to UUB

data are integrated in SD data stream and transported to CDAS

we have now *ONE* system comprising of WCD, SSD, RD

since November 2019
10 prototype stations installed

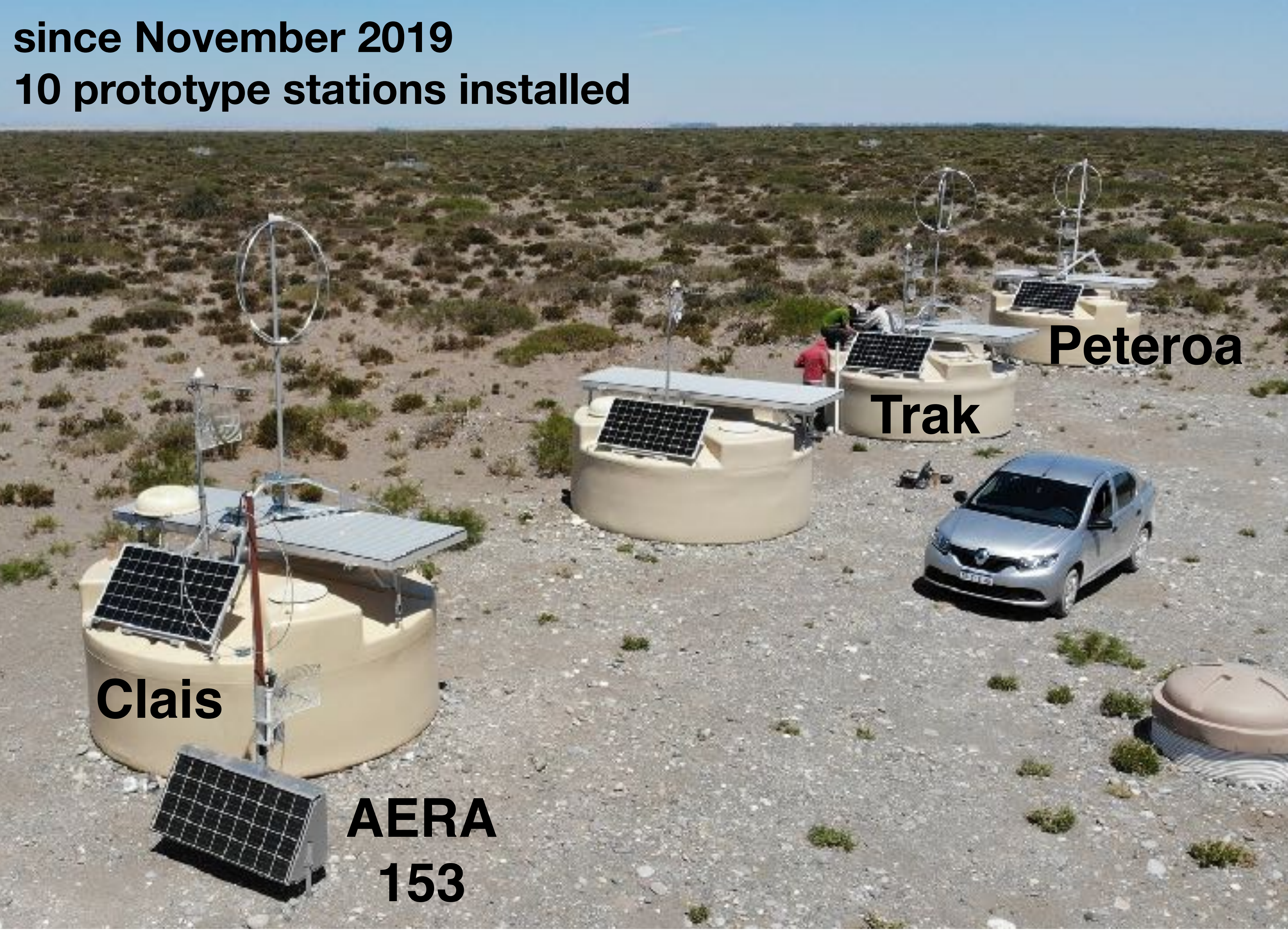

photo: Tim Huege

First Rd Signal

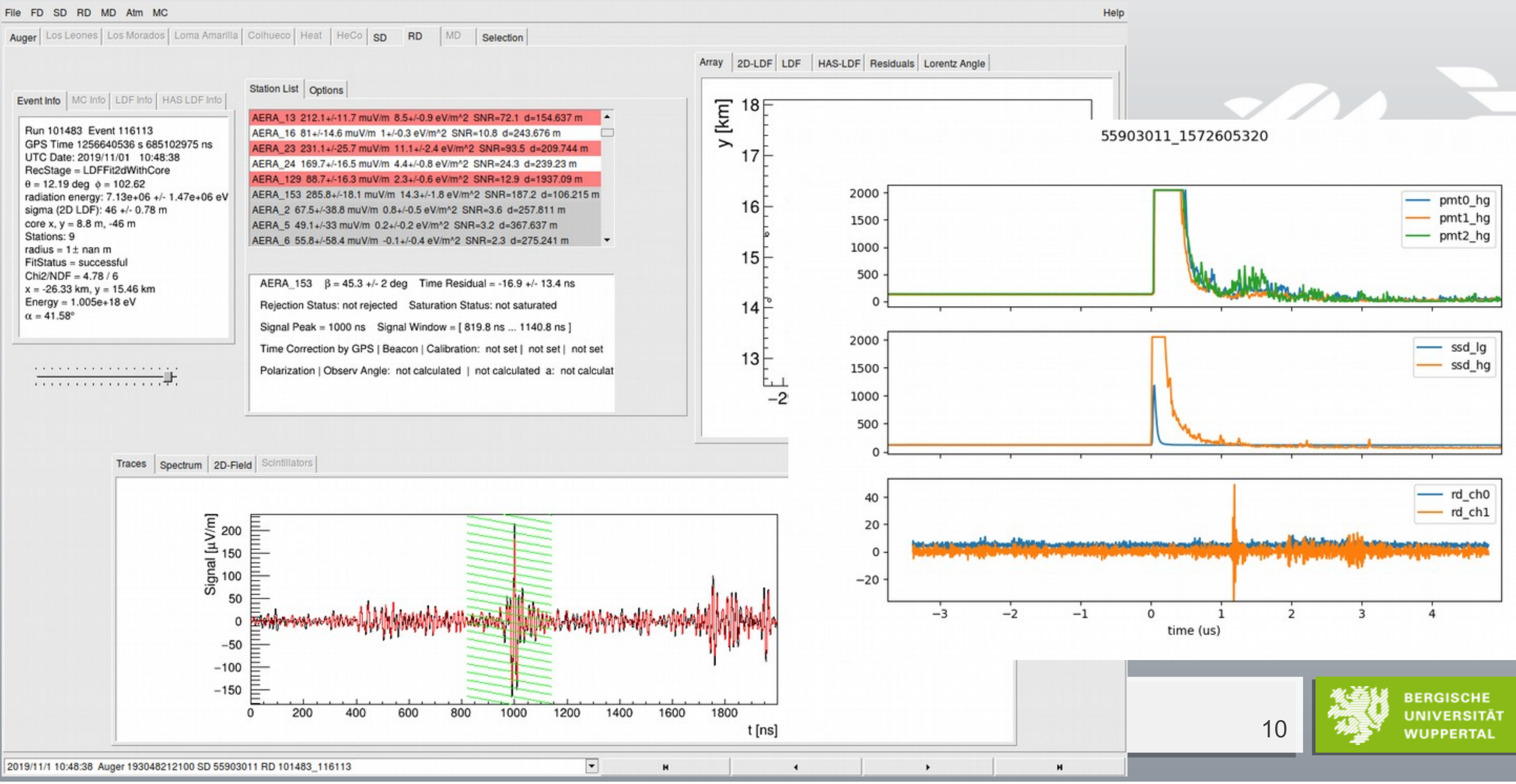

BERGISCHE UNIVERSITÄT WUPPERTAL

J. Rautenberg

mechanical mounting of RD on wcd

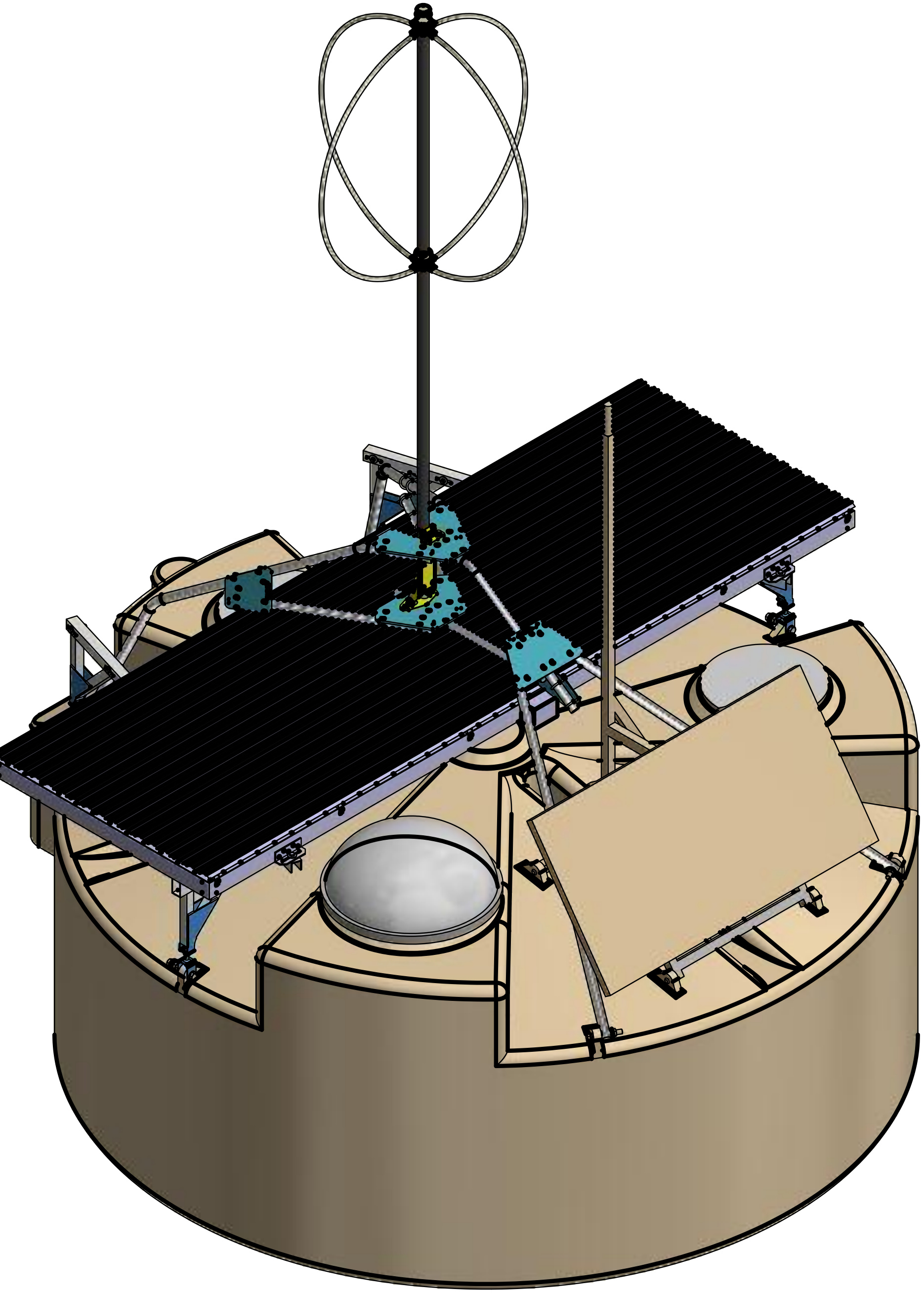

5 m above ground

designed to resist wind speeds of 120 km/h

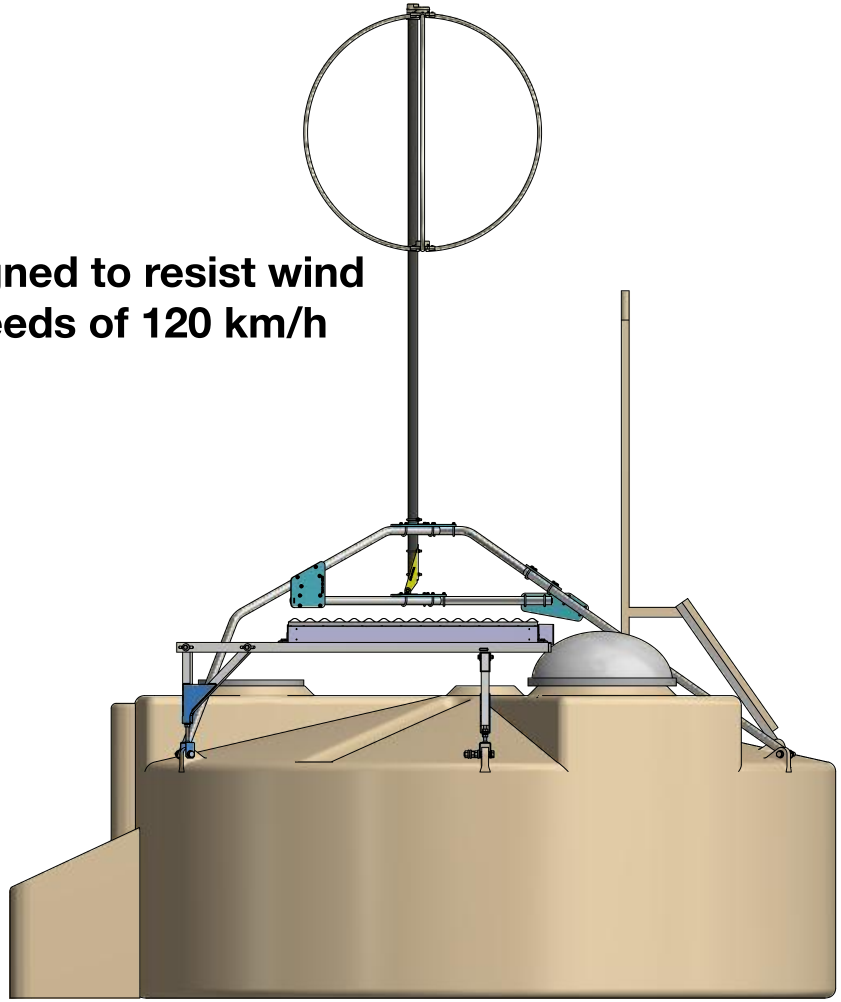

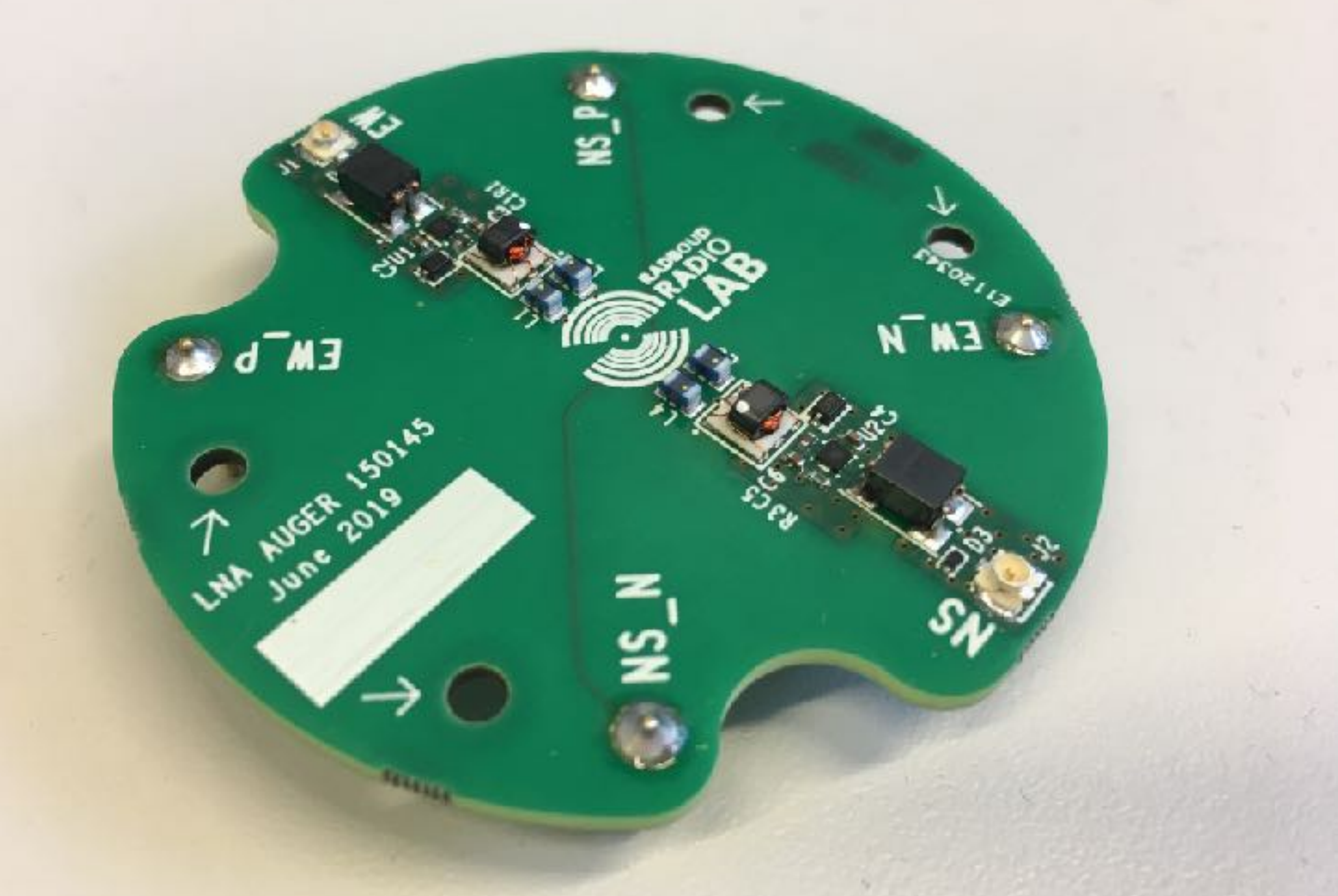

final version of LNA, RU Nijmegen, June 2019

radio digitizer

developed at RU Nijmegen

Detection aperture and event statistics

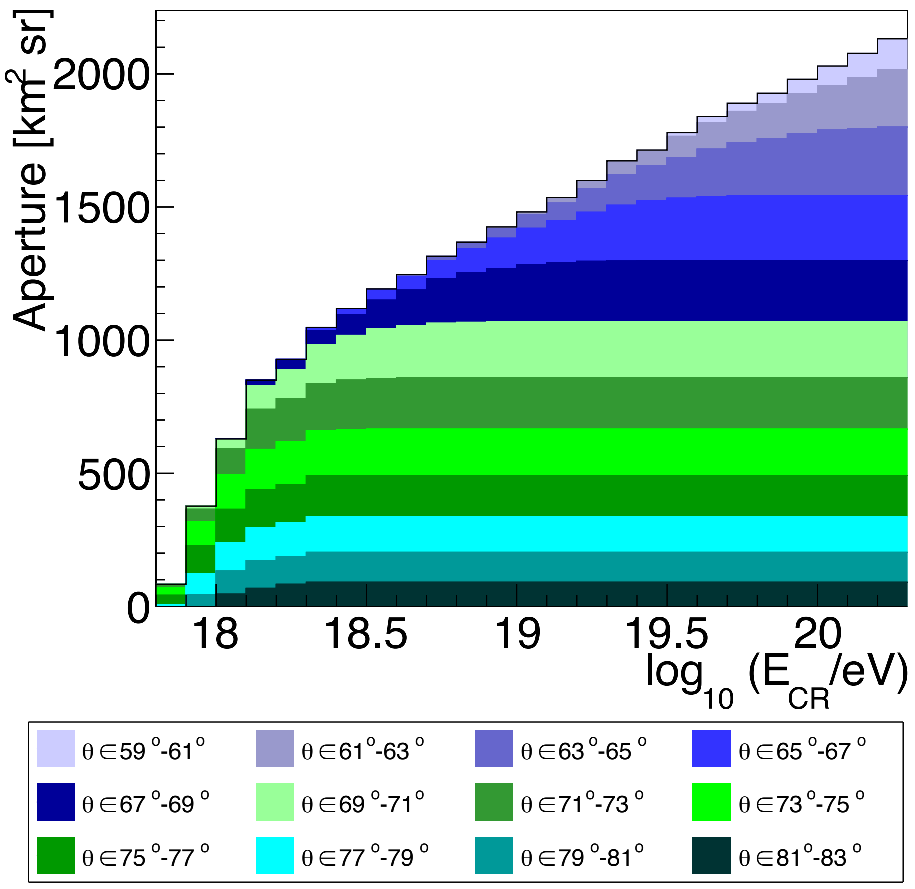

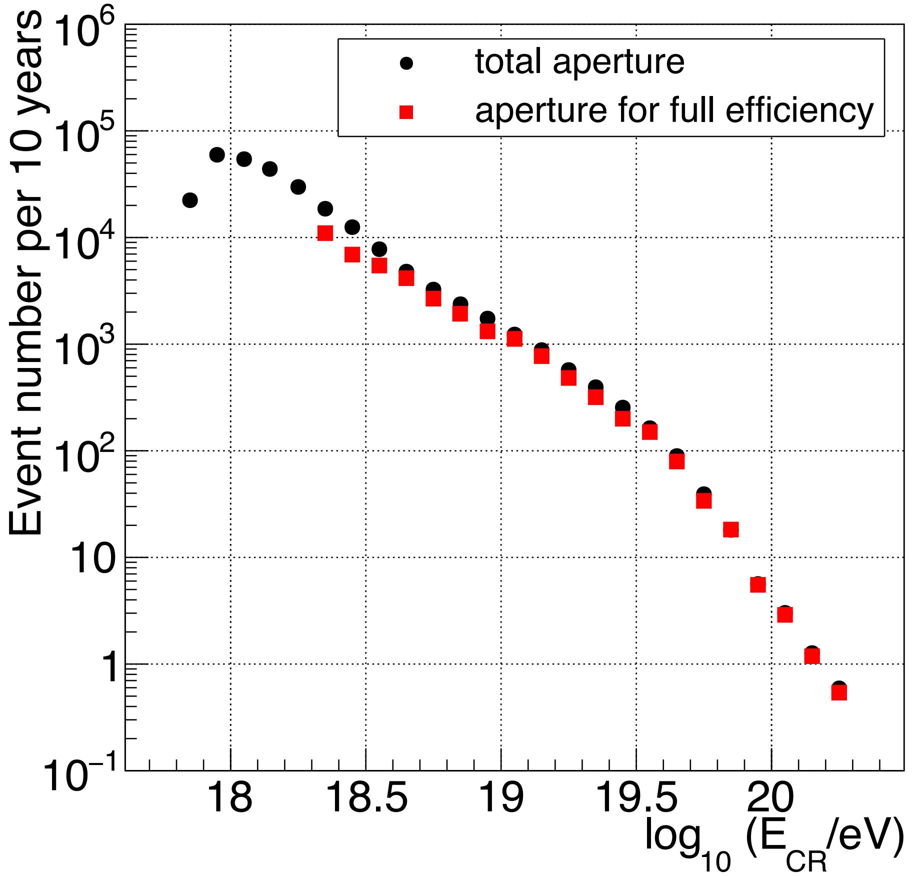

- **High zenith angles become efficient early, contribute smaller apertures**
- **Lower zenith angles contribute larger apertures, become efficient later**
- **3000 fully efficient events above 10^{19} eV in 10 years (300 above $10^{19.5}$ eV)**

Measurement of the fluctuations in the number of muons in inclined air showers with the Pierre Auger Observatory

Felix Riehn[*a] **for the Pierre Auger Collaboration**[†b]

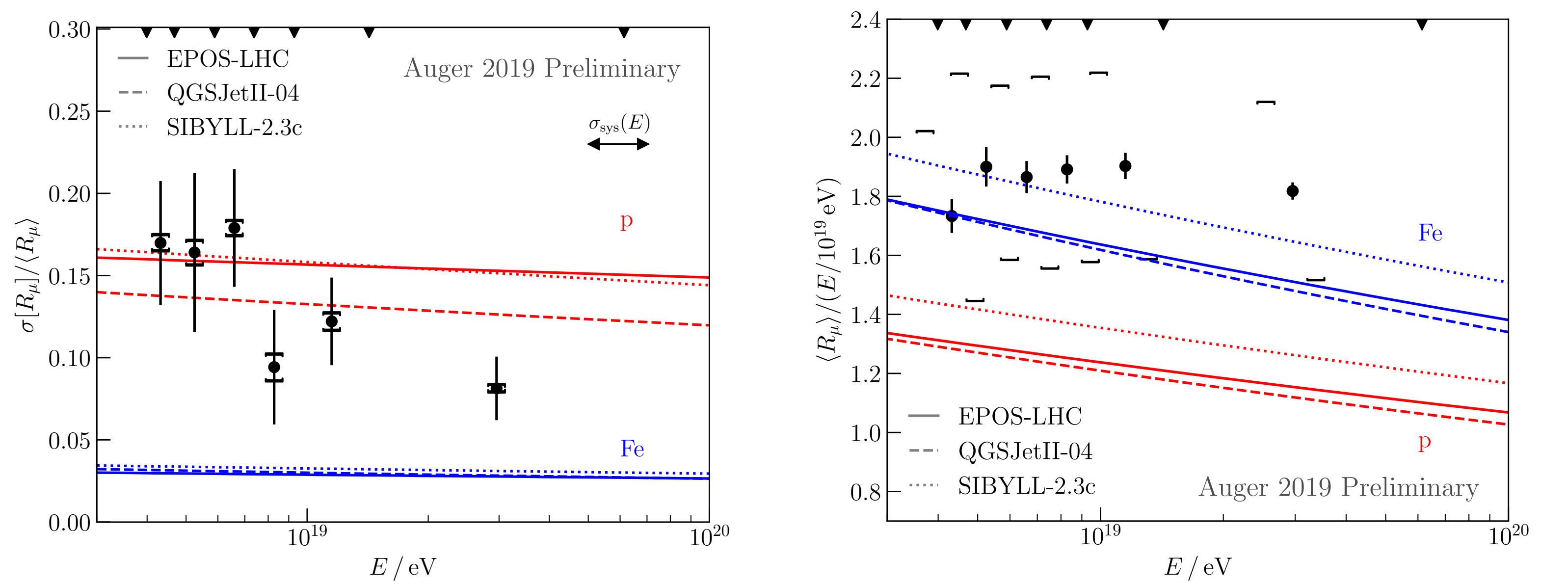

Figure 4: Shower-to-shower fluctuations (left) and the average number of muons (right) in inclined air showers as a function of the primary energy. For the fluctuations, the statistical uncertainty (error bars) is dominant, while for $\langle R_\mu \rangle$ the systematic uncertainty (square brackets) is dominant. The shift in the markers for the systematic uncertainty in the average number of muons represents the uncertainty in the energy scale.

Muon content in horizontal air showers

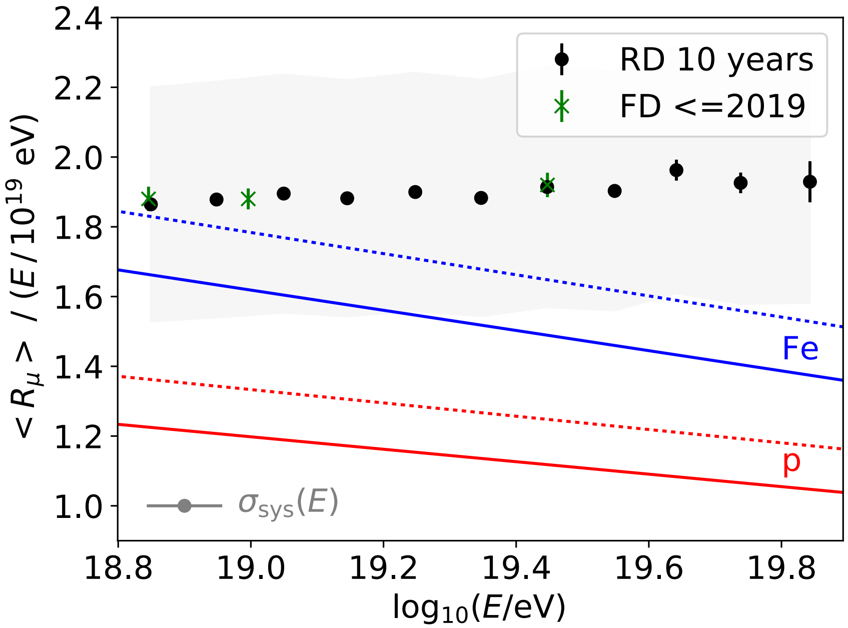

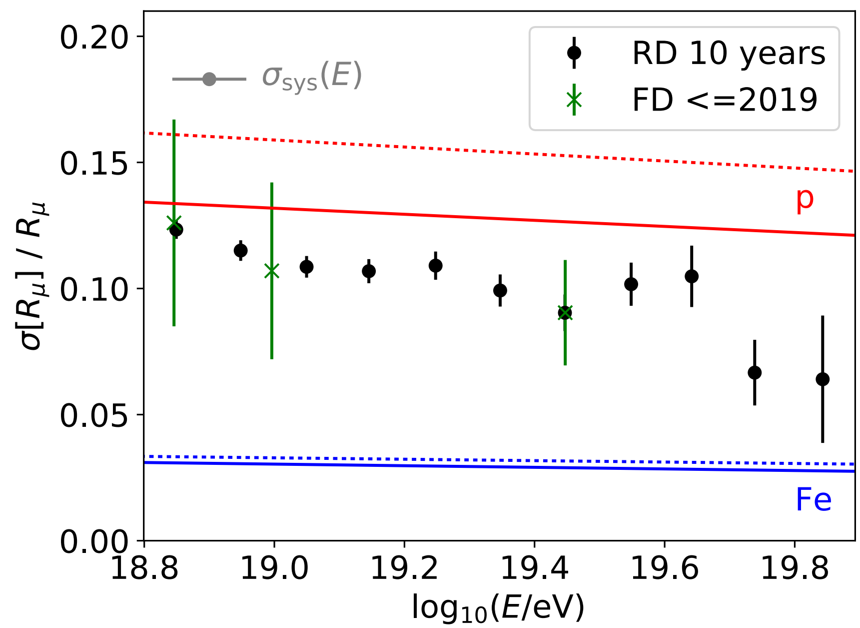

- **More than 6000 showers expected above $10^{18.8}$ eV in 10 years**
- **Energy resolution is not critical (assuming 20% here)**
- **Can also study zenith angle dependence**

Mass composition sensitivity

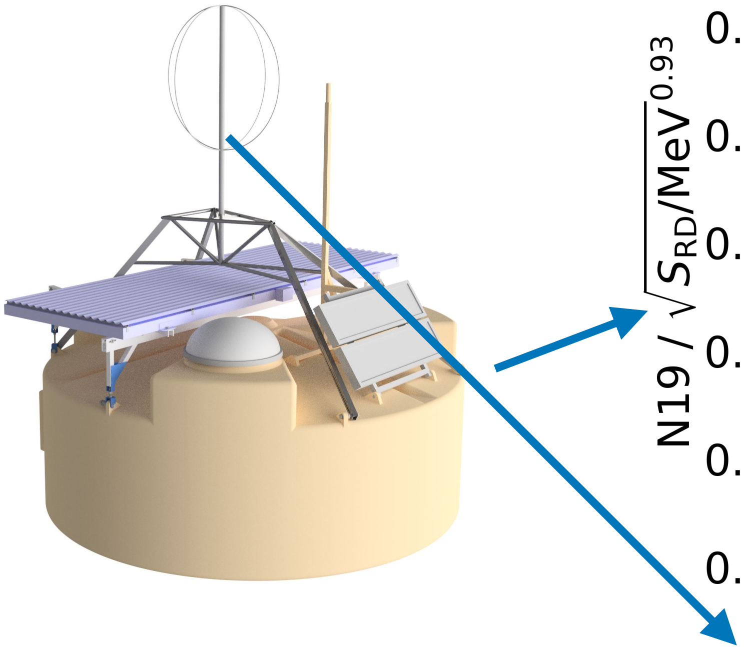

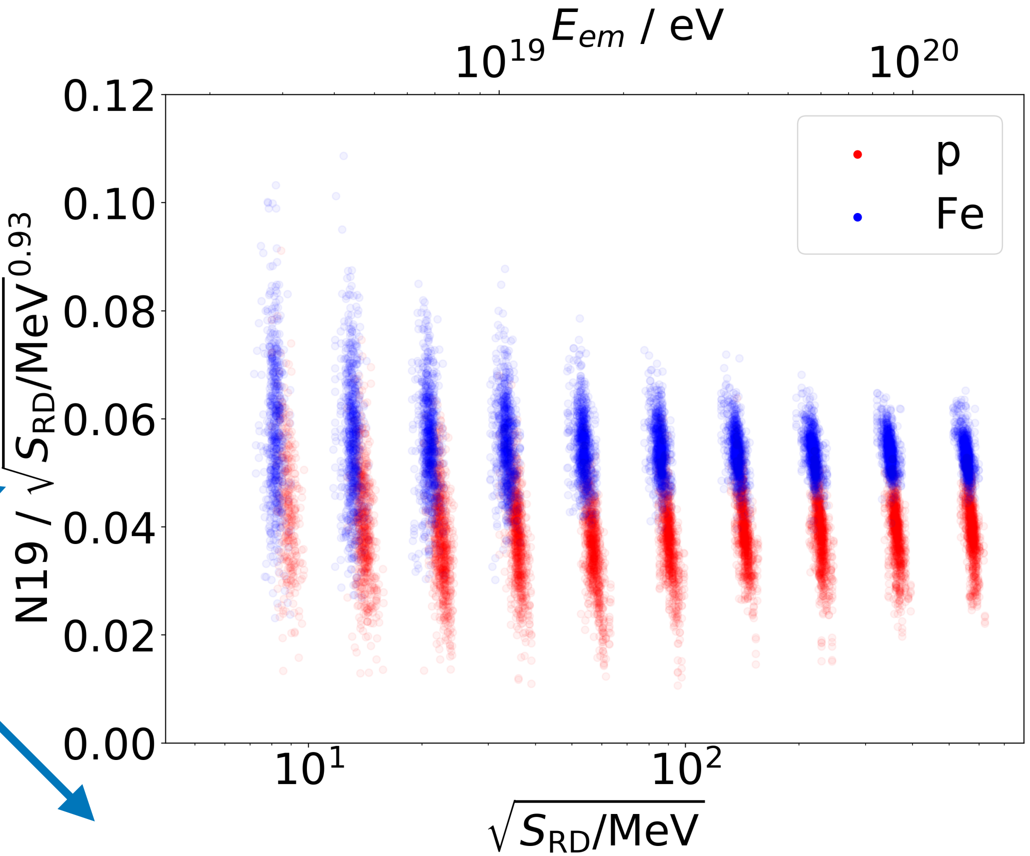

- **Energy from RD**
- **Muon number from WCD**
- **Correct for energy dependence of muon number to exploit its mass composition sensitivity**

Mass composition sensitivity

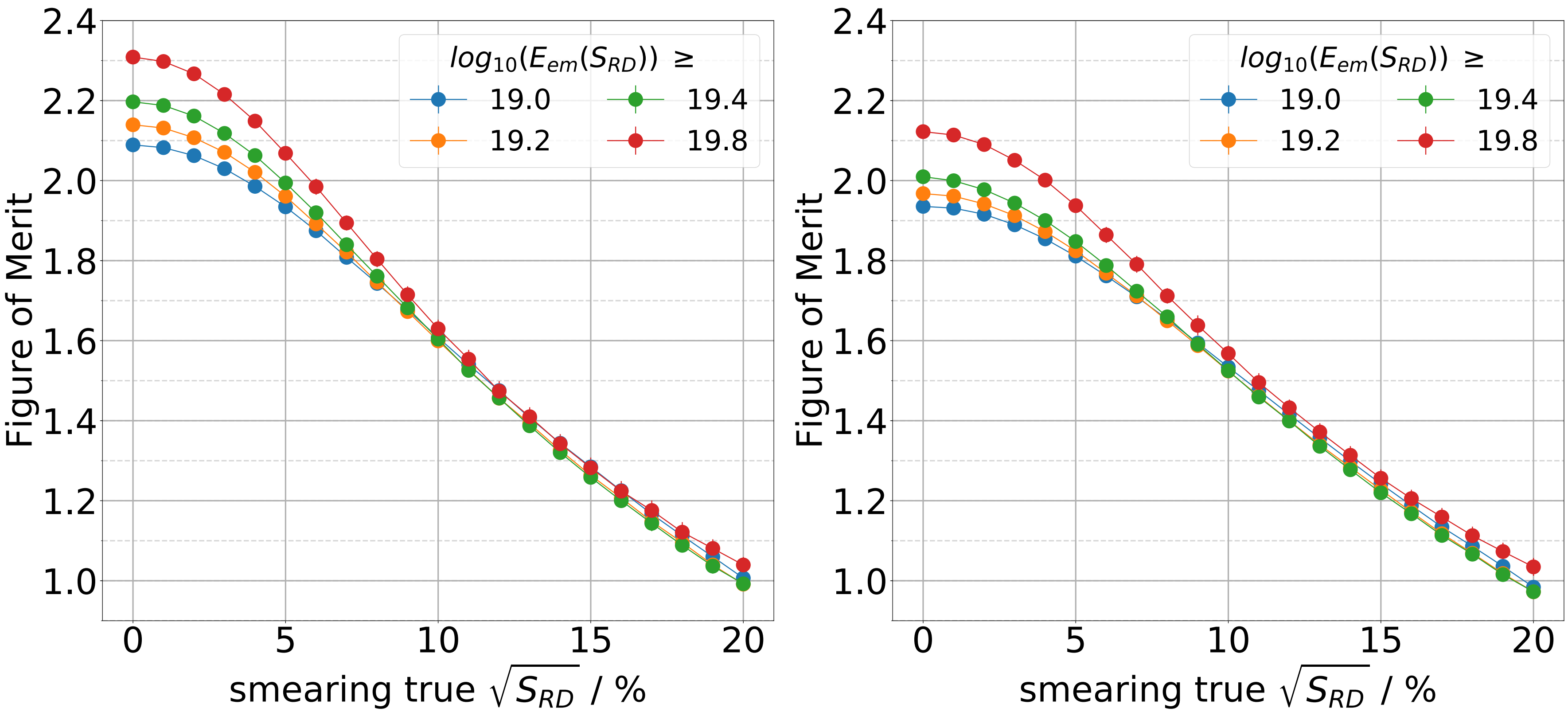

Figure 7: Figure of merit for the separation of proton-induced and iron-induced air showers using the ratio r defined in eqn. (1), various assumed resolutions for the determination of the electromagnetic energy with the Radio Detector, and different cut-offs for the lowest (smeared) electromagnetic energy. Left: using Monte-Carlo true arrival directions and knowledge of X_{max} for each individual air shower. Right: using arrival directions as reconstructed by the Surface Detector and X_{max} values known with a resolution of $100\,g/cm^2$. [33]

Sky coverage with mass sensitivity

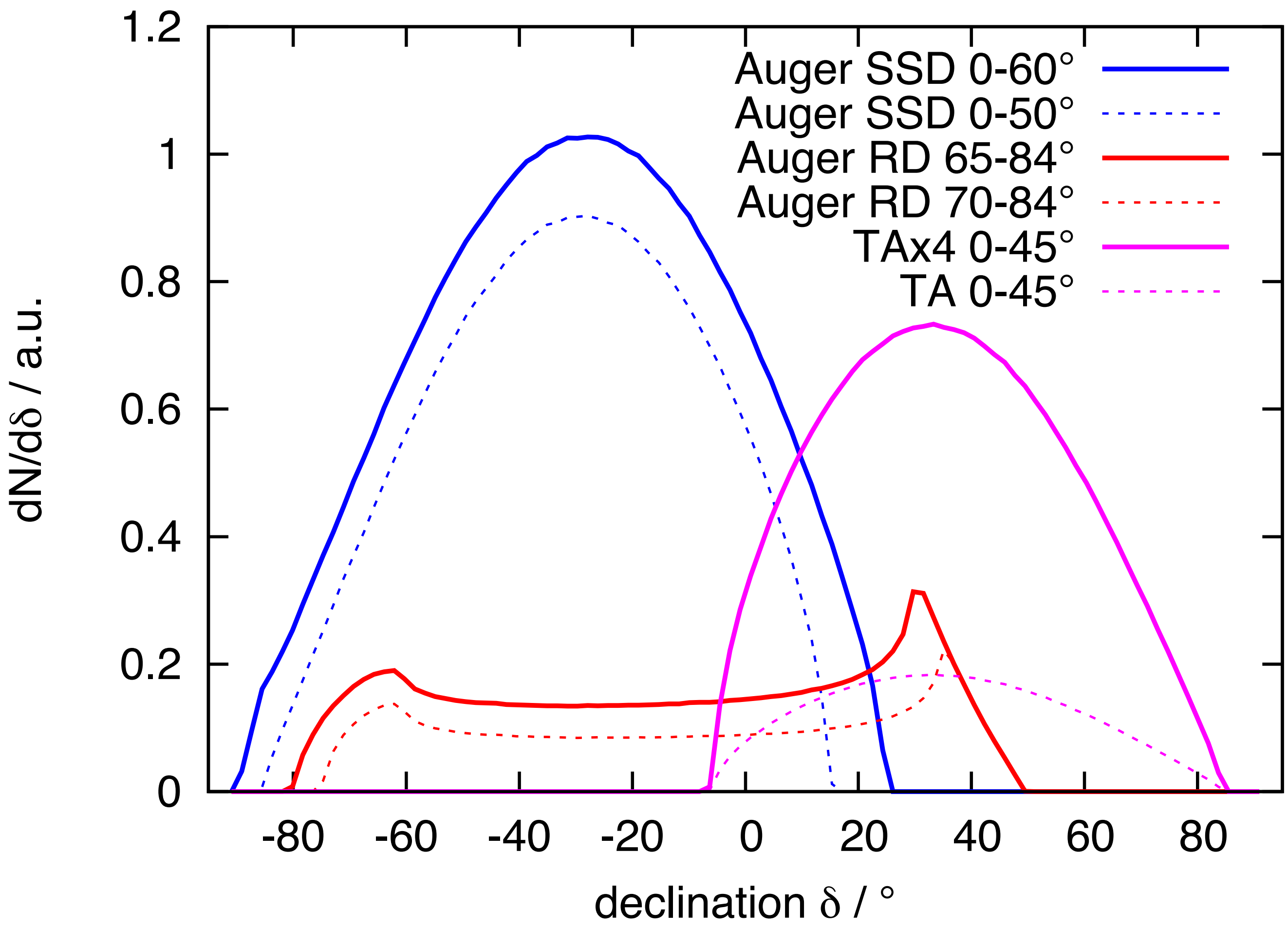

- **Add access at 20° - 45° northern declinations**
- **Shared energy scale**
- **Different systematics than SSD**

Measuring the properties of cosmic rays with the radio technique

The radio technique is now able to characterize cosmic rays:
-direction ✓
-energy ✓
-mass ✓
@100% duty cycle

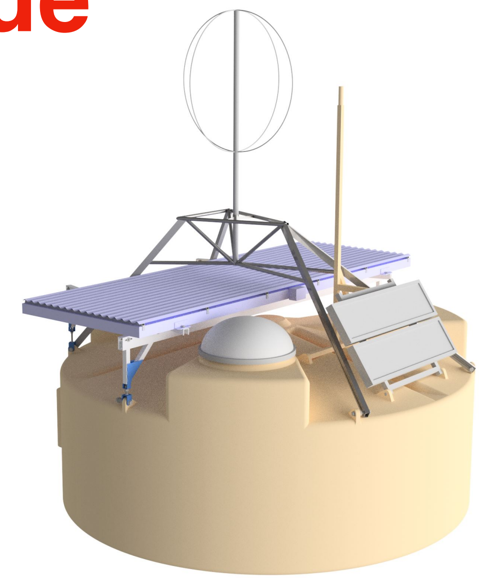

—> application on largest scales at Pierre Auger observatory